

TWO-PHOTON SEQUENTIAL ABSORPTION SPECTROSCOPY
OF ISOTOPIC SPECIES OF IODINE AND
RELATED INTERHALOGENS

By



JEFFREY RICHARD ROBINS, B.Sc., M.Sc.

A Thesis

Submitted to the School of Graduate Studies
in Partial Fulfilment of the Requirements
for the Degree
Doctor of Philosophy

McMaster University

May, 1981

TWO-PHOTON SPECTROSCOPY OF IODINE AND RELATED INTERHALOGENS

DOCTOR OF PHILOSOPHY (1981)
(Chemistry)

McMASTER UNIVERSITY
Hamilton, Ontario

TITLE: Two-Photon Sequential Absorption Spectroscopy of
Isotopic Species of Iodine and Related Interhalogens

AUTHOR: Jeffrey Richard Robins, B.Sc. (Queen's University)
M.Sc. (Queen's University)

SUPERVISOR: Professor G.W. King

NUMBER OF PAGES: xiii, 253

Abstract

Two-photon sequential absorption spectroscopy has been used to study the isotopes of the following diatomic molecules: iodine, $^{127}\text{I}_2$ and $^{129}\text{I}_2$; iodine monochloride, I^{35}Cl and I^{37}Cl ; and iodine monobromide, I^{79}Br and I^{81}Br . The interhalogens were studied via these methods with no special purification or isotope enrichment. Spectra of each isotope individually could be obtained.

In iodine the B state potential function at large internuclear separation and the B state dissociation limit were examined using a combined isotope, mass-scaled version of Le Roy's long-range potential theory. The absolute vibrational numbering and molecular constants were determined for 4 excited g states in the 5eV region of both isotopes. The E state of iodine was measured in sufficient detail in both isotopes to allow calculation of an RKR potential for this state. The fluorescence lifetimes and the effects of self-quenching and foreign-gas quenching were also measured in these high lying excited states in a preliminary fashion.

In the interhalogens, ICl and IBr , single excited states in the 5eV region were observed. Isotopic data were used to determine the absolute vibrational numbering and thus good molecular constants for these states. The intermediate $\tilde{\text{B}}'$ state of IBr was partially measured under high resolution as a necessary prerequisite for the study of the higher lying excited state.

Acknowledgements

I would like to express my gratitude to Dr. G.W. King, my supervisor during this work.

I would like to acknowledge the help, friendship, and encouragement of all the people in the spectroscopy group at McMaster. In particular, I am indebted to Dave Paape, Ian and Tamara Littlewood and Dave Evans for many hours of profitable discussion and all round fun.

I would like to acknowledge financial support from the Natural Sciences and Engineering Research Council Canada in the form of Postgraduate Scholarships in the years 1976-77 and 1977-78. I would also like to thank Diane Clayton for typing this thesis and putting up with my handwriting.

DEDICATED

to my wife Cynthia who has truly made this thesis possible

TABLE OF CONTENTS

<u>Chapter</u>		<u>Page</u>
I	INTRODUCTION.....	1
II	THEORY AND BACKGROUND.....	4
	1. A Description of the Electronic States of Diatomic Halogens.....	4
	1.1 Introduction.....	4
	1.2 The Valence States of Iodine.....	5
	1.3 A Spectroscopic Background of Iodine.	14
	1.4 The Valence States of the Interhalogens.....	21
	1.5 The Spectroscopic Background of Iodine Monochloride.....	29
	1.6 Spectroscopic Summary of IBr.....	34
	2. Long-Range Potential Behaviour.....	37
	2.1 Introduction.....	37
	2.2 Long-Range Internuclear Forces.....	38
	2.3 Limitations and Further Developments.	43
	3. The Use of Isotopic Spectra and Mass Scaling in the analysis of Electronic States.....	46
	3.1 Introduction.....	46
	3.2 Isotope Relationships in the Analysis of the Vibrational and Rotational Levels of an Excited State.....	48
	3.3 Mass-Scaled Long-Range Potential Expressions.....	53

Table of Contents, Continued

III	TWO-PHOTON SEQUENTIAL ABSORPTION SPECTROSCOPIC TECHNIQUES.....	56
	1. Introduction.....	56
	2. Intermediate State Spectra.....	58
	3. High Lying Excited State Spectra.....	63
	4. Discussion.....	66
IV	EXPERIMENTAL.....	68
	1. Introduction.....	68
	1.1 Principles of a Nitrogen-Pumped Dye Laser.....	68
	2. Lasers and Optical Systems.....	73
	2.1 Nitrogen Laser.....	73
	2.2 Dye Laser.....	74
	2.3 Optical Table.....	76
	3. Data Processing Electronics.....	80
	4. Reagents and Laser Dyes.....	85
	5. Procedures.....	91
	5.1 Calibration of the PDL.....	91
	5.2 Calibration of the MDL.....	92
	5.3 Maintenance of the System.....	93
V	RESULTS AND DISCUSSION - IODINE	96
	1. The Dissociation Limit Region in the B $^3\Pi(0^+)$ State of $^{127}\text{I}_2$ and $^{129}\text{I}_2$	96
	1.1 Introduction.....	96
	1.2 Analysis.....	98
	1.3 Discussion.....	115

Table of Contents, Continued

2.	The 5eV Region of $^{127}\text{I}_2$ and $^{129}\text{I}_2$	117
2.1	Introduction.....	117
2.2	Pump Levels and Data Analysis.....	120
2.3	Results for the E and γ States.....	124
2.4	Results for the β , α and δ States....	138
2.5	Discussion.....	149
3.	Fluorescence Decay Measurements on $^{127}\text{I}_2$ and $^{129}\text{I}_2$	158
3.1	Introduction.....	158
3.2	Fluorescence Lifetimes.....	161
3.3	Results and Discussion.....	166
4.	The Effects of Collisions and Deactiva- tions on the Excited States of $^{127}\text{I}_2$	173
4.1	Introduction.....	173
4.2	Saturation of the "E"+B Transitions..	176
4.3	Self-Quenching and Foreign Gas Quenching.....	180
4.4	Time Delay Experiments.....	188
4.5	Discussion.....	189
VI	RESULTS AND DISCUSSION - INTERHALOGENS	
	ICl AND IBr.....	191
1.	The 5eV Region of Iodine Monochloride, I^{35}Cl and I^{37}Cl	191
1.1	Introduction.....	191
1.2	Selection of Pump Lines.....	192

Table of Contents, Continued

	1.3	Analysis of the E State Spectra.....	198
	1.4	Discussion.....	205
	2.	The 5eV Region of Iodine Monobromide, I ⁷⁹ Br and I ⁸¹ Br.....	213
	2.1	Introduction.....	213
	2.2	Selection of Pump Lines.....	214
	2.3	Analysis of the E State Spectra.....	224
	2.4	Discussion.....	232
VII		CONCLUSION.....	239
VIII		REFERENCES.....	245

LIST OF TABLES

IV-1	Filter characteristics.....	79
IV-2	Laser dyes used in the experiments.....	86
V-1	Isotopic masses.....	100
V-2	Summary of rotational line data in the B state dissociation region of iodine.....	101
V-3	Vibrational energy levels for the B state dissociation region of iodine.....	102
V-4	Rotational constants near the B state dissociation limit of iodine.....	111
V-5	Long range constants of the B state of iodine...	113
V-6	Term values and rotational constants for the E state of iodine.....	125
V-7	Vibrational and rotational constants for the E states of iodine.....	128
V-8	A comparison of the E→B results with those of Wieland.....	131
V-9	Term values and rotational constants for the γ state of iodine.....	134
V-10	Vibrational and rotational constants for the γ state of iodine.....	135
V-11	Term values and rotational constants for the β state of iodine.....	142
V-12	Vibrational and rotational constants for the β state of iodine.....	144
V-13	Term values and rotational constants for the α state of iodine.....	146
V-14	Vibrational and rotational constants for the α state of iodine.....	147
V-15	Approximate term values and rotational constants for the δ state of iodine.....	150

List of Tables, Continued

V-16	Approximate vibrational and rotational constants for the δ state of iodine.....	151
V-17	RKR potential for the E state of $^{127}\text{I}_2$	152
V-18	Lifetimes of excited states of iodine.....	169
V-19	Summary of the excited states in the 5eV region of $^{127}\text{I}_2$	174
V-20	Self-quenching of $^{127}\text{I}_2$	185
VI-1	Pump lines in the A \leftarrow X transition of ICl.....	196
VI-2	Term values and rotational constants for the E state of ICl.....	206
VI-3	Molecular constants for the E state of ICl.....	207
VI-4	Rotational constants for the E state of ICl.....	208
VI-5	RKR potential for the E state of ICl.....	209
VI-6	$\tilde{\text{B}}'$ state of IBr.....	220
VI-7	Comparison of the $\tilde{\text{B}}'$ state of IBr with the work of Child.....	221
VI-8	Pump lines in the $\tilde{\text{B}}'$ state of IBr.....	222
VI-9	Term values and rotational constants for the E state of IBr.....	227
VI-10	Molecular constants for the E state of IBr.....	231
VI-11	Rotational constants for the E state of IBr.....	233
VI-12	RKR potential for the E state of IBr.....	234

LIST OF FIGURES

II-1	Molecular orbitals from np^5 electrons.....	7
II-2	Hund's coupling case (c).....	7
II-3	Correlation diagram for homonuclear molecules....	10
II-4	Potential curves in iodine (Mulliken).....	12
II-5	Correlation diagram for heteronuclear molecules..	22
II-6	Schematic of an avoided crossing.....	25
II-7	Subcases of type I predissociation.....	26
II-8	Potential curves for ICl in the B state region...	33
III-1	The basic two-photon experiment.....	57
III-2	Selectivity of two-photon experiment.....	59
III-3	Probe laser overlap.....	61
III-4	Spectrum of $^{129}\text{I}_2$ near the dissociation limit....	64
IV-1	Two-photon laser spectrometer.....	69
IV-2	Hansch design dye laser.....	71
IV-3	γ band with and without lens assembly.....	77
IV-4	Computer spectrum reproduced from digital data...	83
V-1	Birge-Sponer plot of iodine-combined data.....	106
V-2	Plot of G_v versus $(\overline{\Delta G}_v/\rho)^{10/7}$	107
V-3	Plot of η versus $(D_e - G_v)^{0.3}$	109
V-4	Plot of $B(n)$ versus $(\eta_D - \eta)$	114
V-5	RKR potential of the high lying levels in the B state of iodine.....	116
V-6	Spectrum of the E state of $^{127}\text{I}_2$	129
V-7	Spectrum of the F state of $^{129}\text{I}_2$	129

1

List of Figures, Continued

V-8	Spectrum of the α , β and γ states of $^{129}\text{I}_2$	136
V-9	Spectrum of the α and β states of $^{127}\text{I}_2$	140
V-10	Spectrum of the γ and β states of $^{127}\text{I}_2$	148
V-11	Fluorescence decay curve of the γ ($v=1$) transition.	165
V-12	Saturation curves of the E, α , β and γ states of $^{127}\text{I}_2$	178
V-13	Linear plot of the saturation data for the E ($v=3$) transition of $^{127}\text{I}_2$	181
V-14	Self-quenching data from $^{127}\text{I}_2$	186
VI-1	Portion of the 0-24 transition in the A state of ICl	194
VI-2	Spectrum of the E state of I^{37}Cl	199
VI-3	Possible two-photon transitions obeying the e-f selection rules in ICl	201
VI-4	Diagram of the B state region of IBr	216
VI-5	Numbering schemes for the $\tilde{\text{B}}'$ state of IBr	218
VI-6	Portion of the $\tilde{\text{B}}'$ state spectrum in IBr	223
VI-7	Spectrum of the E state of I^{79}Br	225

Chapter I

INTRODUCTION

The development of the laser has made possible many new forms of spectroscopy; one of these was the opportunity to go beyond conventional single photon processes and to observe two-photon and higher order multiphoton interactions. This type of experiment is referred to as double-resonance spectroscopy and it has been defined as "... the use of two resonant one-photon interactions in a single molecule, to probe molecular structure and relaxation processes". [1]

In the literature, when a double-resonance experiment is performed using two visible lasers it is referred to as optical-optical double-resonance spectroscopy (OODR) [1], or as in this study two-photon sequential absorption spectroscopy [2]. In this type of experiment one photon is used to populate the intermediate state and then a second photon induces transitions to excited states of higher energy. This stepwise excitation has a number of distinct advantages:

1. The opportunity of reaching states not attainable by a direct transition from the ground state because of selection rules;
2. The extension of high resolution spectroscopy beyond the 2 - 3eV region within reach of tunable lasers to the

4 - 5eV region where a laser matching the direct uv transition is lacking;

3. The possibility of state selectivity, where the first laser prepares the molecule in one particular quantum state before the subsequent excitation spectrum, in contrast to the usual excitation process where a large number of vibrational and rotational states can occur.

A number of excellent examples exist in the literature of the application of these techniques to diatomic molecules. In a series of papers by Gottscho et al [3-5] two simultaneously pumped, single mode, cw dye lasers were used to investigate the low-lying and high-lying (4eV) electronic states of BaO. Two cw dye lasers have been used to study CaF [6] and a combination of a cw dye laser and a pulsed dye laser were applied to the rotational analysis of the E-B system of CaCl [7]. Iodine and the related interhalogen iodine monochloride have been extensively studied using two pulsed dye lasers. Danyluk and King [8,9] and King et al [10] have used two-photon methods to examine the gerade state of iodine in the 5eV region. In the same manner Bernheim et al [11] have studied the gerade states of Li_2 . These states are not accessible from the ground state via normal one-photon absorption. The high degree of selectivity of this technique has been demonstrated in the examination of the detailed long-range behaviour of the B state of iodine [12-14]. This same selectivity allows for the study of individual isotopic species of iodine monochloride near

the intermediate A state dissociation limit [15] and in the 5eV region [16].

This present study undertook a detailed scrutiny of various isotopic species of iodine and the interhalogens iodine monochloride and iodine monobromide. The study of isotopic data from these molecules was a necessary step in firmly defining the absolute vibrational numbering in the electronic states measured and thus fixing their molecular constants. The selectivity of these two-photon methods was a perfect tool for the study of the isotopic species of the interhalogens without special enrichment or purification difficulties. It also became evident during this work that the next step in the development of the laser spectrometer involved in these experiments was the addition of a mini-computer to facilitate data handling, storage and analysis. The availability of such a powerful tool stimulated experiments not previously attempted with this equipment, in the field of fluorescence lifetime measurement.

Chapter II

THEORY AND BACKGROUND

1. A Description of the Electronic States of Diatomic Halogens

1.1 Introduction

The interpretation of the rich ultraviolet and visible spectra of the diatomic halogens has required that some form of theoretical description of the electric states involved be made. An ordering of the energy levels as a function of the electronic configuration was necessary. The diatomic halogens, in particular iodine, have been the focus of two important papers by R.S. Mulliken [17,18]. In these papers the extensive valence-shell states of iodine have been given a theoretical interpretation. The methods involved have employed molecular orbitals (MO) constructed from linear combinations of atomic orbitals (LCAO).

Mulliken's treatment essentially involved two aspects:

- (a) interpretation of electronic states in terms of electron configurations and predictions of their properties; and
- (b) dissociation product correlations. The latter involved deciding what atomic states the products of the dissociation of a particular molecular state yield. Mulliken's treatment of this problem has been central to many interpretations of

experimental observations. This discussion will be primarily based on the work of Mulliken and, because of the large amount of experimental data available, will focus primarily on the homonuclear molecule iodine.

The electronic states of the heteronuclear halogens are analogous to those of the homonuclear molecules. There is, however, one important difference and that arises from the absence of the g, u -symmetry properties of the MO's in the heteronuclear molecule. The presence of this symmetry property allows the adiabatic crossing of various states in I_2 . In the interhalogens, where the interactions are strong enough, its absence can result in two electronic states avoiding each other. The non-crossing rule states that the potential curves of two electronic states of the same species (i.e. electronic states with, in case (c), the same Ω values and the same symmetry properties) cannot cross each other [19]. Section 1.4 of this discussion will deal with this difference in more detail as it affects certain states of interest in the diatomic interhalogens.

1.2 The Valence States of Iodine

If one considers two ground-state $^2P_{3/2,1/2}$ halogen atoms with np^5 outermost electron configurations (^{17}Cl : $[\text{Ne}], 3s^2, 3p^5$; ^{35}Br : $[\text{Ar}], 3d^{10}, 4s^2, 4p^5$; ^{53}I : $[\text{Kr}], 4d^{10}, 5s^2, 5p^5$), a simple LCAO treatment results in the molecular

orbitals in Figure II-1 [21,22]. Of course the heteronuclear halogens will have no defined g, u-symmetry properties.

In the simplest LCAO approximation the MO's σ_g , σ_u are of the forms $ns \pm ns$ and $np\sigma \pm np\sigma$ and the MO's π_g and π_u are of the form $np\pi \pm np\pi$. Mulliken [17,18] defines the valence-shell states to have MO electron configurations of the type $\sigma_g^2 \sigma_u^2 \sigma_g^m \pi_u^p \pi_g^q \sigma_u^n$ where $m + n + p + q = 10$. These configurations are abbreviated to mpqn. The lowest energy arrangement of the ten valence electrons $\sigma_g^2 \pi_u^4 \pi_g^4 \sigma_u^0$ defines the ground state and is abbreviated as 2440.

The classification of states derived from a particular mpqn configuration must take into account the various interactions of rotational and electronic motions. The relative strengths of these will dictate what quantum numbers can be used to describe the rotational levels in the different types of electronic states and how their energies depend on these quantum numbers [19]. In an isolated molecule the total molecular angular momentum results from the vectorial coupling of electronic spin angular momentum, electronic orbital angular momentum, and the nuclear rotational angular momentum. There are several limiting coupling cases that serve to describe fairly well the large majority of molecules. These are known as Hund's coupling cases (a) through (e) [19]. Heavy molecules such as the halogens have to be treated using Hund's coupling

Figure II-1. Molecular Orbitals

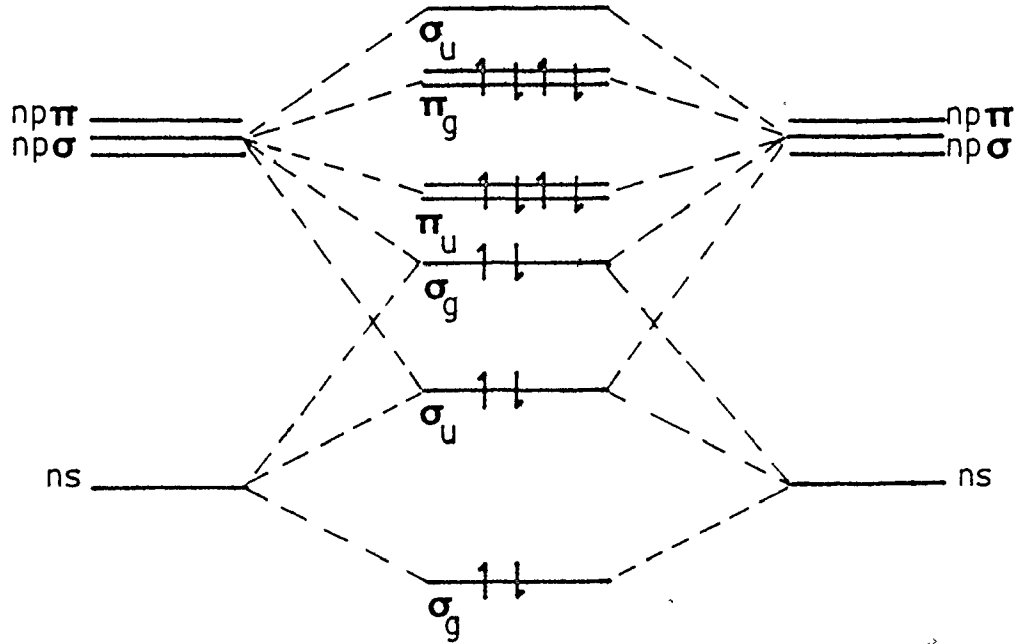
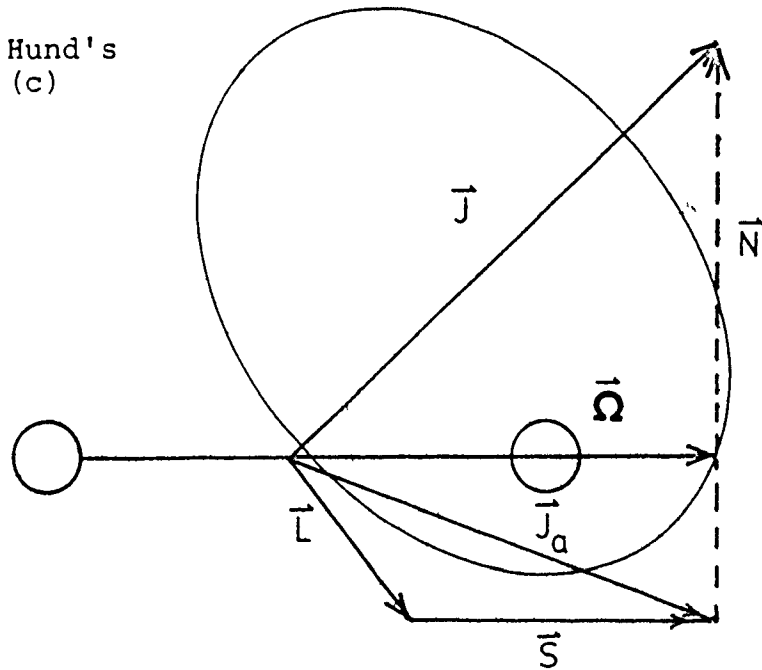


Figure II-2. Hund's Coupling Case (c)



case (c). In case (c) the interaction between \vec{L} , the electronic orbital angular momentum, and \vec{S} , the spin, is stronger than the interaction of these with the internuclear axis (Figure II-2). In this case $\vec{\Lambda}$, the component of the electronic orbital angular momentum along the internuclear axis, and $\vec{\Sigma}$, the component of the spin along the axis, are not defined. Instead \vec{L} and \vec{S} form a resultant vector \vec{J}_a which is then coupled to the internuclear axis with a component $\vec{\Omega}$. The total electronic angular momentum $\vec{\Omega}$ and the angular momentum of nuclear rotation \vec{N} then form the resultant total angular momentum \vec{J} [19]. States under case (c) must be classified by their values of Ω , the axial projection of the total electronic angular momentum, only. The rotational energy levels and their J values are given by the same formulae as for case (a) coupling (where the strongest interaction is the electrostatic correlation that couples the electron spin and orbital angular moments individually to the molecular axis).

Mulliken [17] has classified the valence states of iodine according to two types of case (c) coupling. One type of classification of the electronic states of iodine is similar to case (a) (or (b) or Ω -s type) and has a well-defined meaning only for fairly small r values. The normal case (c) classification is applicable for large r values and is important for dissociation product correlations. Mulliken

[20] has given a series of tables showing the Ω values and symmetry properties of the molecular states obtainable from the union of two atoms with specified J values, assuming case (c) coupling in the molecule. Using these rules and the non-crossing rule, the correlations for the 23 Ω -components derived from two 2P atoms is shown in Figure II-3 [17,21]. For heteronuclear halogens the correlations will be somewhat different and will be discussed later. Similar diagrams can be constructed for higher-lying valence-shell configurations that will correlate with excited or ionic states of the halogen atoms.

This diagram is only a qualitative way of describing the relative energy levels of the molecule. A different ordering of the molecular levels in energy will alter the correlation with atomic J values. A correct determination of the correlation of molecular Λ and s values (small r) with atomic J values depends heavily on a knowledge of the energy order of the molecular levels [20]. For example, for larger multiplet splittings of the $2341\ ^3\Pi_g$ state into its component 0_g^+ , 0_g^- , $1g$ and $2g$ states, the relative positions of $2341\ ^3\Pi_g(0_g^+)$ and $2422\ ^3\Sigma_g^-(0_g^+)$ in Figure II-3, could be reversed. Application of the non-crossing rule would cause $2341\ 0_g^+$ to correlate with $^2P_{3/2} + ^2P_{1/2}$ atoms rather than with $^2P_{3/2} + ^2P_{3/2}$ atoms as it does in the diagram [21]. There are usually one or two unique levels for

Figure II-3. Schematic correlation diagram for molecular iodine [21]

which the J correlation can be given without any knowledge of the energy order of the molecular levels. A unique level is a level whose Ω value and symmetry type occur only once in the manifold of states derivable from two atoms with given L and S values [20]. Such a case occurs for the B state of iodine; the 0_u^+ level from $2p_{3/2} + 2p_{1/2}$ must correlate with the $2431 \ ^3\Pi(0_u^+)$ level. In heteronuclear halogens the $^3\Pi(0^+)$ state would correlate with $2p_{3/2} + 2p_{3/2}$ atoms.

It should be noted from Figure II-3 that only the $2440 \ X \ ^1\Sigma_g^+$ and $2431 \ ^3\Pi_{0,1,2}$ form bound states. Other bound states of higher energy exist but are ionic in character and correlate with excited atoms. In 1971 Mulliken revised [18] his earlier descriptions of iodine [17] using more recent experimental data. Using predicted vertical energies of the valence-shell states measured from the bottom of the X state potential well, Mulliken has developed a diagram showing electron configurations, term assignments, dissociation products and estimated forms of the potential curves; this is shown in Figure II-4. In this diagram, except for the $2440 \ X \ ^1\Sigma_g^+(0_g^+)$ state and the $B \ ^3\Pi_u(0_u^+)$ state, the potential curves are not known well and have been drawn by considerations of the bonding and antibonding characteristics of the MO's involved and the non-crossing rule [18].

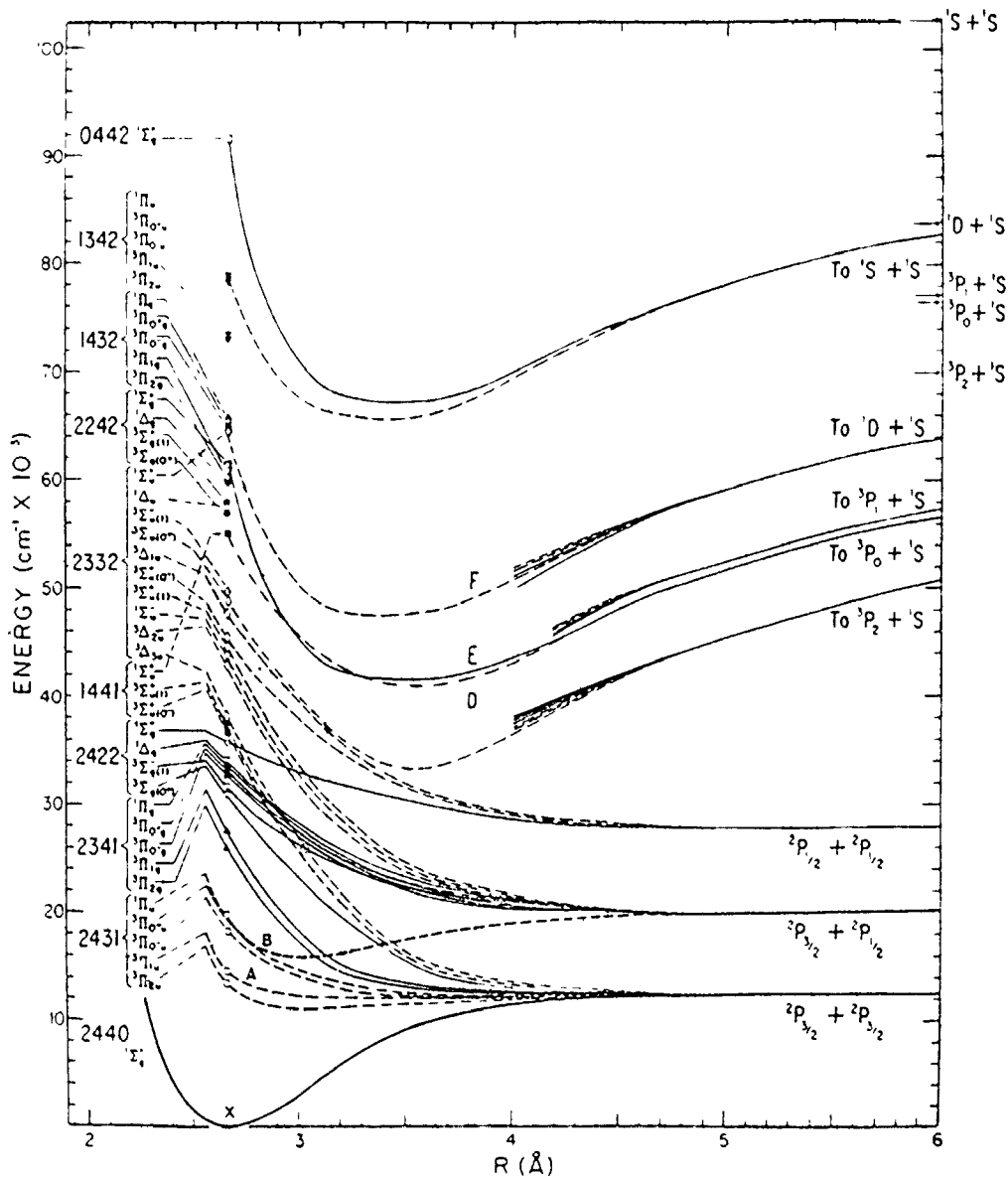


Figure II-4. Mulliken's estimated potential curves for valence-shell states of iodine (Figure 1 of reference 18). The solid curves are gerade (g) states; the dashed curves are ungerade (u) states.

Recent pseudopotential calculations [23,24] have been made to answer points that were not clear from Mulliken's work. These studies show slightly different ordering for some of the molecular states and give some idea of configurational mixing that may be occurring in the states. In general, however, Figures II-3 and II-4 are very useful aids in the assignment of observed transitions.

Two-photon studies of iodine, originating from the ground $X\ ^1\Sigma_g^+$ state and using the $B\ ^3\Pi(0_u^+)$ state as an intermediate, must terminate on an excited state of g-symmetry. There are a large number of gerade states lying above the 2431 configuration of the B state. These can be divided into two classes on the basis of their dissociation products. The g states belonging to the lower lying 2341 and 2422 configurations (see Figure II-4) are predicted to dissociate to (2P) atoms. These levels have estimated vertical energies between 3 and 4eV. There are 9 gerade states in this region; 2341 configuration $^3\Pi_g(0^+, 0^-, 1, 2)$, $^1\Pi_g$ and the 2422 configuration $^3\Sigma_g^-(0^+, 1)$, $^1\Delta_g$, $^1\Sigma_g^+$. The g states in the higher lying 2242 and 1432 configurations are expected to exhibit ion-pair character [18] (large equilibrium internuclear separation r_e and small vibrational frequency ω_e). These are predicted to dissociate into $I^-(^1S)$ and $I^+(^3P_{2,1,0}, ^1D, ^1S)$ atoms. These levels have estimated vertical energies between 7 and 8eV. There are 9 gerade states in this region; 2242 configuration $^3\Sigma_g^-(0^+, 1)$,

$1\Delta_g$, $1\Sigma_g^+$ and the 1432 configuration $3\Pi_g(0^+, 0^-, 1, 2)$, $1\Pi_g$.

1.3 A Spectroscopic Background of Iodine

The spectroscopic literature concerning iodine is extremely extensive and no attempt will be made here to completely summarize it (summaries of some of the work can be found in reference 18 up till 1971 and reference 21, for low-lying valence states, up till 1973) Instead, the more recent work on states that are relevant to these studies will be discussed.

The B-X system of iodine has been the subject of intensive study for the last 58 years beginning with the early work by Mecke in 1923 [25]. The two-photon studies all originate in the ground X $1\Sigma_g^+$ state and use the B $3\Pi_u(0_u^+)$ state as an intermediate. Detailed knowledge of these states is important. The analyses of the B and X states are closely tied together. The determination of spectroscopic constants for these two states has not always yielded consistent results. In 1970 Le Roy extensively re-analysed the existing data on the X state [26] and produced an improved set of vibrational terms and rotational constants up to $v_X = 82$. In 1972 Barrow and Yee [27] produced the most comprehensive study of the B-X spectrum to date. Barrow and Yee analysed bands in the range $v_B' = 4-77$ and $v_X'' = 0-5$. They gave constants for the X state that held over the range $v_X = 0-5$. Barrow and Yee

found that the vibrational energies and distortion constants for the B state could not be adequately represented by simple polynomials. They listed polynomial expansion coefficients for the vibrational constants only over the range $v_B = 0-50$. Barrow and Yee did give a comprehensive table of molecular constants obtained from term value analysis for $v_B = 4-77$ in the B state. In 1974 Wei and Tellinghuisen [28] re-examined the B-X transition and the results obtained in various previous studies were critically analysed. Using a method involving band-by-band direct fitting procedures, followed by a correlated least squares treatment of the intermediate results, Wei and Tellinghuisen produced what they termed the "best" spectroscopic parameters for the X and B states [28].

Recent work has superseded all of these studies of the B-X system. Gerstenkorn and Luc have used high resolution Fourier transform spectroscopy to measure accurately ($\pm 0.002 \text{ cm}^{-1}$) the iodine absorption spectrum from 14,800 to 20,000 cm^{-1} [29,30]. With these measurements they have assigned about 14,000 transitions belonging to 139 bands of the B-X system [31,32]. Using these band-by-band studies, they have produced molecular constants and Dunham expansion parameters describing the B-X system [32]. Their work has determined the values of 365 molecular constants σ_0' , B' , D' and H' in the excited state $B^3\Pi(0_u^+)$ (for $1 \leq v' \leq 62$)

and 20 values of B'' and D'' in the ground state $X \ ^1\Sigma_g^+$ (for $0 \leq v'' \leq 9$). These values were used to produce 60 polynomial expansion parameters for the molecular constants G_v' , B_v' , D_v' , H_v' and G_v'' , B_v'' , D_v'' . Luc [32] has extensively compared their results with previous studies. Provided the J values of the calculated wavenumbers are less than or equal to the maximum J values detected for each band by Barrow and Yee [27] the agreement between the two studies is within $\pm 0.030 \text{ cm}^{-1}$.

Where possible in these studies of iodine the values of Luc [32] have been used to calculate B-X transition energies. For levels beyond these regions the term values of Barrow and Yee [27] were used. The values of Danyluk and King [13] were used for very high B state levels. For the isotopic species $^{129}\text{I}_2$, standard isotope relationships and the constants of Luc [32] were employed below $v = 62$. The work of Yee [33] was used where possible above this region.

The work of Gerstenkorn and Luc provides the best description of the B state up to $v_B = 62$ and the X state up to $v = 9$. However, the X state of iodine has been observed [26] up to $v_X = 84$, and recent laser fluorescence studies have extended this to $v_X = 96$. Gerstenkorn and Luc made very detailed assignments of portions of the B-X system in the vicinity of various laser lines [34]. Using these assignments, the B-X transition has been studied by laser-

induced fluorescence-high resolution Fourier transform spectroscopy [35] (LIF-FTS) and with a cw optically pumped iodine laser [36,37]. In this work X state levels from $v_X = 10-103$ with rotational values of $J_X = 0-110$ were studied (exact details of the study have not as yet been published). Bacis et al [35] and Koffend et al [36] have applied the long-range potential theory of Le Roy and Bernstein to obtain values of D_e , v_D and C_6 for the X ground state. The LIF-FTS study [35] found two states perturbing the X state, a 0_g^+ and a $1g$ state. These affect the levels in the X state from $v_X = 85$ up. Transitions into three consecutive levels of the 0_g^+ state and four levels of the $1g$ state from the $B^3\Pi(0_u^+)$ state were observed [35]. Because of interest in the optically pumped I_2 laser, Tellinghuisen et al [38] have also examined the X state by looking in detail at the $D \rightarrow X$ fluorescence. Using methods they have developed [39,40] to calculate centrifugal distortion constants and incorporate these values in the data analysis, they calculated a detailed set of least-squares expansion parameters for the vibrational energy, rotational constants and first two centrifugal distortion constants for levels in the X state from $v_X = 0$ to $v_X = 99$. Such detailed knowledge of the ground state of a diatomic molecule is rare.

The emission and fluorescence spectra of iodine have been studied by conventional spectroscopy for over 50 years,

but firm assignments of the higher-lying electronic states are few. It has been found that the emission spectrum of iodine exhibits a different structure with and without an inert buffer gas present [18]. In the absence of foreign gases the spectrum consists of one or more typical resonance series at short wavelengths, followed at longer wavelengths by groups of diffuse bands. In the presence of a buffer gas, the diffuse bands become faint and are replaced by some well-defined, red-degraded systems of sharp bands. Despite the large number of possible transitions from the high lying electronic states, only four transitions have been assigned with a high degree of certainty using conventional spectroscopy. Only two of these transitions originate from gerade states and the constants of only one excited state (the E state) have been firmly established.

In the absence of any inert buffer gas, an ungerade state has been identified from the fluorescence excited by absorption of light between 1800 and 2000 Å. This fluorescence corresponds to the D (1441, $1\Sigma_u^+$) \rightarrow X $1\Sigma_g^+$ transition between 3100-3460 Å [18,38,41]. The other assigned transitions appear in the presence of an inert buffer gas. These bands correspond to the F (2332, $1\Sigma_u^+$) \rightarrow X $1\Sigma_g^+$ transition between 2500-2720 Å [18,42]; the D' (1432, $3\Pi_{2g}$) \rightarrow A' (2431, $3\Pi_{2u}$) transition between 3000-3450 Å [18,43,44] and the E (1432, $3\Pi_g^+$) \rightarrow B $3\Pi(0_u^+)$ transition between 4000-4360 Å

[†]As will be discussed later in Section 2.3, Chap. V, the E state has also been assigned to 2242 $1\Sigma_g^+$

[18,42,45]. The presence of these bands when an inert gas is added has been attributed to initial excitation to a D state level and then collisional energy transfer to vibrational levels of lower excited states [18].

The advent of lasers and sequential multiphoton spectroscopy provided a technique for detailed study of the higher lying states of iodine. States that were forbidden via single photon transitions from the ground state could be accessed using two-photon absorption via an intermediate state. Selective population of individual vibrational and rotational levels yielded much less complex spectra of the excited state than was available using conventional means. Rousseau and Williams [46,47] in an early study, used two-photon techniques to study the E state of iodine using one tunable and one fixed frequency laser. They resolved the ~~fluorescence~~ out of this state into the B state and studied the discrete structure of the B state. In addition, they observed a series of diffuse bands originating from the "internal-diffraction" effects predicted by Condon in 1928 [48]. These are transitions originating in the discrete levels of the E state and terminating in the continuum levels of the B state. In an attempt to pin down the electronic assignment of the E state (either $^3\Pi(0_g^+)$ or $^1\Sigma_g^+$) they made a single measurement of the lifetime of the E→B emission [47]. Their argument was that the fully

allowed $^3\Pi(0_g^+) \rightarrow ^3\Pi(0_u^+)$ transition would be expected to have a short fluorescence lifetime in comparison to the spin forbidden $^1\Sigma_g^+ \rightarrow ^3\Pi(0_u^+)$ transition. This work was followed by the two-photon studies of Danyluk and King [9] using two tunable dye lasers. Danyluk and King established the existence of 5 excited g states in the 5eV region of iodine. Similar experiments on one of these observed states were performed by Cunha et al [49] and Williamson [50]. These latter two studies used completely different regions in the intermediate B state for pump levels as had Danyluk and King, and they observed different regions of the excited state potential well. All of these studies [9,49,50] were made on the E state potential well.

Multiphoton studies in iodine have been made involving three-photon absorption as well. The D'-A' system has been studied in this manner [51]. Resonance enhanced three-photon absorption using a cw intracavity absorption technique [52] has accessed the D-X transition. Excited states have also been studied but not identified using third harmonic generation based on simultaneous resonances in one- and two-quantum transitions [53] and by multiphoton resonance ionization spectroscopy [54]. Recently the fluorescence spectrum of iodine was reexamined in the presence and absence of buffer gases following excitation by an ArF excimer laser at 193.3 nm [55]. Two- and three-photon absorption of the iodine molecule via dissociative states

has also been studied [56]. Optical-optical double-resonance, using polarized light, has been applied to the study of the role of dissociation states that lie above the B state dissociation limit, as intermediate levels.

All of these laser studies have yielded further information on the excited states of iodine; however, these studies have not ended the confusion about what upper states are actually present. For example, the interpretation of the results of Danyluk and King [9] has been questioned by Tellinghuisen et al [44], and even the very existence of some of the states observed has been doubted [50]. A laser study of the D'-A' system [51] has produced a calculated T_e value for the A' state that is appreciably below all other estimations and measurements [44].

1.4 The Valence States of the Interhalogens

The valence-shell states of ICl and IBr are similar to those of I_2 , and a diagram (Figure II-5), analogous to Figure II-3, showing schematically the correlations involved, can be constructed. The use of the designations such as 2341, referring to electronic configurations in terms of the molecular orbitals $\sigma\pi\pi^*\sigma^*$, in heteronuclear molecules, refer to orbitals that are no longer equally associated with the two atoms. For the molecule XY, the MO configuration [17] is $(\sigma_X + \sigma_Y, \sigma)^m, (n_Y p\pi)^p, (n_X p\pi)^q, (n_Y p\sigma - n_X p\sigma, \sigma^*)^n$.

Figure II-5. Schematic correlation diagram for iodine monobromide

The main differences between Figures II-3 and II-5 arise from the lack of g , u -symmetry and the fact that the separated atom state $I(^2P_{3/2}) + I(^2P_{1/2})$ will now be split into two states $I(^2P_{3/2}) + X(^2P_{1/2})$ and $I(^2P_{1/2}) + X(^2P_{3/2})$. These differences are important in that they produce examples of avoided crossings of potential curves. It is the lower of the two avoided crossings in Figure II-5 that is important in this study. The 2422 configuration and the 2341 configuration lie very close in energy and their relative positions could be reversed [17]. However, this will not effect the discussion, as they both have 0^+ symmetry.

The lower energy avoided crossings in both ICl and IBr have been studied. The states involved are a 0^+ repulsive state which correlates with two ground state atoms and an attractive $^3\Pi(0^+)$ state that correlates with one ground $I(^2P_{3/2})$ atom and one spin-orbit excited $X(^2P_{1/2})$ atom ($X = \text{Cl or Br}$). The interaction of these two states is a form of homogeneous perturbation ($\Delta\Omega = 0$), a perturbation between states of the same type, as opposed to a heterogeneous perturbation where $\Delta\Omega = \pm 1$. The strength of the interaction between these states varies in the different interhalogens. It can be sufficiently weak to simply give rise to predissociation from the adiabatic $^3\Pi(0^+)$ state, or strong enough to cause an avoided crossing which will result in the appearance of a new heavily predissociated $\tilde{B}'(0^+)$ state. This latter interaction will also produce a potential maximum

in the B $^3\Pi(0^+)$ state (Figure II-6).

The process of predissociation or the possibility of going over without radiation from a discrete state into a repulsive one, has been divided by Herzberg into types [19]. Type I predissociation, which occurs in the interhalogens, is the overlapping of the vibrational or rotational levels of a certain electronic state by the dissociation continuum belonging to another electronic state. Predissociation occurs as a radiationless transition into this other dissociated electronic state. Herzberg has divided case I into three subdivisions, which are distinguished according to whether the point of intersection of the two potential curves lies at about the height of the asymptote of the state, giving rise to the predissociation, or whether it lies below or above this asymptote (Figure II-7). The curve crossings in the interhalogens ICl and IBr correspond to case (c) of type I, where the point of intersection lies above the asymptote of the repulsive curve. The probability of predissociation becomes large for levels in the state α in Figure II-7 (c) that lie above the point of intersection. At the onset of predissociation the observed bands will become diffuse in absorption and break off in emission. The energy corresponding to this point is referred to as the predissociation limit [19]. Information on the forms of the potential curves involved can be obtained from individual linewidth measurements and the energy shifts around the

4

Figure II-6. Schematic diagram of an avoided crossing
(diagram is not to scale)



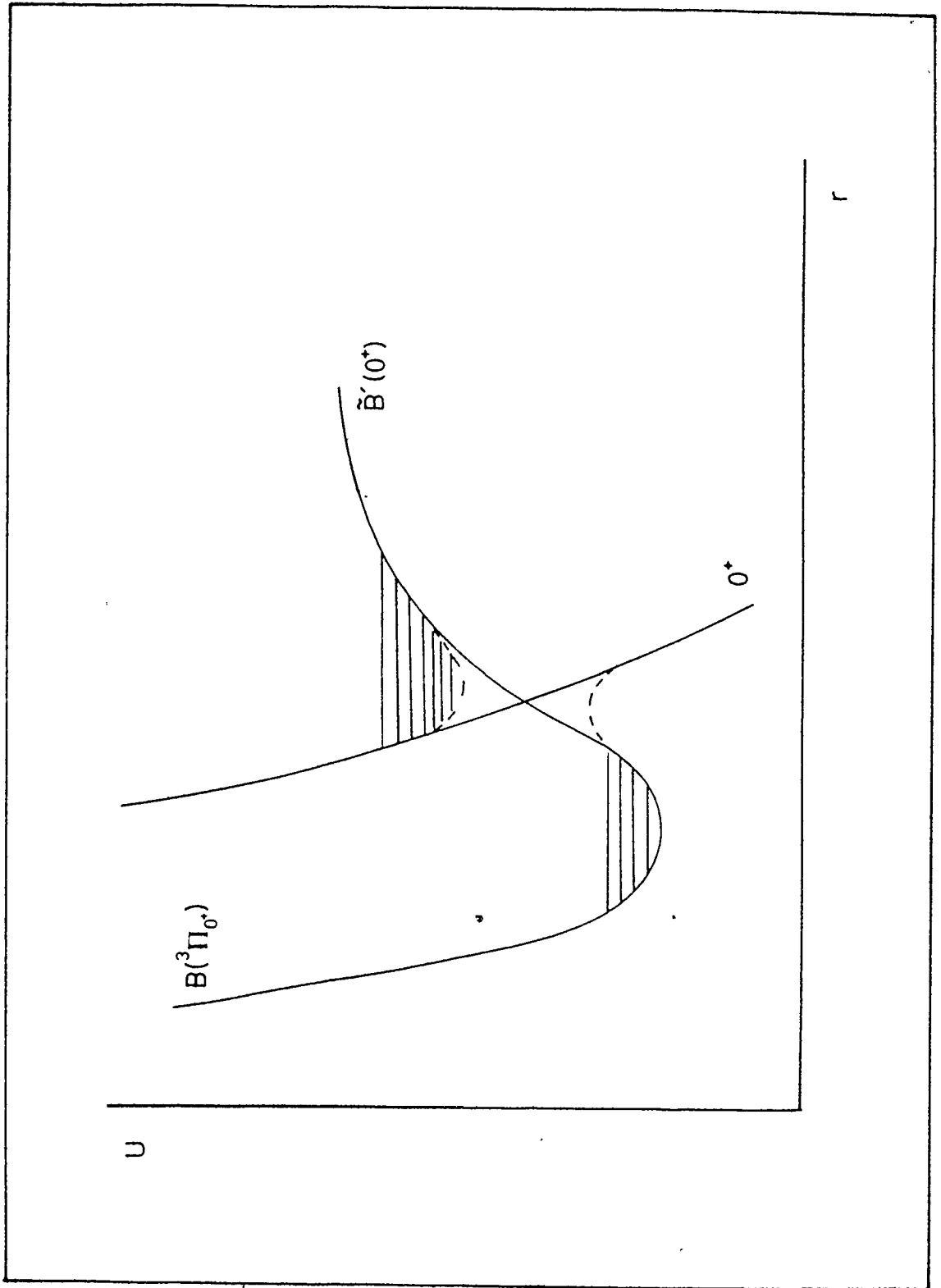
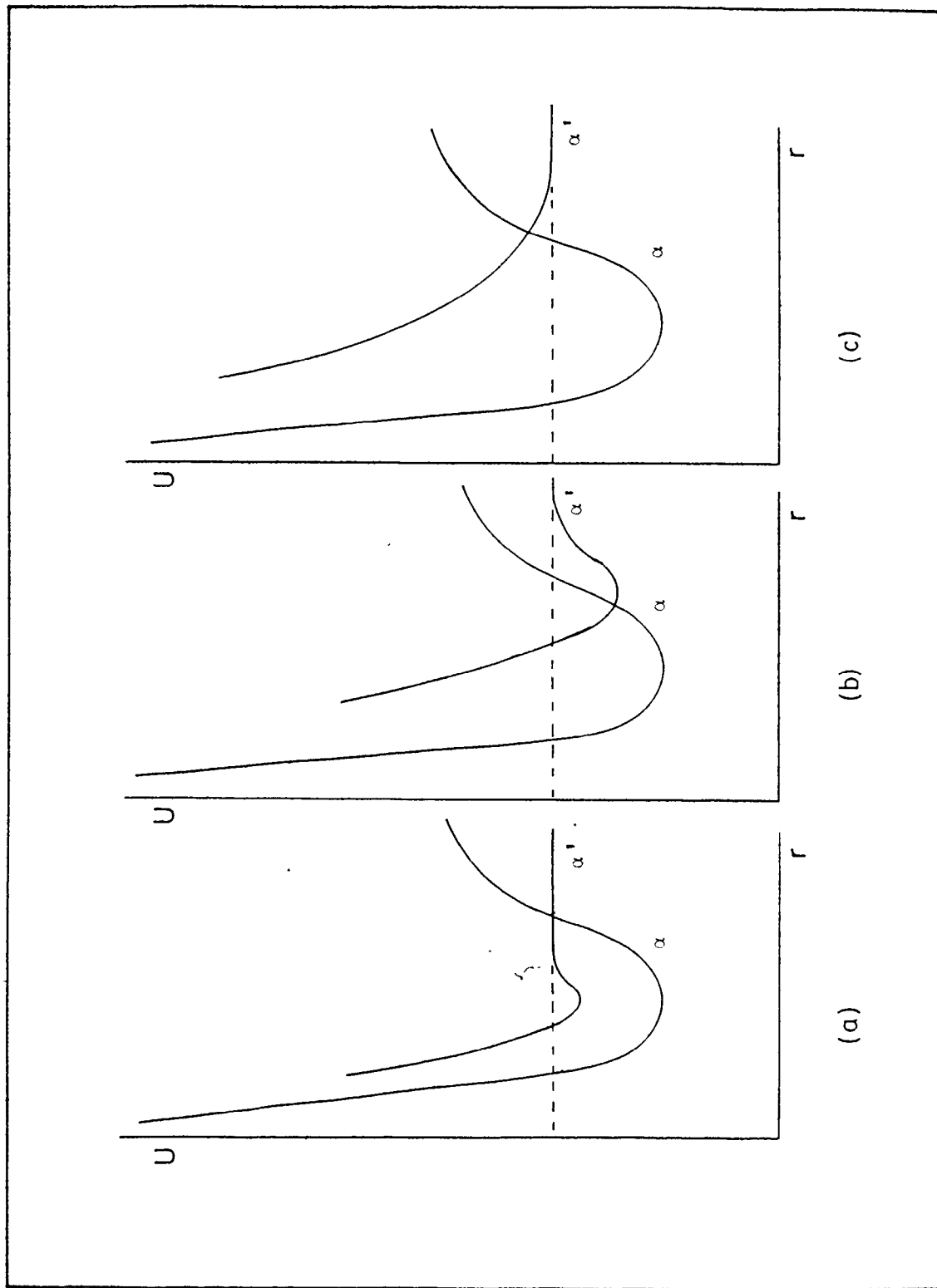


Figure II-7. Three subcases of case I of predissociation. In each case, the broken line gives the position of the asymptote of the potential curve α'



interaction.

The observed spectra in these regions of ICl and IBr consist of a series of discrete absorption transitions from the X state to the B $^3\Pi(0^+)$ state breaking off at a false dissociation limit, to be followed at higher frequencies by fragments of other weak diffuse bands. On the evidence of a change in the rotational constant, this is attributed to the presence of a new Born-Oppenheimer (or adiabatic) state $\tilde{B}'(0^+)$ formed by a strongly avoided potential curve crossing (Figure II-6). To interpret these observations (primarily in IBr) and obtain information on the interacting states, Bandrauk and Child [57] in 1970 developed analytical expressions for the predissociation linewidths from the scattering solutions to a two-state curve crossing problem. They considered both inner and outer curve crossings and distinguished between "strong coupling" in which new adiabatic states are formed, and "weak coupling" in which they are not. The outer crossing, strong coupling case was applied to IBr. In the strong coupling model, a molecule of energy E_{vJ} and rotational quantum number J is considered to be initially in the bound $\tilde{B}'(0^+)$ state. The probability that it will make a nonradiative transition to a dissociative adiabatic curve is considered and the result of this interaction is that the linewidth of the level broadens and the level is shifted in energy. The energy shift and the increase in the linewidth will both vanish at the occurrence of a bound level of

the same energy E_{vJ} in the diabatic potential $B \ ^3\Pi(0^+)$. Thus whenever a pair of levels in the $B \ ^3\Pi(0^+)$ state and the $\tilde{B}'(0^+)$ state have the same energy and the same value of J a sharp, unshifted line is expected. As this accidental degeneracy becomes less exact, the lines broaden and shift in energy. This results in fragmentary branches, broadening on each side of the sharp central line.

In 1973 Child and Bernstein [58] systemized the curve crossings in the diatomic interhalogens and in 1974 Child [59] extensively summarized the theory to that date on diatomic predissociation linewidths. In 1976 Child extended the strong coupling model to cases of intermediate coupling [60], which he felt was a better explanation of the fragmentary bands observed in IBr. The evidence against the adiabatic picture of a new state $\tilde{B}'(0^+)$ being formed by a strongly avoided potential curve crossing, came from photodissociation from the $B \ ^3\Pi(0^+)$ state continuum and the appearance of the $\tilde{B}' + X$ spectrum in absorption. There was no adiabatic interpretation completely consistent with the fact that fragments of bands observed in IBr were seen for some but not all the excited vibrational levels. This would not be expected if, as most experimentalists had assumed, the vibrational spacings in the $B \ ^3\Pi(0^+)$ state and the $\tilde{B}'(0^+)$ state were the same; if the spacings were identical, a sharp level coincidence should occur for every vibrational state [60].

1.5 The Spectroscopic Background of Iodine Monochloride

The discrete absorption spectrum of ICl in the visible and near infrared comprises three electronic transitions, $A^3\Pi_1 + X^1\Sigma^+$, $B^3\Pi(0^+) + X^1\Sigma^+$ and $0^+ + 1^1\Sigma^+$. Of the known excited states the $A^3\Pi_1$ state lies at lowest energy and like the ground $X^1\Sigma^+$ state correlates with ground state $I(^2P_{3/2}) + Cl(^2P_{3/2})$ atomic dissociation products.

In contrast with the B-X system in iodine the strong visible absorption in ICl corresponds to the A+X transition. This state in ICl is well suited to two-photon studies as its vibrational levels are well established and more extensive than the perturbed $B^3\Pi(0^+)$ state. The bands of the A-X system are readily identified since they each contain one P, Q and R branch. Extensive, accurate work was done on this system by Hulthén et al [61,62]. They analysed the $v_X'' = 0$ progressions of $I^{35}Cl$ ($v_A' = 3-35$) and $I^{37}Cl$ ($v_A' = 11-32$) and gave molecular constants for a few bands in the $v_X'' = 1$ and 2 progressions. The A-X system has been studied in emission by Clyne and Coxon [63] who analysed the chemiluminescent recombination of $Cl(^2P_{3/2})$ and $I(^2P_{3/2})$ atoms. Hulthén et al [62] identified the existence of anomalous "X-bands" lying close to dissociation in the A state. In $I^{35}Cl$ the vibrational levels broke off after $v' = 35$ and six levels labeled $X_1 - X_6$ were identified with vibrational and rotational constants that suggested a

homogeneous perturbation was present. King and McFadden [15] examined the dissociation limit region of the A state using two-photon techniques and confirmed the presence of these bands in $I^{35}\text{Cl}$ and identified four bands in $I^{37}\text{Cl}$ due to transitions to vibrational levels in the same region. They applied Le Roy's long-range potential equations to the levels in this region and established the dissociation limit of the A state ($D_e = 17557.514 \text{ cm}^{-1}$). They also found two different C_5 coefficients (the leading term in the $-C_n/R^n$ long-range potential for ICl covalent dissociation should have $n = 5$) for the two isotopes. This indicates a probable breakdown of the Born-Oppenheimer approximation caused by the homogeneous perturbation responsible for the occurrence of the X bands [62,15].

The A-X system of ICl has been recently extensively reexamined by Coxon et al in absorption [64] and emission [65]. They have obtained new molecular constants for the X and A states. This reanalysis was prompted by the fact that although Hulthén's measurements were made with great precision, the molecular constants were obtained by graphical techniques with no estimate of the error involved. In addition, the A $^3\Pi_1$ state has $\Omega = .1$ and will exhibit Ω -type doubling. That is a splitting of rotational levels into two components for each J value, caused by interaction between the rotation of the nuclei and \vec{L} the electronic orbital angular momentum. Hulthén examined the Ω -doubling

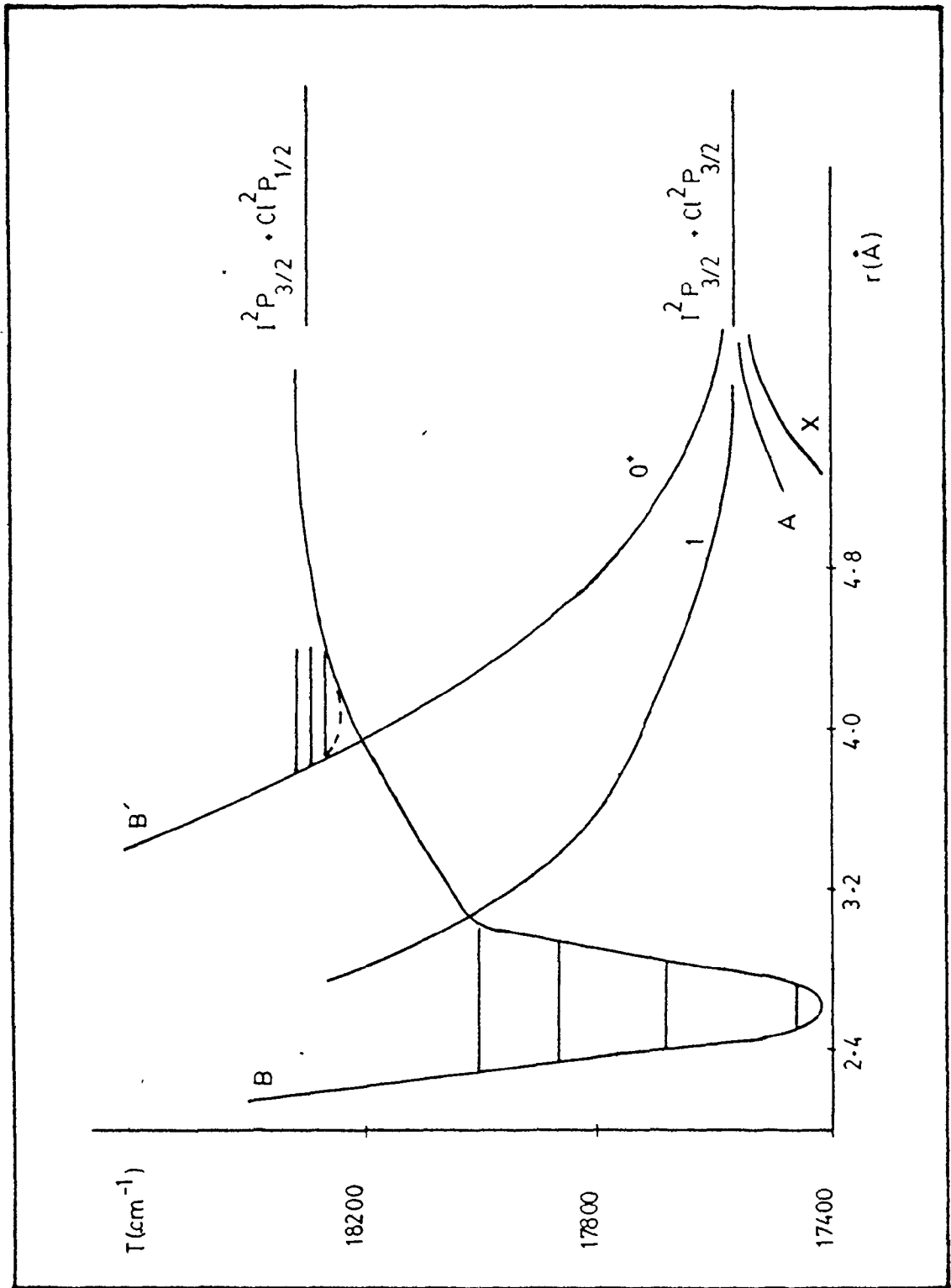
in the A state of $I^{35}Cl$ and showed that the difference $T^e(J) - T^f(J)$ increased linearly with $J(J + 1)$ for all vibrational levels up until $v_A' = 28$. Coxon et al [64] felt that a more complex pattern of Ω -doubling was actually present for the molecule and linear dependence only occurred up to $v' = 20$. In this two-photon work, the measurements of Hulthéns et al [62] were used to establish the term values for the A state pump lines used. In Sec. 1.2, Chap. VI, the impact of Coxon's studies on the values used will be discussed. The lifetimes and fluorescence quenching of some vibrational levels of the A $^3\Pi_1$ state have also been studied [66-68].

The B $^3\Pi(0^+)$ state correlates diabatically with $I(^2P_{3/2}) + Cl(^2P_{1/2})$, but crosses and interacts strongly with a repulsive 0^+ state which dissociates to ground state atoms. The few vibrational levels ($v \leq 3$) of the B $^3\Pi(0^+)$ state below the crossing point and the predissociation caused by the interaction of the 0^+ state, were first studied in detail in 1932 by Brown and Gibson [69]. The B state levels in IF, ICl and IBr were reexamined by Clyne and McDermid [70a] who calculated RKR turning points and Franck-Condon factors for the B-X system [70b]. Olson and Innes [71] examined single rotational level lifetimes from linewidth measurements in the B state. They were looking for information on the avoided crossing and homogeneous predissociation effects caused by the repulsive 0^+ state. They also suggested

a heterogenous perturbation might also be present. Clyne and McDermid [72] obtained further fluorescence decay lifetimes and quenching cross sections for levels in the B state. Recent work [73] has been completed on a more detailed study of predissociation of the B state in both $I^{35}\text{Cl}$ and $I^{37}\text{Cl}$. Profiles of lines in the vibrational bands of the $B^3\Pi(0^+)$ state and several fragmentary P and R branches associated with the adiabatic \tilde{B}' state were recorded. Figure II-8 shows the potential curves calculated [73]. These observations were analysed using the intermediate coupling model of Child [60]. The spectroscopic constants of the $B^3\Pi(0^+)$ state were published separately [74].

The higher lying excited states of ICl are not very well known, although they ~~should~~ exist as they do in I_2 [17]. Most of these states will be unstable (repulsive) because they dissociate into $\text{I}(5p^5, 2P) + \text{Cl}(3p^5, 2P)$ atoms. Others should be stable, giving a strongly excited atom on dissociation. States should exist due to combinations such as the excited atomic states of $\text{I}(p^5, 2P) + \text{Cl}(p^5, 2P)$ and the ionic states due to $\text{I}^+(p^4) + \text{Cl}^-(p^6, 1S)$ or $\text{I}^-(p^6, 1S) + \text{Cl}^+(p^4)$. Cordes and Sponer [17,75] have observed two states tentatively identified as components of a Π state. Haranath and Rao [76] identified another band in emission in the region 4400-3800 Å. Using two-photon methods, what appears to be the same excited state, was observed by Barnes et al [77] and analysed in both isotopes by King et al [16]. This

Figure II-8. Potential curves for the B $^3\Pi(0^+)$ state of ICl and other low-lying states of 0^+ or 1 [case (c)] symmetry (Figure 1 of reference 73)



state has been tentatively assigned to a $2332, 3^{-}(1^{-})$ state.

1.6 Spectroscopic Summary of IBr

The close generic relationship between IBr and ICl not unexpectedly leads to very similar absorption spectra. There are three distinct band systems in IBr first observed in detail in the visible and near infrared by Brown in 1932 [78]. The visible bands are due to the $B\ 3\Pi(0^{+}) - X\ 1\Sigma^{+}$ and $\tilde{B}'(0^{+}) - X\ 1\Sigma^{+}$ transitions. The $A\ 3\Pi_1 - X\ 1\Sigma^{+}$ transition now occurs in the near infrared (540-880 nm), since the energy splitting between the A and B states increases with molecular weight. In a series of papers Selin et al [79-81] studied these three transitions under high resolution and produced spectroscopic constants for the X, A, B and \tilde{B}' states for both $I^{79}\text{Br}$ and $I^{81}\text{Br}$. The A-X system has also been observed in emission [82] from chemiluminescence due to combination of ground state atoms.

The visible bands are of interest to two-photon studies and these correspond to the occurrence of an avoided crossing. Classically the $\tilde{B}'(0^{+})$ state is formed by the avoided crossing of the repulsive 0^{+} state with the higher vibrational levels ($v \geq 5$) of the $B\ 3\Pi(0^{+})$ state. Brown observed these bands [78] but the first detailed study of the vibrational levels in the two wells was undertaken by Selin in absorption [80,81]. Selin established the vibrational

numbering and positions of the $v = 2, 3$ and 4 levels of the $B^3\Pi(0^+)$ state below the interaction, in both isotopes. In ICl the $\tilde{B}'(0^+)$ well is relatively shallow and few transitions were observed, in IBr it is much deeper and Selin observed levels which he numbered $v' = 8-27$ (only 9 actual levels were observed between $v' = 8$ and $v' = 27$). The observed transition were fragmentary (i.e. of limited range in J) and irregularly distributed over the whole range of the 0^+ state.

The magnetic rotation spectrum of IBr was studied by Eberhardt et al [83,84]. Their initial work [83] assigned only the frequencies of the lines of maximum intensity in the $v' = 25$ and 26 levels of both isotopes. In the subsequent study [84] they covered the spectrum of the 0^+ well more extensively and listed term values for band fragments for $v' = 27-31$ in $I^{79}\text{Br}$ and $I^{81}\text{Br}$. They were also able to extend some of the fragmentary vibrational bands observed by Selin in absorption [81].

As outlined earlier, Child [60] has analysed IBr in terms of intermediate strength coupling. The absorption work of Selin [81] and the MRS spectra of Eberhardt [84] were used by Child in the construction of new potential for these two states. In Child's two states the vibrational numbering and spacings were different. A recent paper using laser excitation spectroscopy [90] has measured the line-widths of rotational transitions of several vibrational

bands in the $\tilde{B}'(0^+) - X^1\Sigma^+$ system of IBr. The observed change of linewidth as a function of the rotational quantum number J was attributed to predissociation of the \tilde{B}' state. Krockel et al [90] demonstrated that their observations agreed with Child's interpretation of intermediate coupling [60].

Laser-induced fluorescence has been used to determine the molecular constants of the X state with greater precision and measure intensities of the (20,1) band of the $\tilde{B}'-X$ system. Weinstock et al [85,86] excited the predissociated levels of the \tilde{B}' state of $I^{79}\text{Br}$ and $I^{81}\text{Br}$ using a single mode cw dye laser. The fluorescence spectra showed long progressions of bands in the ground state vibrational quantum number ($v_X'' = 0-19$). This yielded much improved X state spectroscopic constants [86]. Laser-induced fluorescence has also been used by Wright and Havey [87] to measure lifetimes of the $v' = 2, 3$ and 4 levels of the B state. Wright and Havey employed broad band excitation with 150 nsec pulses from a flash lamp pumped dye laser and could not assign the quantum state of the emitting IBr. More recent work [88] involving laser-induced fluorescence has been done on the $B^3\Pi(0^+)$ state using a narrow band pulsed laser (≈ 10 nsec pulses, 10^{-3} nm bandwidth). Clyne and Heaven [88] studied the 3-3, 2-2, 2-3, 4-3 and 4-4 bands in the $B-X$ system, and in the 2-2 and 3-3 bands made a series of measurements of the lifetimes of resolved rovibronic states in $I^{79}\text{Br}$ and $I^{81}\text{Br}$. The lifetimes of the

rotational lines in the $v' = 2$ and 3 levels show strong dependence on J , which can be interpreted as a natural predissociation. The dependence indicated the perturbation was heterogeneous [88].

Unlike ICl and I_2 there was no body of accurate unambiguous measurements of the intermediate \tilde{B}' state of IBr to draw upon. The ground state constants of Weinstock et al [86] were used but our own measurements of levels in the \tilde{B}' state were made to determine accurate pump frequencies.

As is the case for ICl, knowledge of higher lying electronic states in IBr is extremely limited. Early work by Cordes and Sponer [17,75] indicated the presence of a $^3\Pi$ state observed in emission between 1600 and 2000 Å. Haranath and Rao [89] have observed bands in emission in the region 3800-3900 Å. They have assigned the upper state of this emission to $2422 \ ^1\Sigma^+$ which seems unlikely.

2. Long-Range Potential Behaviour

2.1 Introduction

The form of the long-range portion of the interatomic potential of diatomic molecules and the distribution of the vibrational levels in this region received a great deal of attention in the early 1970's. This is illustrated in R.J. Le Roy's review article [91] and its extensive list of references. The developments made by Le Roy in this form of analysis have been successfully applied to the halogen

molecules, particularly the B $^3\Pi(0_u^+)$ state of iodine [13,14, 27,91].

Up until the work of Le Roy and Bernstein, the Birge-Sponer extrapolation procedure was one popular method of determining diatomic dissociation limits from experimental measurements of the vibrational spacings. This procedure involved plotting the experimental vibrational spacings $\Delta G_{v+1/2} = (G_{v+1} - G_v)$ versus the vibrational quantum number v . To obtain the dissociation limit, the Birge-Sponer plot of $\Delta G_{v+1/2}$ versus v generally must be extrapolated in some manner from the highest observed vibrational level to the dissociation limit. In terms of the Morse potential there exists a linear relationship between $\Delta G_{v+1/2}$ and v [100]. For more realistic potentials the Birge-Sponer plot in most cases shows positive curvature in the region just prior to dissociation, due to the dominating influence of the long-range portion of the interatomic potential [92]. The methods developed by Le Roy and Bernstein, and later just Le Roy, for studying the vibrational spacing near dissociation [91-95,98,99] take this into account.

2.2 Long-Range Internuclear Forces

For two atoms at large internuclear separation R , their interaction energy $V(R)$ can in general be expanded as:

$$V(R) = D - \sum_{m \geq \tilde{n}} C_m / R^m \quad \text{II-1}$$

where D is the dissociation limit, \bar{n} and m are integers and C_m is a constant from perturbation theory. The nature of the atoms to which a given molecular state dissociates determines which terms are prominent in this equation and what their signs are. If the leading terms in equation II-1, all have the same sign, the interaction potential in the long-range region may be approximated by:

$$V(R) \approx D - C_n/R^n \quad \text{II-2}$$

where n (in general non-integer) is some weighted average of the powers of the locally important terms. Asymptotically this n becomes equal to \bar{n} , the integer power of the leading term in equation II-1. Le Roy has given various rules for determining the limiting asymptotic power [91,92 Appendix B]. This representation of the potential is only valid at large internuclear separation and breaks down in molecular states that are perturbed by other states.

To develop expressions governing the distribution of vibrational levels near dissociation, Le Roy applied the first-order WKB approximation for the eigenvalues of the potential $V(R)$ [96,99]:

$$v + 1/2 = (2\mu)^{1/2}/\pi\hbar \int_{R_1(v)}^{R_2(v)} [G_v - V(R)]^{1/2} dR \quad \text{II-3}$$

Application of these methods and the use of the inverse power form of the long-range potential $V(R)$ (equation II-2),

yielded a differential expression for the vibrational levels:

$$dG_v/dv = K_n [D - G_v]^{(n+2)/2n} \quad \text{II-4}$$

where $K_n = \bar{K}_n/\mu^{1/2} (C_n)^{1/n}$ and \bar{K}_n is a numerical factor involving the gamma function summarized in Table 1 of reference 91.

The differential expression (II-4) demonstrates the possibility of positive curvature in the Birge-Sponer plot:

$$\begin{aligned} d^3G_v/dv^3 &= [(n+2)/n^2] K_n^3 [D - G_v]^{(3/n-1/2)} \\ &= d^2 \Delta G_v / dv^2 \\ &= 1/2 [d^2 (\Delta G_{v-1/2} + \Delta G_{v+1/2}) / dv^2] \end{aligned} \quad \text{II-5}$$

By inspection of the power $(3/n - 1/2)$ of the term $(D - G_v)$ it can be seen that for $n = 6$ this curvature is a constant; for $n > 6$ it increases with increasing v , becoming infinite at dissociation; for $n < 6$ it decreases to zero at D [92].

A more convenient integrated form of equation II-4 can be developed:

$$G_v = D - [(v_D - v) H_n]^{2n/(n-2)}, \quad n \neq 2 \quad \text{II-6}$$

where $H_n = [(n-2)/2n] K_n = \bar{H}_n / (\mu^{1/2} (C_n)^{1/n})$. \bar{H}_n is a numerical constant. For $n > 2$ the integration constants v_D can be interpreted as the effective (in general, non-integer) vibrational index at the dissociation limit.

The most general way of applying these results to experimental data involves the least-squares fitting of experimental energies to equation II-6 to obtain the four parameters D , n , C_n and v_D . If the levels are sufficiently near dissociation the resulting n will closely approximate the known asymptotic value \tilde{n} . However, methods that assume "a priori" knowledge of the asymptotic value \tilde{n} can be just as useful.

In practice one can approximate derivatives with energy differences:

$$\begin{aligned} dG_v/dv \approx \overline{\Delta G}_v &\equiv 1/2(\Delta G_{v+1/2} + \Delta G_{v-1/2}) \\ &= 1/2(G_{v+1} - G_{v-1}) \end{aligned} \quad \text{II-7}$$

Using this approximation, equation (II-4) can be rewritten as:

$$(\overline{\Delta G}_v)^{2n/(n+2)} = (D - G_v) (K_n)^{2n/(n+2)}$$

or

$$G_v = D - (\overline{\Delta G}_v / K_{\tilde{n}})^{2\tilde{n}/(\tilde{n}+2)} \quad \text{II-8}$$

Once the dissociation limit D has been determined either from a graphical or least-squares analysis of equation (II-8), the parameters C_n and v_D can be determined from a rearranged form of equation II-6:

$$(D - G_v)^{(\tilde{n}-2)/2\tilde{n}} = H_{\tilde{n}}(v_D - v) \quad \text{II-9}$$

Both expressions II-8 and II-9 should yield straight lines when applied to experimental data in the dissociation limit region.

Le Roy has also developed expressions for the dependence of the rotational constant B_v on the long-range internuclear potential [91,95]. In this case the electronic interaction potential $V(R)$ is replaced by a total effective potential:

$$V_J(R) = V(R) + (h^2/2\mu)J(J + 1)/R^2 \quad \text{II-10}$$

Once again using the WKB eigenvalue criterion, an integral expression for B_v can be developed analogous to equation II-3: [96,98,99]

$$B_v = \left(\frac{h}{4\pi\mu c} \right) \frac{\int_{R_1(v)}^{R_2(v)} R^{-2} [G_v - V(R)]^{-1/2} dR}{\int_{R_1(v)}^{R_2(v)} [G_v - V(R)]^{-1/2} dR} \quad \text{II-11}$$

This expression yields

$$B_v = (\bar{P}_n/\mu (C_n)^{2/n}) (D - G_v)^{2/n} \quad \text{II-12}$$

Combining this with the vibrational energy expression II-6 gives a more useful equation:

$$B_v = Q_n (v_D - v)^{4/(n-2)} \quad \text{II-13}$$

where $Q = \bar{Q}_n / (\mu^n (C_n)^2)^{1/(n-2)}$. The factors \bar{Q}_n and \bar{P}_n are again collections of numerical constants given in Table 1 of reference 91.

In his early work Le Roy pointed out [91,95] that the constant P_n was always a relatively poorer representation of the exact integral ratio in equation II-11, than K_n was of the integral appearing in the derivation of the vibrational levels. Any values of the parameter C_n calculated from relationship II-13 will tend to be too large. Most of the error is due to the effect of higher-power terms in the long-range potential that have not been taken into account.

2.3 Limitations and Further Developments

In the limit, as the vibrational energy approaches dissociation, the potential at the level's outer turning points becomes dominated by the leading term in equation II-1. This has led to the substitution of the limiting single-term approximation to the potential (equation II-2) into the appropriate first-order semiclassical expressions for various molecular properties to yield the simple analytic expressions that have been outlined above. The observed spacings of the highly-excited vibrational levels of the B state of iodine exhibit the predicted limiting behaviour of $n = \bar{n} = 5$ [13,14,27,91]. However analysis of

the RKR potential and the vibrational turning points has established values for the higher order terms ($m > \tilde{n}$) in equation II-1 [13,27,97] and in the case of the B state of iodine it has been shown that the R^{-6} term makes a substantial contribution to the potential. The equations involving the rotational constants of these levels, although expected to be less reliable than those involving the vibrational bands, exhibit larger deviations than expected for the limiting behaviour [91,13,14]. In view of this, Le Roy has reexamined the limiting behaviour of a diatomic molecule in more detail [98].

This examination shows that the vibrational energy spacings often obey the limiting near-dissociation equations even when the term C_n/R^n is responsible for only a fraction of the potential. It also confirms that, in the limiting approximation, the values of the integral which determines the vibrational level spacing (equation II-3) generalized

to $I_\ell(E) = \int_{R_1}^{R_2} dR/R^\ell [E - V(R)]^{1/2}$ [98,99] are exactly zero

when $m = n + 1$ in the expression $V(R) = D - \sum_{m \geq n} C_m/R^m$ [91,98].

Thus the equations involving the vibrational spacings will be unexpectedly accurate since they will be valid far into the region where the $R^{-(n+1)}$ term in the potential has become significant. On the other hand, the rotational

constants B_v have been found to be quite sensitive to the presence of additional contributions to the long-range potential.

This reexamination of the long-range behaviour [98] has led to a rederivation of the expressions describing the behaviour near dissociation, starting with a potential $V(R)$ that involves at least two terms in the approximation for the long-range potential i.e. $V(R) = D - C_n/R^n - C_m/R^m$. Two major conclusions can be drawn from Le Roy's reexamination. One is that the application of the limiting near-dissociation equations II-8 and II-9 to experimental data is still the most accurate method for determining diatomic molecule dissociation energies. This results from the fact that the experimental vibrational energies are often expected to obey the limiting near-dissociation equations even when the single term C_n/R^n is responsible for only a fraction of the total potential. The second conclusion is that observed B_v values can never be expected to quantitatively obey the simple limiting behaviour. In the future, for strongly bound species, the deviations from this limiting behaviour of the B_v values may be used as a more accurate method for obtaining experimental values of the higher-order coefficients C_m ($m > n$) than the method involving RKR turning points [98].

3. The Use of Isotopic Spectra and Mass Scaling in the analysis of Electronic States

3.1 Introduction

Within the Born-Oppenheimer approximation, the internuclear potential energy of any given electronic state is precisely the same for all isotopic forms of a diatomic molecule. For two isotopic molecules such as $I^{79}Br$ and $I^{81}Br$, not only are the forms of the potential curves the same, the relative positions of the potential curves of different electronic states, that is the electronic energies T_e (relative to the bottom of the ground state potential well), are the same for the two isotopic molecules. The mass difference affects only the vibrational and rotational energies of the molecules in each electronic state.

Although the intensity distribution of the vibrational bands may give an indication of which is the first vibrational level in a state, it may also simply be that bands to longer wavelength are too weak to observe. In the case of two-photon sequential absorption measurements, it is primarily the shape of the dye profile that dictates intensity trends over large numbers of vibrational bands. Thus it is generally not possible to determine more than a relative numbering for the vibrational bands observed for an individual molecule. However, when an isotope effect is observed, the absolute numbering can be determined since the isotopic substitution shifts the vibrational band positions in a

manner that is dependent on the absolute vibrational quantum number.

The fact that within the Born-Oppenheimer approximation the internuclear potentials are precisely the same, allows for the data from different isotopes to be treated concurrently in the analysis of long-range potential behaviour. There are distinct values of D_0 for each isotope since the dissociation limit D_0 is measured relative to the $v = 0$ level of the ground state. The values of D_e will be identical however, and the D_0 values are related to each other by the ground state zero-point energy. The values of v_D at the dissociation limit obey a relationship involving just the reduced masses of the isotopes [91]:

$$(v_D(i)+1/2)/(v_D(j)+1/2) = [\mu(i)/\mu(j)]^{1/2}$$

All of these similarities allow for combined isotope analysis. This will reduce the number of independent parameters that must be determined and allows for a larger independent data set than is often possible in any given region for one isotope alone. A combined isotope approach can also prove useful in situations where data for different isotopes happens to be available in mutually exclusive or only partially overlapping regions of the potential well.

3.2 Isotope Relationships in the Analysis of the Vibrational and Rotational Levels of an Excited State

In general, the rovibronic data from an excited electronic state is usually processed in such a manner as to yield energies $T(v', J')$ that are relative to the ground state $v_X'' = 0, J_X'' = 0$ level. These $T(v', J')$ values can be fit to the equation [19,101]:

$$T(v', J') = T_0(v', J'=0) + B(v')J'(J'+1) - D(v')J'^2(J'+1)^2 + \dots \quad \text{II-14}$$

The term values $T_0(v', J'=0)$ thus produced can themselves be fit to the expression:

$$T_0(v', J'=0) = T_e^* + G(v') \quad \text{II-15}$$

where

$$G(v') = \omega_e'(v'+1/2) - \omega_e x_e'(v'+1/2)^2 + \omega_e y_e'(v'+1/2)^3 + \dots \quad \text{II-16}$$

T_e^* is the electronic states energy relative to $v_X'' = 0, J_X'' = 0$.

The introduction of measurements on an isotopic molecule can be handled by first returning to the harmonic approximation where the classical vibrational frequency ν_{osc} is given by:

$$\nu_{osc} = (1/2\pi)(k/\mu)^{1/2} \quad \text{II-17}$$

where the force constant k , since it is determined by the electronic potential only, is exactly the same for different isotopic molecules. However the reduced mass μ does differ. If the heavier isotope is distinguished with a superscript i , then a ratio ρ ($\rho < 1$) can be calculated:

$$\nu_{\text{osc}}^i / \nu_{\text{osc}} = (\mu / \mu^i)^{1/2} = \rho \quad \text{II-18}$$

If anharmonicity is taken into account, to a good approximation a relationship similar to equation II-16 can be developed [19,101]:

$$G^i(v') = \rho \omega_e(v'+1/2) - \rho^2 \omega_e x_e(v'+1/2)^2 + \rho^3 \omega_e y_e(v'+1/2)^3 + \dots \quad \text{II-19}$$

and $T_0^i(v', J'=0) = T_e^{i*} + G^i(v')$. The vibrational constants are thus related by the following isotope relationships:

$$\begin{aligned} \omega_e^i &= \rho \omega_e \\ \omega_e x_e^i &= \rho^2 \omega_e x_e \quad \text{and} \\ \omega_e y_e^i &= \rho^3 \omega_e y_e \end{aligned} \quad \text{II-20}$$

The term values T_e^* and T_e^{i*} will differ by the zero-point energy difference in the ground state.

The vibrational dependence of the rotational constants of an electronic state can be expressed as [19]:

✱

$$B(v) = B_e - \alpha_e(v+1/2) + \dots \quad \text{II-21}$$

$$D(v) = D_e - \beta_e(v+1/2) + \dots \quad \text{II-22}$$

The rotational constants of a molecule also depend on the reduced mass; thus, the rotational constants of two isotopes can be related to each other. Since it is only the equilibrium internuclear distance which remains the same in the isotopes, the relationships must be developed in terms of the equilibrium rotational coefficients [19]. In general the rotational constants of the isotope can be related to those of the normal molecule by [33]:

$$B_v^i = \sum_{n=0} \rho^{n+2} B_n (v+1/2)^n,$$

$$D_v^i = \sum_{n=0} \rho^{n+4} D_n (v+1/2)^n \quad \text{II-23}$$

Since the ground state of a diatomic molecule is usually well known, a general expression for the observed isotope shift in the vibrational bands can be developed. It involves both the well known results for the ground state and the less well known excited state parameters. The general expression is:

$$\begin{aligned} \Delta v &= v - v^i \\ &= (1-\rho) [\omega_e' (v'+1/2) - \omega_e'' (v''+1/2)] \\ &\quad - (1-\rho^2) [\omega_e x_e' (v'+1/2)^2 + \omega_e x_e'' (v''+1/2)^2] \\ &\quad + (1-\rho^3) [\omega_e y_e' (v'+1/2)^3 - \omega_e y_e'' (v''+1/2)^3] \\ &\quad + \dots \end{aligned} \quad \text{II-24}$$

A more useful quadratic expression can be given for isotope shifts measured relative to $\nu_X'' = 0$:

$$\begin{aligned} \Delta\nu &= \nu - \nu^i \\ &= (1-\rho) [\omega_e' (v'+1/2) - 1/2\omega_e''] \\ &\quad - (1-\rho^2) [\omega_e x_e' (v'+1/2)^2 - 1/4\omega_e x_e''] \end{aligned} \quad \text{II-25}$$

A very similar linear isotope shift relationship can be constructed for the rotational constants $B(v)$:

$$\begin{aligned} \Delta B(v) &= B(v) - B(v)^i \\ &= B_e (1-\rho^2) - \alpha_e (1-\rho^3) (v+1/2) \end{aligned} \quad \text{II-26}$$

An elegant method to determine the coefficients and establish the vibrational numbering can be developed employing all the data concurrently by the use of mass-scaling. Stwalley [102,103] and Le Roy [91] have introduced a mass-reduced quantum number:

$$\eta = (1/\mu^{1/2}) (v+1/2) \quad \text{II-27}$$

If the reduced mass of the normal molecule is defined as $\mu = 1.0$, the ration ρ becomes:

$$\rho = 1/(\mu^i)^{1/2} \quad \text{II-28}$$

The mass-reduced quantum number η can then be expressed as:

$$\eta = \rho (v+1/2) \quad \text{II-29}$$

The expansion of the term energy II-15 and II-16, in a quadratic approximation becomes:

$$T(v', J'=0) = T_e + \omega_e(v+1/2) - \omega_e x_e (v+1/2)^2 \quad \text{II-30}$$

If the isotope relationships are required to hold rigorously:

$$\begin{aligned} T(v', J'=0) &= T_e + \omega_e [\rho(v+1/2)] - \omega_e x_e [\rho^2(v+1/2)^2] \\ &= T_e + \omega_e(\eta) - \omega_e x_e(\eta^2) \end{aligned} \quad \text{II-31}$$

or in general:

$$T(\eta) = \sum_{n=0} T_n(\eta^n) \quad \text{II-32}$$

In order to apply equation II-32 the vibrational terms must now be corrected to be relative to the ground state potential minimum rather than $v_X'' = 0, J_X'' = 0$ as before. This simply involves adding the ground state zero-point energy to each of the previously calculated $T(v', J')$ values. In this manner all the available data can be fit to a single equation that exactly satisfies the isotope relationships. A very distinct minimum in χ^2 space is obtained with the correct excited state vibrational numbering.

The rotational constants can be handled in a similar manner. A reduced-mass rotational constant can be defined:

$$B(\eta) = B(v)/\rho^2 \quad \text{II-33}$$

By applying the isotope relationship for B_e and α_e an expression in $(v+1/2)$ can be developed:

$$\begin{aligned}
 B(v) &= \rho^2 B_e - \alpha_e \rho^3 (v+1/2) \\
 B(\eta) &= B(v)/\rho^2 \\
 &= B_e - \alpha_e [\rho (v+1/2)] \\
 &= B_e - \alpha_e (\eta)
 \end{aligned}
 \tag{II-34}$$

or in general:

$$B(\eta) \equiv B(v)/\rho^2 = \sum_{n=0} B_n (\eta^n)
 \tag{II-35}$$

3.3 Mass-Scaled Long-Range Potential Expressions

As was outlined in the introduction to this section the internuclear potential energy, within the Born-Oppenheimer approximation, is identical for the isotopes of a molecule. Using the mass-reduced quantum number η and the ratio ρ , it is possible to recast Le Roy's long-range potential equations in mass-reduced form. To use this form, as was noted in the previous section for the term energies, the G_v values must be expressed relative to the bottom of the ground state potential well.

The three major equations (from Sec. 2, Chap. II) involved in this analysis are equations II-8, II-9, and II-13. In this analysis it would be most convenient to express the constants K_n and H_n in terms of their values for the normal molecule. The constant K_n for an isotope i , where \bar{K}_n is a numerical constant given in tables by Le Roy [91], can be expressed as:

$$\begin{aligned}
 K_n^i &= [2n/(n-2)] \bar{H}_n / [(\mu^i)^{1/2} (C_n)^{1/n}] \\
 &= (\mu/\mu^i)^{1/2} [2n/(n-2)] \bar{H}_n / [\mu^{1/2} (C_n)^{1/n}] \\
 &= \rho [2n/(n-2)] \bar{H}_n / [\mu^{1/2} (C_n)^{1/n}] \\
 &= \rho K_n
 \end{aligned}
 \tag{II-36}$$

where μ is the reduced mass of the original molecule in the same units as the constant \bar{K}_n . Thus for any isotope

$$G_v = D_e - (\bar{\Delta G}_v / \rho K_n)^{2n/(n-2)}
 \tag{II-37}$$

where D_e is the dissociation limit relative to the bottom of the ground state potential well and $\bar{\Delta G}_v = 1/2(G_{v+1} - G_{v-1})$ for each isotope separately.

The expression $(v_D - v)$ can be reexpressed in terms of n as $(v_D - v) = \mu^{1/2} (n_D - n)$. Using this the second expression can be written in terms of an isotope i as

$$(D_e - G_v)^{(n-2)/2n} = (\mu^i)^{1/2} H_n^i (n_D - n)
 \tag{II-38}$$

where $H_n^i = \bar{H}_n / [(\mu^i)^{1/2} (C_n)^{1/n}]$ and \bar{H}_n is a numerical constant given by Le Roy [91]. It can be seen that the values of H_n for the various isotopes are simply related through the reduced mass:

$$H_n^i / H_n = (\mu/\mu^i)^{1/2}$$

and thus:

$$(\mu^i)^{1/2} H_n^i = \mu^{1/2} H_n
 \tag{II-39}$$

As such, equation II-38 can be written in terms of the constant H_n for the original molecule, for any isotope as:

$$(D_e - G_V)^{(n-2)/2n} = \mu^{1/2} H_n (\eta_D - n) \quad \text{II-40}$$

or if the reduced mass of the original molecule is defined as equal to 1.0:

$$(D_e - G_V)^{(n-2)/2n} = H_n (\eta_D - n) \quad \text{II-41}$$

The equation involving the rotational constant can also be reexpressed in terms of an isotope i as:

$$(\mu^i)^{1/2} (\eta_D - n) = (B_V/Q_n^i)^{(n-2)/4} \quad \text{II-42}$$

where $Q_n^i = \bar{Q}_n (1/\mu^i)^{n/(n-2)} (1/C_n^2)^{1/(n-2)}$ and \bar{Q}_n is a numerical constant. Equation II-42 can be rearranged by factoring out the reduced mass μ^i to give:

$$(\eta_D - n) = (1/\mu^i)^{-(n-2)/4} (B_V/Q_n^i) \quad \text{II-43}$$

where $Q_n^i = \bar{Q}_n / (C_n^2)^{1/(n-2)}$. If the redefinition of the reduced mass of the original molecule being equal to 1.0 is used and the ratio $\rho = 1/(\mu^i)^{1/2}$ is applied, equation II-43 becomes:

$$(\eta_D - n) = (B_V/\rho^2 Q_n^i)^{(n-2)/4} \quad \text{II-44}$$

Thus, for any isotopic species of a molecule, the long range behaviour can be analysed using equation II-37, II-41 and II-44 where the constants H_n and K_n are normalized to their values for the original molecule.

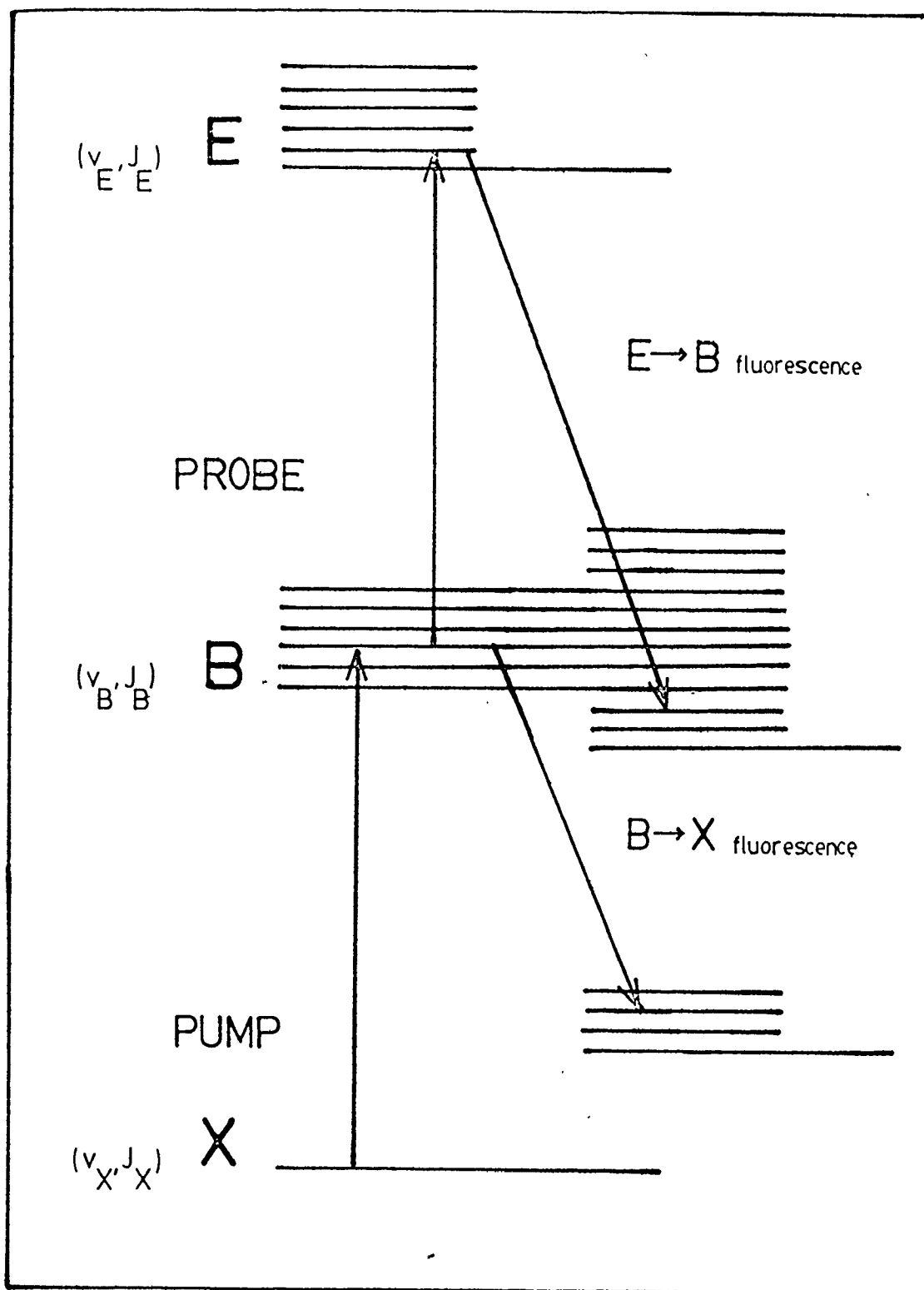
Chapter III

TWO-PHOTON SEQUENTIAL ABSORPTION SPECTROSCOPIC TECHNIQUES

1. Introduction

Two basic types of two-photon experiments were performed: one was intended to map out the detailed rotational and vibrational structure of an intermediate state; the other was designed to yield information on the rotational and vibrational levels of a high-lying excited state. Figure III-1 shows schematically how two-photon sequential absorption spectroscopy produced spectra of the various excited states of iodine (the same ideas apply to the interhalogens). A narrow bandwidth (0.07 cm^{-1}) pressure scan laser (or pump laser) was used to populate individual rotational levels in a vibrational band of the intermediate B state (ν_B, J_B). A broad bandwidth (1.5 cm^{-1}) mechanical scan laser (or probe laser) was then used to stimulate transitions from the intermediate level to other excited states, collectively referred to as E states (ν_E, J_E). The occurrence of an E+B+X transition could be monitored in two different ways. Either a decrease in the B+X fluorescence or the occurrence of E+B (or in general E+ some lower state) fluorescence could be detected. In all of these experiments it was the fluorescence out of the E state that was detected.

Figure III-1. The two-photon sequential absorption experiment as it applies to iodine. Similar considerations apply to the interhalogens



In the first type of experiment, where information on the intermediate state was required, the probe laser was fixed on the frequency of a known E+B transition and the pump laser was scanned over the discrete rotational, vibrational levels in the intermediate state. In the second type of experiment, where information on the excited E state was required, it was the pump laser that was fixed in frequency and was used to pump molecules up to one particular discrete level in the intermediate state. The probe laser was then scanned to induce transitions to the excited state.

2. Intermediate State Spectra

The intermediate state levels of any specific isotope of a molecule could be individually studied with little or no overlap from other isotopic species using these two-photon methods. It was possible to study diatomic species with isotopes in natural abundance (i.e. ICl with $^{35}\text{Cl}/^{37}\text{Cl} = 75.592\%/24.471\%$, and IBr with $^{79}\text{Br}/^{81}\text{Br} = 50.537\%/49.463\%$). This was accomplished by fixing the E state probe laser on an E+B transition corresponding to the specific isotope desired. Then as the pump laser was scanned the intermediate state spectrum of that isotope alone was obtained.

Figure III-2 illustrates the process for an intermediate state level low in the potential well. The probe laser is fixed such that the E+B fluorescence



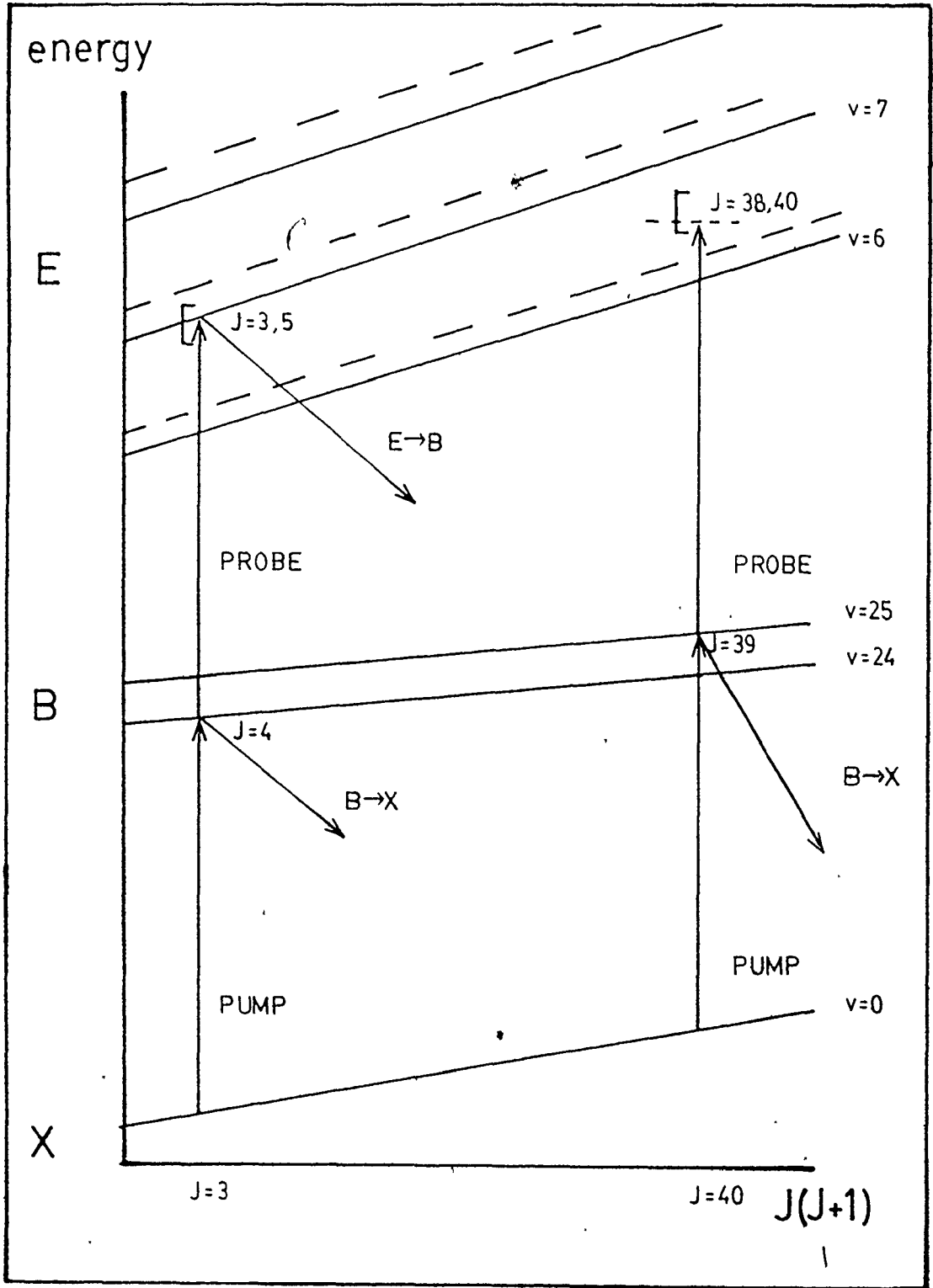


Figure III-2. Illustration of the selectivity of two-photon experiments. The dashed lines correspond to levels in the isotope.

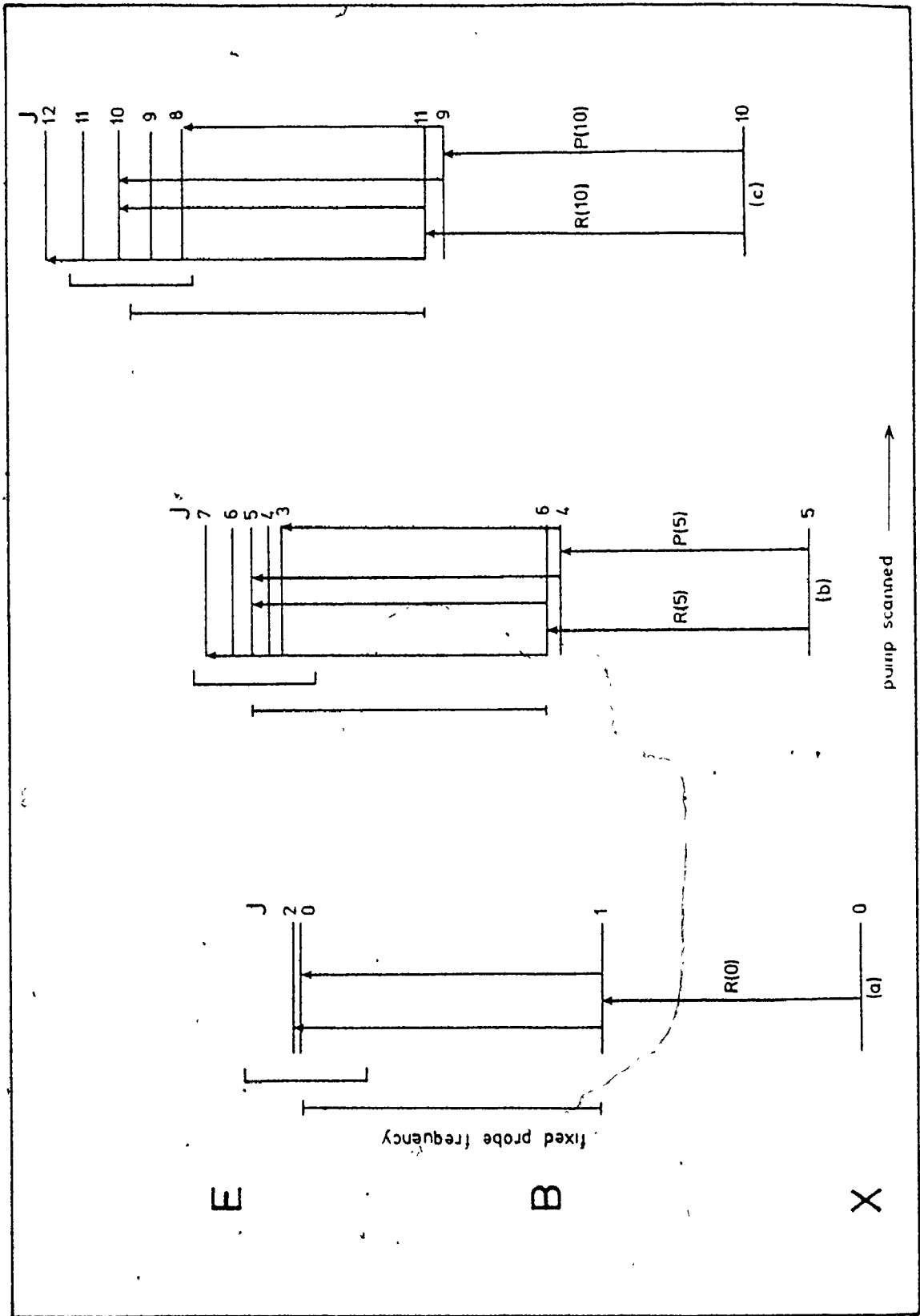




observed is due to the combination ($v_X = 0, J_X = 3$) \rightarrow ($v_B = 24, J_B = 4$) \rightarrow ($v_E = 7, J_E = 3,5$). Two rotational levels are excited in the E state because of the $\Delta J = \pm 1$ selection rule ($\Delta J = 0$ transitions were not observed in this work) and the fact that the probe laser has a wide bandwidth. The pump laser will also populate other underlying levels of higher J in higher vibrational states (eg $v_B = 25, J_B = 39$ in Figure III-2). These levels will produce B \rightarrow X fluorescence but, because of the different rotational constants in the two states and the $\Delta J = \pm 1$ selection rule, no E \rightarrow B fluorescence will be observed; the fixed frequency of the probe laser does not coincide with the necessary E state level. Under most circumstances, the probe laser will not coincide with any levels in the isotope to which allowed transitions could occur.

Figure III-3 illustrates how the spectrum will proceed as the pump laser is scanned towards lower wavenumbers (or higher J). Due to the differing rotational constants in the E and B states, eventually the separation of the rotational levels in the upper state, to which transitions are allowed, will exceed the bandwidth of the probe laser and the observed E \rightarrow B fluorescence will decrease. In Figure III-3 (c) the $\Delta J = \pm 1$, E \rightarrow B transition stimulated from the R(10) pump line has exceeded the probe laser bandwidth resulting in a decrease in the number of molecules excited to the E state and a corresponding decrease in the

Figure III-3. Successive stages in the two-photon process for a single v_B level as the pump laser is scanned and the probe laser is fixed. The rotational level separations are greatly exaggerated and are not drawn to scale



observed fluorescence due to the R(J) pump lines. The R(J) lines will eventually disappear. The intensity of the P J) lines will also follow this pattern.

This type of experiment worked best when the rotational constant in the E state was significantly larger than the rotational constant in the intermediate state. The lower in the E state well the probe level was, and thus the farther apart the vibrational levels, the better the intermediate state spectra were because of fewer chance overlaps.

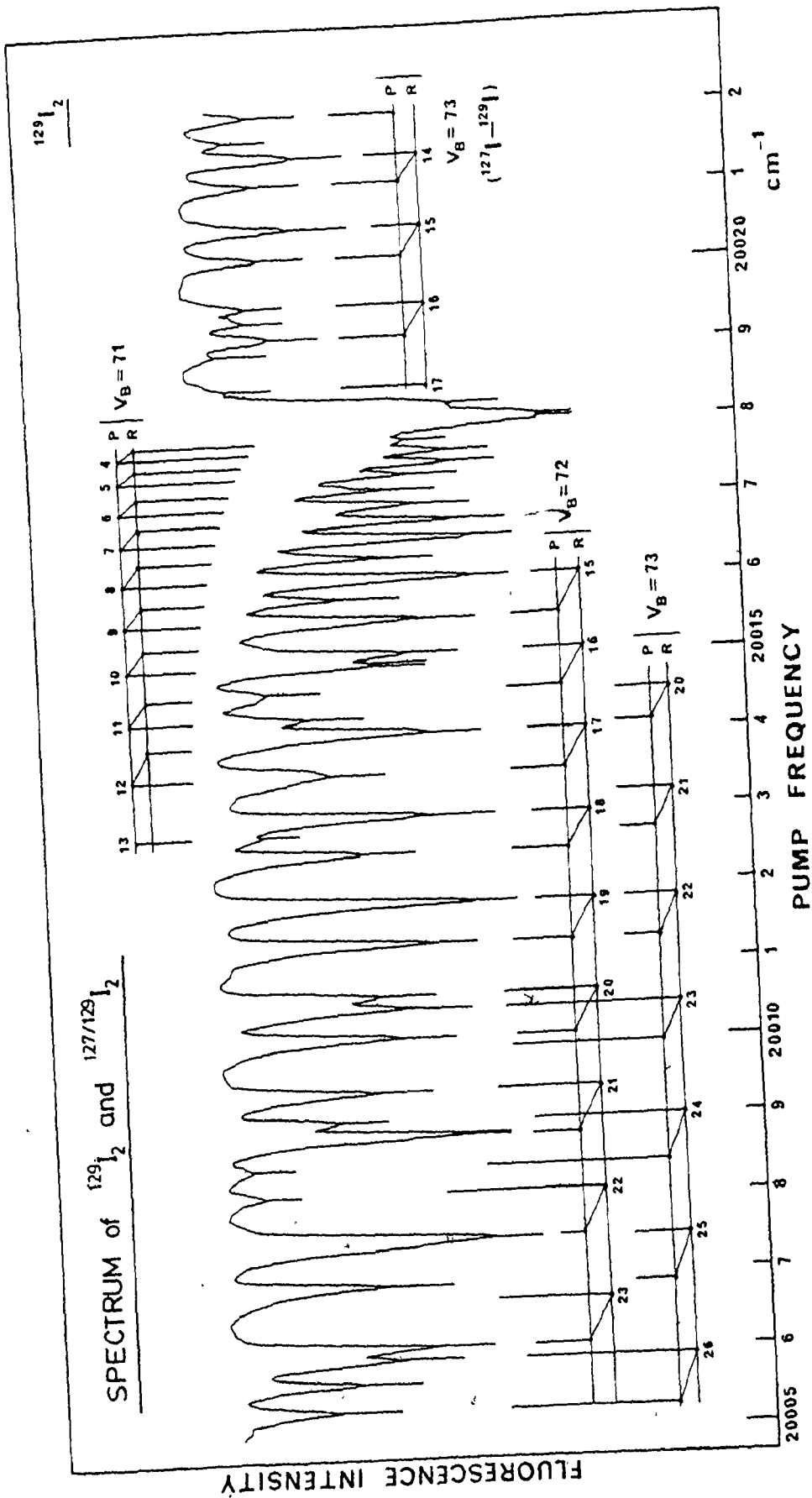
This same experiment can be used to study the discrete rotational structure of vibrational bands near the dissociation limit of the intermediate state. In this region the vibrational levels of this state are very dense, and at any one energy many differing J levels of different vibrational levels occur. The dissociation limit can be approached by successively scanning the pump laser to the highest observed transition before the differing rotational constants, the ΔJ selection rule and the probe laser bandwidth combine to result in the loss of overlap between the E and B states. The probe laser frequency is then decreased slightly and the scan is repeated. This process will gradually converge the pump laser on levels of high v and low J in the intermediate state. Because of the dense spectrum, a number of vibrational bands are observed at the same time. The range of J values observed for each level

is determined by the relative magnitudes of the rotational constants in the respective states and by the bandwidth of the probe laser. Figure III-4 illustrates a spectrum of $^{129}\text{I}_2$ near the dissociation limit. In this spectrum the probe frequency was maintained at 23361 cm^{-1} , such that the E+B excitation was to the $v_E = 21$ level with $T_0 = 43379 \text{ cm}^{-1}$ and $B = 0.019 \text{ cm}^{-1}$. Calculations of the frequencies of the E+B transitions induced by the probe laser bandwidth of 1.5 cm^{-1} predict that the B-X spectrum should contain groups of lines with maximum intensities at about $J_B = 5, 20$ and 25 for the bands with $v_B = 71, 72$ and 73 respectively.

3. High Lying Excited State Spectra

Once the intermediate state spectrum has been identified the narrow bandwidth pumps laser can be set to one of the rovibronic B-X transitions and the probe laser scanned across its entire dye profile. This will produce E+B spectra of the vibrational levels in the E state, corresponding to the selection rule $\Delta J = \pm 1$. This process was also isotopically selective, since when the pump laser was fixed on a level for one given isotopic species, the probe laser only induced E+B transitions corresponding to that one isotope. The probability that an overlap of isotopic levels occurs became higher if levels in the more dense region of the intermediate state near dissociation were used as pump lines.

Figure III-4. Rotational structure of the $v_B = 71, 72$ and 73 bands of $^{129}\text{I}_2$. Some lines of the $v_B = 73$ band of the mixed isotope $^{127/129}\text{I}_2$ also appear



Frequently, along with the main set of strong transitions, there occurred satellite sets of bands in the E state spectra. These transitions were due to "off-resonance" pumping. For example, in the dense B state spectrum of iodine, even with a narrow bandwidth laser (0.07 cm^{-1}), it was possible to encompass several rotational transitions within the laser's bandwidth. These underlying transitions, as the probe laser reached the appropriate frequency, can themselves stimulate E+B spectra. If the underlying rotational level was of a significantly different J from the pump line, the splitting resulting from the $\Delta J = \pm 1$ selection rule in the E state spectra would be sufficiently noticeable that the off-resonance pump line responsible could be readily picked out from sorted lists of transitions to the intermediate state. Otherwise it was necessary, if the satellite bands were to be used as data, to fix the probe laser on one of these transitions and run an intermediate state spectrum to identify the pump line. The probe laser was now at a different frequency and in resonance with a different portion of the E state than it was when the original pump line was identified.

4. Discussion

Line broadening effects were kept at a minimum during these experiments. Because the samples were gases at room temperature and low (~ 1 torr) pressures, collisional broadening was small. The use of counterpropagating laser beams reduces the Doppler broadening [104]. However, in the end, these efforts were not necessary. The linewidths of the observed transitions were entirely determined by the bandwidth (1.5 cm^{-1}) of the probe laser, which was a larger effect than any of these other broadening effects.

There are two limitations to this technique of measuring high-lying excited electronic states. The first is that the resolution is substantially less than that obtainable with conventional spectrographs. The overall precision of these measurements was limited by the bandwidth of the lasers. In the case of the intermediate state spectra, the resolution was quite high ($\sim 250,000$); however, in the E state spectra, with the broad bandwidth of the probe laser, the resolution was substantially less ($\sim 30,000$). This was a problem when trying to resolve the rotational lines in transitions involving low J. The separation between the P and R branch lines was less than the laser bandwidth. In some cases, discussed in later chapters, this was important, because possible $\Delta J = 0$ transitions (or Q branch lines), whose intensity in some transitions falls off rapidly with J, could become too weak to observe before the

splitting between P and R lines was sufficient for the system to resolve the three lines.

The other limitation was related to the quantity of data on the E state available through this technique. Conventional spectra, in general, can simultaneously show a large number of rotational lines associated with a significant number of vibrational levels in an excited state. This large body of data, often of the order of thousands of measurements, greatly over-determines any molecular constants calculated from it. With the current equipment, in this experiment, a typical E+B spectrum, for a given pump line, extends over about 600 cm^{-1} around the maximum of the probe laser gain profile. This spectrum usually contained 5 to 8 vibrational levels each consisting of a pair of rotational lines. Even with off-resonance lines a large number of runs generated relatively few rotational lines (over one hundred measurements was uncommon). The range of J observed was also limited to what various intermediate state pump lines could be identified and used.

Chapter IV

EXPERIMENTAL

1. Introduction

The two-photon laser spectrometer and the systems built around it have undergone a series of developments during the course of this work. This development began with the system originally described in reference 2 and culminated in the interfacing of a minicomputer with the system. The spectrometer consisted of a nitrogen laser simultaneously pumping two independent dye lasers. Both of the independently tunable dye lasers were based on the Hänsch design [107-109]. One dye laser was mechanically scanned, the other pressure scanned. These lasers were associated with the appropriate optical elements, calibration devices and the necessary electronic components to generate, detect, record and analyse the two-photon signals (Figure IV-1).

1.1 Principles of a Nitrogen-Pumped Dye Laser

A nitrogen laser provides a convenient pump laser for such a system. The 3371 Å output of the nitrogen laser is well matched to the $S_1 + S_0$ absorption of most organic dyes. A slowly rising pump pulse will transfer most of the molecules to the triplet state and deplete the ground state

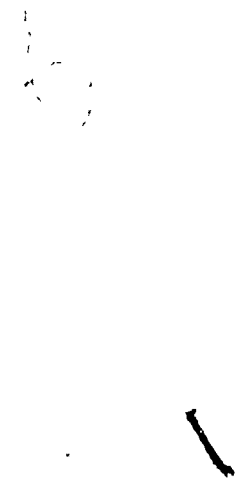
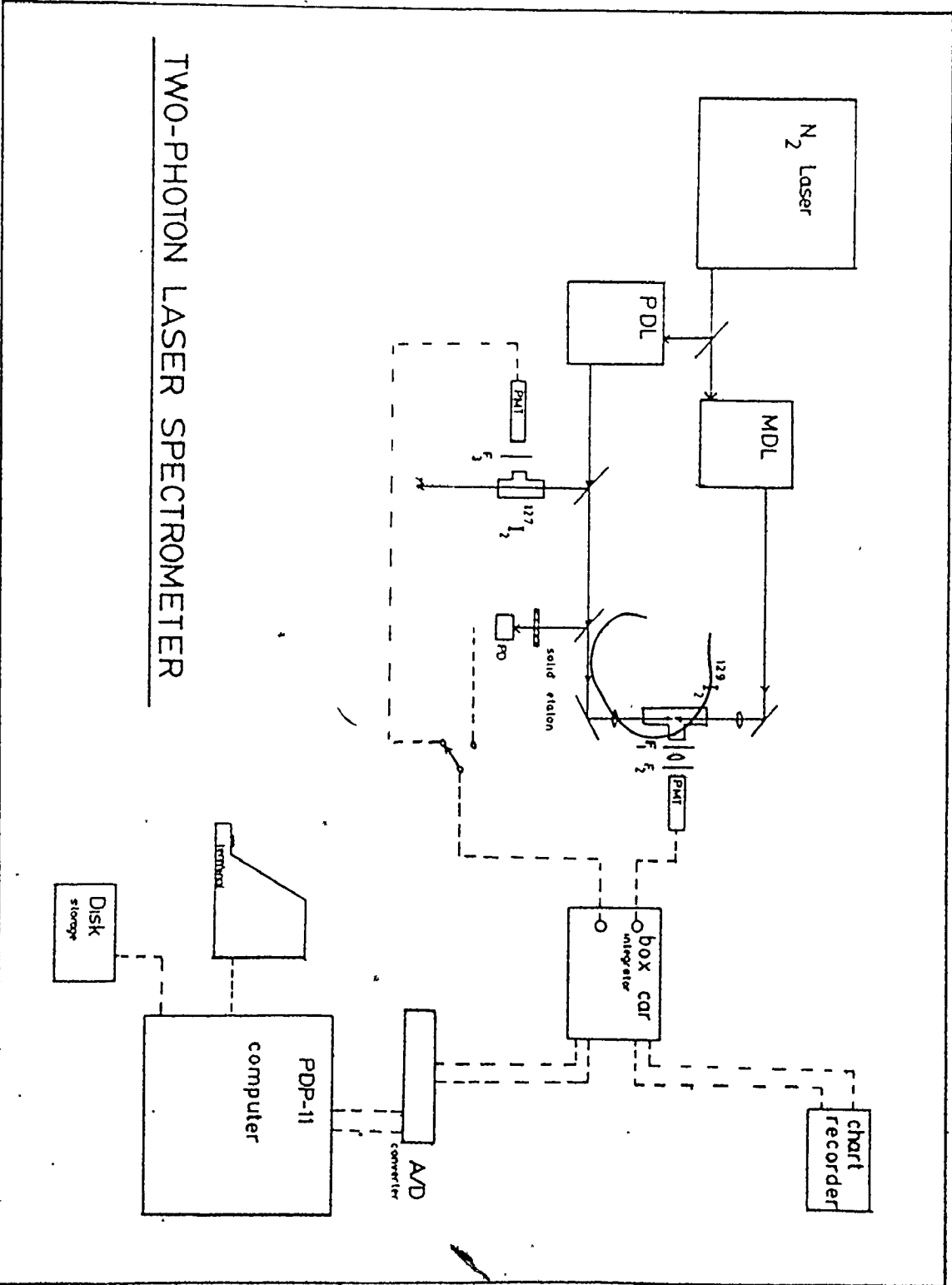


Figure IV-1. Schematic diagram of the two-photon laser spectrometer



TWO-PHOTON LASER SPECTROMETER

[105]. The fast rise time (< 2 nsec) of the nitrogen laser eliminates this problem of triplet state absorption. The nitrogen laser has a high pulse repetition rate at moderate output intensity. Dye laser output can be obtained over a large range of wavelengths from the near ultraviolet through the visible to the near infrared.

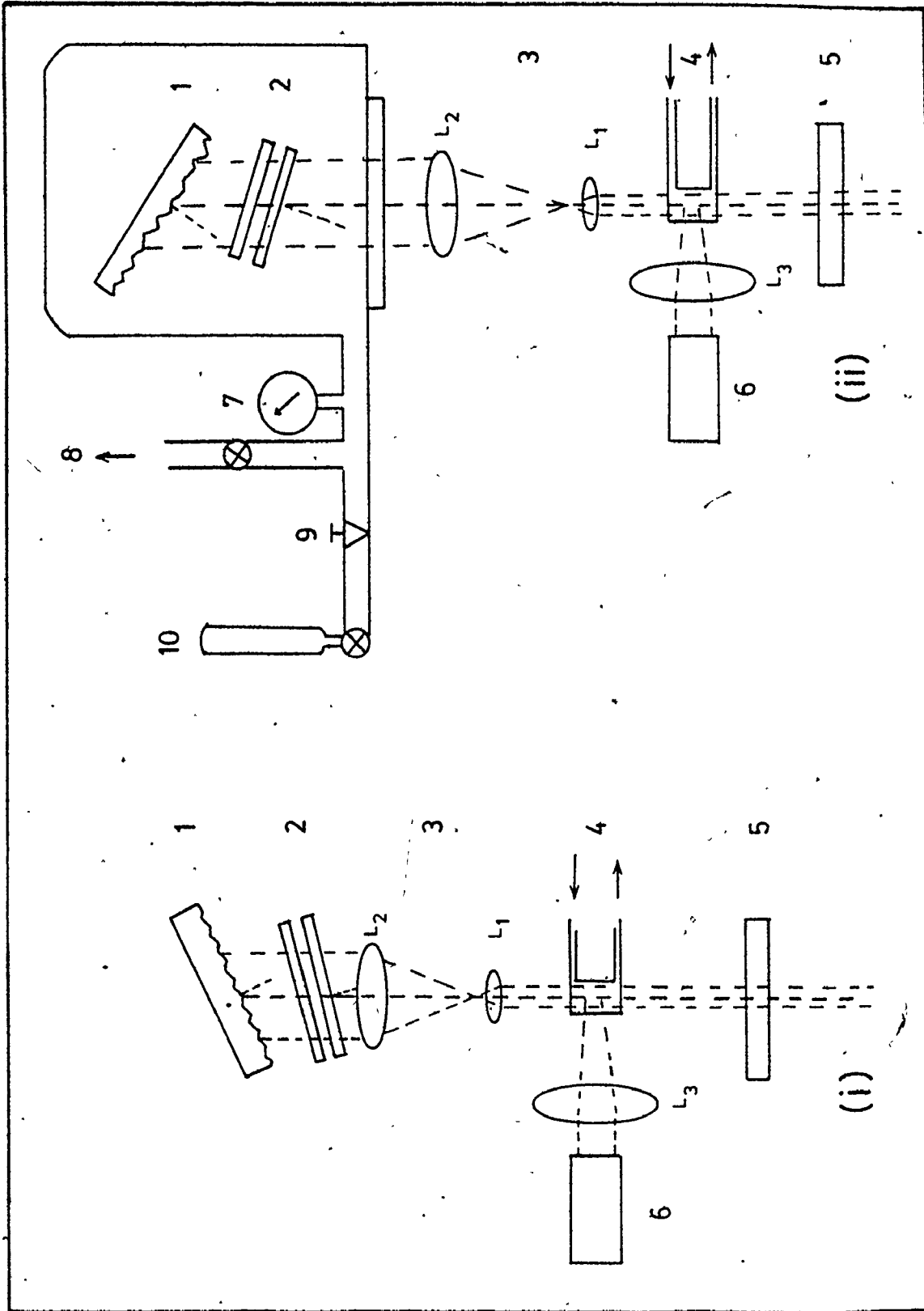
The Hänsch design [107-109] consists of a rapidly flowing dye solution transversely excited by the nitrogen laser focussed to a line in the dye cell. The dye cell is placed inside a cavity with a high dispersion grating in Littrow mount as a wavelength selective end reflector. The stimulated fluorescence from the dye cell is collected and collimated by an intercavity telescope in front of the grating. This insures that the beam is well collimated and illuminates a large enough area of the grating for good resolution. For narrower bandwidth operation an air-spaced, tilted Fabry-Perot etalon can be inserted in the cavity in front of the grating (Figure IV-2, i). With just a single dispersive element--the grating--the dye laser can be scanned using a stepping motor drive. With multielement operation, mechanical scanning becomes impractical. Not only is there an increase in the always present problem of vibration due to the stepping motors, but there is the further difficulty of synchronously tuning two dispersive elements, the grating and the etalon, in two independent, nonlinear manners. This problem is eliminated by the use

Figure IV-2. Hänsch design dye lasers:

- (i). Mechanical scan dye laser with internal etalon
- (ii). Pressure scan dye laser

Legend:

- 1) Grating
- 2) Fabry-Perot etalon
- 3) Telescope
- 4) Dye cell
- 5) Output reflector
- 6) Nitrogen pump laser
- 7) Pressure gauge
- 8) Vacuum pump
- 9) Fine needle valve
- 10) Propane cylinder



of pressure scanning techniques [108,110,111].

Both the grating and the etalon in a pressure scanned dye laser are mounted in a common pressure chamber (Figure IV-2, ii). As the index of refraction of a medium between the plates of the etalon, and in contact with the grating changes, the effective transmission wavelength λ ($\lambda = \lambda_0/n$) also changes. In terms of the vacuum wavelength λ_0 , and the index of refraction n , the equations describing a Fabry-Perot etalon and a diffraction grating, may be written

$$2t \cos \theta/m = \lambda_0/n$$
$$d(\sin \alpha + \sin \beta)/n = \lambda_0/n$$

where d and t are lengths, α , β and θ angles and m and n orders of interference. Both of these equations have the general form $\lambda_0 = nK_i$ ($i = 1,2$) where the K 's are independent of λ . When the two dispersive elements are positioned such that the same radiation is passed by both, the K 's become equal. Then the dispersive elements can be scanned synchronously if a medium of the same index of refraction surrounds them both. Since the refractive index of a gas depends on its density and thus on the gas pressure, to a good approximation the light dispersed by the two devices changes frequency linearly with pressure.

Pressure scanning produces a scan free from vibration, with excellent linearity. If care is taken with the vacuum system the laser can be maintained on a given frequency to within half the bandwidth of the laser for a period of 1 - 1 1/2 hours.

2. Lasers and Optical Systems

2.1 Nitrogen Laser

The nitrogen pump laser used was a National Research Group model NRG-0.6-8-300. At a 60 Hz repetition rate it operated at a peak power of 0.6 MW and an average power of 300 milliwatts. The pulse duration was 8 nsec FWHM. The basic design behind this laser is outlined in reference 106. The laser was triggered by a free running nitrogen pressurized spark gap. The nitrogen gas flowed through the spark gap, a filter, a regulating needle valve and into the laser tube. It was important to use a high purity nitrogen gas supply, otherwise a rapid build up of carbon deposits in the spark gap increased its breakdown pressure. Satisfactory operation was obtained using the boil-off gas from liquid nitrogen that was piped into the lab, instead of high purity tank nitrogen.

Repetition rates of the nitrogen laser could be varied between 5 Hz and 60 Hz. A 60 Hz repetition rate was used most frequently since this resulted in a good duty cycle for the boxcar-integrator and allowed the dye lasers

to be scanned more rapidly than would have been possible at slower repetition rates. These two advantages offset the overall loss in output power from the nitrogen laser as the output power decreased from 1.0 MW at a 5 Hz repetition rate to 0.6 Mw at 60 Hz.

2.2 Dye Lasers

The mechanical scan dye laser (MDL) was a modified Molelectron DL200 with the intercavity etalon and associated scanning mechanism removed. Using a 600 l/mm grating in 5th and 6th orders an output bandwidth of $1.2 - 1.5 \text{ cm}^{-1}$ was obtained throughout the scanning region. A stepping motor system was employed to scan the grating. The stepping motor ran at various fixed rates based on fractional multiples of the line frequency. A typical scan usually covered an entire dye profile, approximately 300 \AA , and took upwards of 40 minutes to complete.

The pressure scan dye laser (PDL) was operated as outlined in reference 2. With a 600 l/mm grating used in 4th order and a 2mm invar spacer in the intercavity etalon, the output bandwidth was measured with a Spectra Physics model 470 thermally stabilized confocal interferometer as 0.075 cm^{-1} . High purity propane gas ($n = 1.001023$ at 760 torr and 20°C) was used as the scanning gas. Propane was bled into the pressure chamber through a fine needle valve across a 40 psig pressure differential. As high a pressure

drop as possible was desired, because a supersonic flow through the orifice into the chamber would result in near linearity of gas mass transfer with time [111,112].

A scan of approximately 15 cm^{-1} was possible when the pressure was increased from 0 to 760 torr of propane. The results of computer measurement of etalon fringes generated by a solid quartz etalon showed good linearity[†]. With careful alignment it was possible to achieve a constant output power from the laser across the entire scan. Accurate pressure measurement was not necessary since the frequency of the laser output was always measured by various calibration methods, rather than being referred back to any absolute pressure.

In the experiments performed here, certain dye combinations were always used in each of the lasers. These combinations were those appropriate to the study of I_2 , ICl and IBr . The PDL was operated in the yellow and green region, as it was used to pump vibrational transitions from the ground state to an intermediate state such as the B-X absorption system of iodine. The MDL was operated in the blue region, as it was used as a broadband probe for transitions from the intermediate state to higher electronic states, collectively referred to as E states, in the 5eV region.

[†]Over a full 15 cm^{-1} scan, the equation used to describe the fit of the fringes deviated from linearity by less than 0.07%

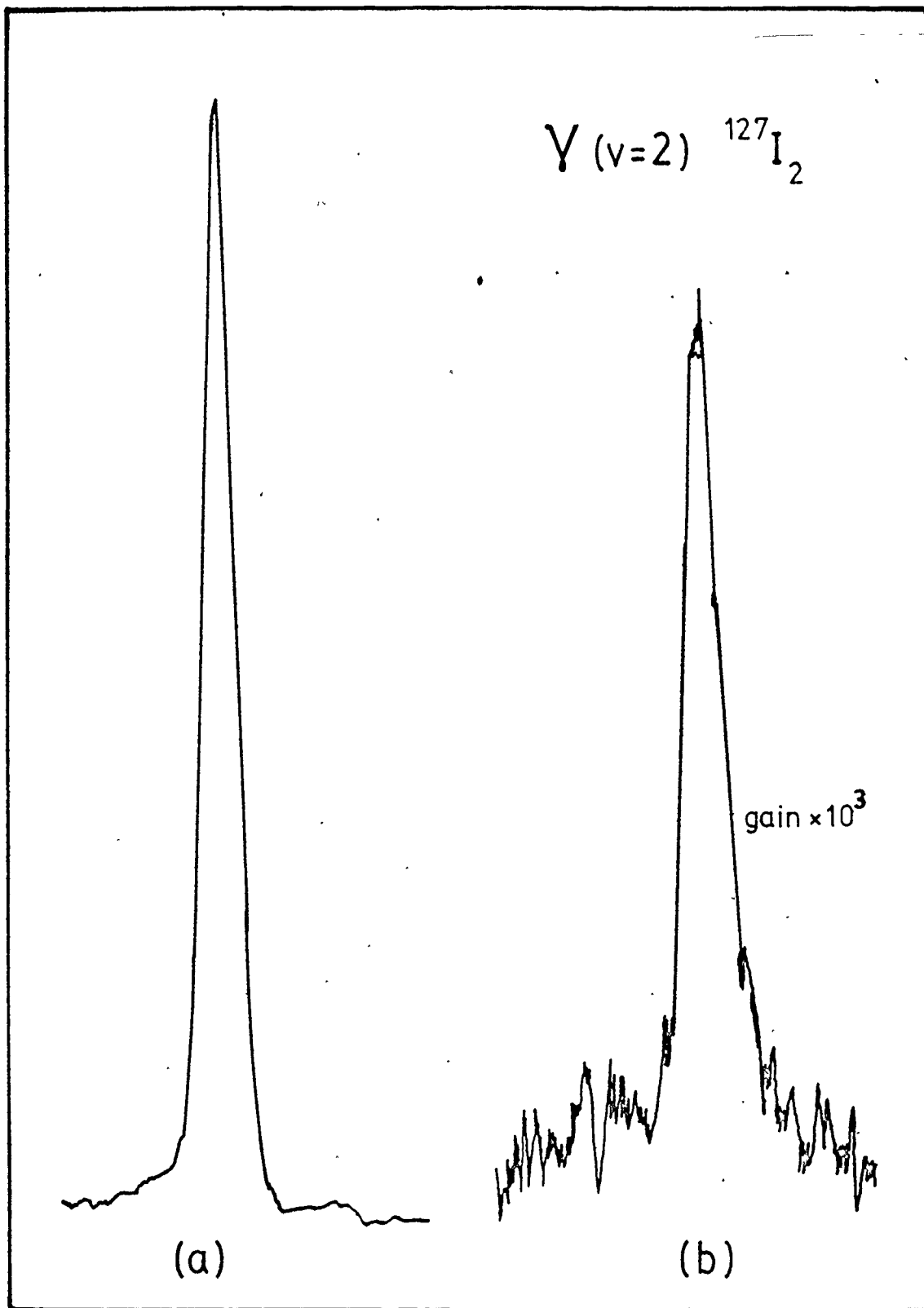
2.3 Optical Table

All the lasers and optical systems were mounted on an NRC isolation table. An overall diagram of the equipment is shown in Figure IV-1. The output beams from the two dye lasers were directed around the edge of the table top until finally they were counterpropagated through the sample cell. The optical paths were matched so that the laser pulses arrived coincident in time at the center of the cell. The two beams were each focussed to the same 750 μ diameter spot in the cell center. The focussing of the beams in the sample cell greatly improved the signal-to-noise ratio. However, it was theoretically possible that the high light intensity in each focussed beam could itself cause non-linear multiphoton events. This possibility was eliminated by the fact that no fluorescence signal was observed when each beam was successively blocked. Spectra could generally be obtained, with significantly higher background, when the lasers were either singly focussed, partially focussed or not focussed at all (Figure IV-3). These observations indicated that only single photon excitation was produced by each beam.

A number of other components could be inserted in the optical paths on the table when required. The basic two-photon spectrometer required various calibration devices. The insertion of beam splitters allowed for the inclusion of a solid quartz etalon or an iodine reference cell in

Figure IV-3. The γ_2 band of $^{127}\text{I}_2$, using P₇₈(13) as the B-X pump line

- (a). Both pump and probe laser beams focussed into the absorption cell
- (b). No focussing lens in either beam



the optical path of the PDL (Figure IV-1). The MDL was calibrated using a Spex monochromator located off the main optical table.

To study decay effects in the intermediate state, the probe beam, which stimulated transitions to the upper E states, could be delayed relative to the intermediate state pump beam. The optical delay consisted of the mirror system from a 1.86m White cell [114]. This allowed for the delay of one laser pulse relative to the other in multiples of approximately 25 nsec., up to a maximum of 100 nsec. The delay intervals were calibrated by placing a corner cube reflector in the cell position and focussing the two counter-propagating beams onto a high speed photodiode detector [113]. The time differences between the two pulses were measured on an oscilloscope. Delays beyond 100 nsec were impractical. This resulted from the difficulty in maintaining the critical alignment needed for beam overlap. It was also found to be difficult to compensate, using neutral density filters, for the intensity lost in the delayed beam due to the large number of mirror reflections involved.

The two-photon sequential absorption was monitored by detecting the broadband fluorescence out of the E state with a thermoelectrically cooled EMI9816QB photomultiplier. This fluorescence was monitored at right angles to the beams through an optical filter and lens assembly. The pump and

probe beams were carefully screened and baffled before entering the sample cell. The sample cell itself was designed with baffles and a Wood's horn to reduce stray light. Despite these precautions there was sufficient residual scattered light to lower the S/N ratio of the broadband fluorescence to the point where weak signals became lost in the background without the use of filters. These filters were chosen to transmit as much fluorescence as possible while excluding scattered laser light and unwanted fluorescence from the intermediate to the ground state. A number of filter combinations were employed consisting of either a Corning 7-60 or 7-54 filter combined with a Schott BG12. These filters and their characteristics are listed in Table IV-1.

Table IV-1. Filter characteristics

Filters	Transmission region (Å)	Maximum transmission
7-60/BG12	3960-3275	35% T @ 3700 Å
7-54/BG12	4200-3200	45% T @ 3700 Å

All but a few spectra were obtained using the 7-60/BG12 filter combination.

Reference signals from the B→X fluorescence of iodine were produced in the reference cell and monitored with a RCA 1P21 photomultiplier. A series of Corning sharp cut-off yellow and red filters were used to filter out scattered laser light in the cell from the photomultiplier.

Etalon transmission peaks produced by passing the PDL beam through a solid quartz etalon were detected using a Molectron model 141 photodiode, preamplifier combination.

3. Data Processing Electronics

The two signals, one from the sample cell and one from the reference system, were processed through a Molectron Laser Spectroscopy Detector system. This consisted of two amplifier/shapers, a dual gate generator, and two differential gated integrators all making up a two channel boxcar integrator. The amplifier/shaper was a low noise, high gain bandpass amplifier, which also shaped the pulses. Noise sources outside the amplifier and in the first amplifier stage had bandwidths which were large compared to the useful components of the signal. Pulse shaping improved the signal-to-noise ratio by limiting the bandwidth and reducing the unwanted noise contribution. The differential gated integrator was an RC integrator that was only active during an externally supplied gate window. A pair of gates, separated in time, were supplied by the dual gate generator. The initial time delay of the gates, their width and their

separation in time were all variable. The first gate sampled the signal pulse, the second the interpulse baseline.

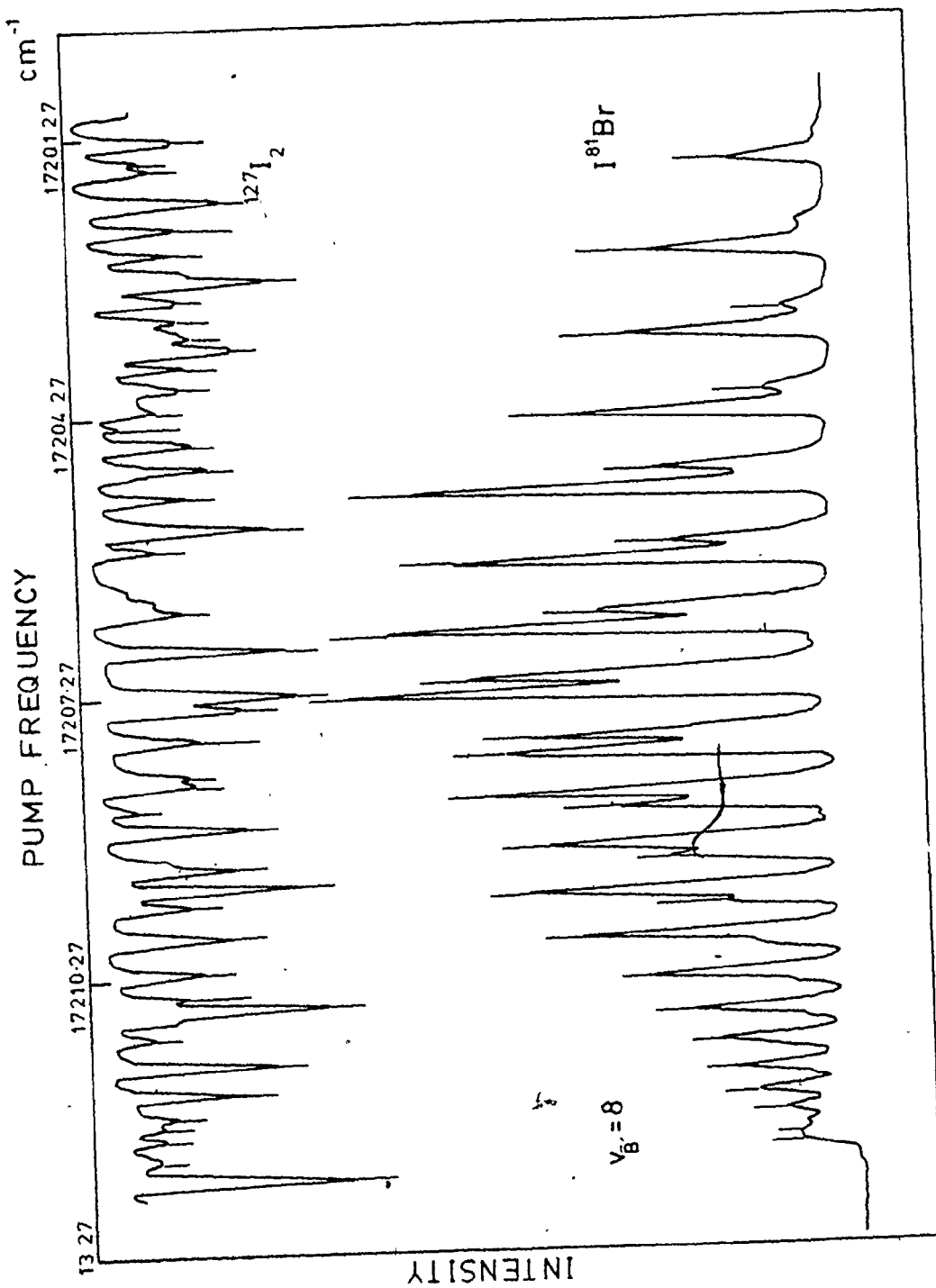
The two signals after pulse amplification, shaping and integration were sent simultaneously to a chart recorder and to the analog-to-digital converter of an on-line mini-computer. A buffer amplifier, consisting of an operational amplifier, isolated the computer system from possible feedback from the chart recorder. The boxcar's output of 0 to 10V had to be matched to the computer's input of -5 to +5V. A level shifter consisting of an operational amplifier biased with a Zener diode was inserted to match the baseline of the signal to the computer input.

The minicomputer was a Digital Equipment Corp. MINC 11 system. This consisted of a PDP-11 microcomputer, a RX02 twin floppy disk drive, a VT105 video graphics terminal, and a set of laboratory interface modules. The set of modules used consisted of a real-time clock, a 12 bit analog-to-digital converter (A/D), and a 12 bit digital-to-analog (D/A) converter. The 12 bit A/D converter gave a resolution of 1 part in 4096, or in terms of the input voltage range of $\pm 5.12V$, a resolution of 2.5 mV. The software supported the high level languages Basic and RT-11 Fortran as well as the assembler language Macro. Software routines were available in Basic and Fortran for controlling the lab modules. Graphics routines in Macro have been developed for the VT105 terminal to supplement the graphics

supplied. A large body of programming was developed for data acquisition and manipulation. This included routines to store, smooth, average and display spectral data, as well as routines to output various signals to analog devices. Programs were also written to identify peaks, calculate line frequencies and analyse the resulting numerical results.

In the recording and digitization of spectra the output signals from the boxcar were sampled at a rate of between 2 and 4 samples per second, depending on the length of the scan. With no further processing, the digital representations of the two signals were simultaneously displayed on the computer terminal and stored in an unformatted data file on disk. The data was stored with a maximum of 10,000 data points per channel per scan. In the case of the short 15 cm^{-1} scans of the PDL this resulted in a highly defined spectrum with a large number of data points over a given peak. In the case of the longer and much less spectrally dense MDL scans fewer points over a peak were stored. A minimum of 20 points over a peak was always maintained. A typical example of a computer stored spectrum of I^{81}Br is included in Figure IV-4 along with the $^{127}\text{I}_2$ calibration spectrum. This trace has had the peak maxima identified and the I^{81}Br spectrum calibrated. It was then reconverted to analog form using the D/A converter of the computer and the chart recorder.

Figure IV-4. A computer-generated spectrum of the $v = 8$ band origin of $I^{81}Br$. The single-photon $^{127}I_2$ calibration spectrum is illustrated and all the peaks in the spectrum have been flagged by the peakfinding routine



Peak maxima in a data file were determined and flagged using a modified version of the Stavitsky Peakfinder routine [115]. In this program it was found unnecessary to use the cubic least squares interpolation subroutine to establish peak positions. Peak maxima determinations were visually checked by displaying the results of the peakfinding routine on the terminal. Peak positions in a data file could also be determined manually directly on the terminal using a cursor program. Line frequencies were calculated from quadratic fits to the calibration spectra.

The use of the computer speeded up the handling of spectral information. In less than 15 minutes the peak positions on a spectrum could be accurately measured, the calibration line frequencies fit to a quadratic, and calculated line frequencies of the sample spectrum printed out. The accuracy of frequency calibration using the computer was greater than that available using hand measurements.

A series of measurements of the fluorescence lifetimes of various excited states were made. The broadband fluorescence from the excited state was detected by the EMI photomultiplier. The normal high speed dynode chain associated with this tube was replaced by a dynode chain operating at a higher current and containing large capacitors across the last few stages to maintain a constant voltage drop across the dynode when large input signals were received.

The photomultiplier output was monitored on a Phillips sampling oscilloscope which consisted of a PM3410 mainframe, a PM3419A sampling dual trace amplifier with 350 picosecond risetime and 50 ohm input impedance and a PM3419B sampling time base. The sampling scope was stepped across the displayed fluorescence decay under computer control. At each discrete point on the decay curve the y-output from the dual trace amplifier was digitized by the computer and averaged over a predetermined time period. Where applicable, a standard least squares fit to an exponential was used to analyse the decay curves, but when lifetimes that approached the width of the laser pulse (~ 10 nsec) were measured, a deconvolution program was used. Deconvolution involving the division of the Fourier transform of the signal by the transform of the laser pulse was quite unsatisfactory due to the need for division by values very close to zero. Instead, a series of assumed exponential decays were convolved with the measured laser pulse, and the results compared to the signal until a minimum χ^2 was obtained [116]. A more detailed explanation of this procedure is contained in Sec. 3.2, Chap. V.

4. Reagents and Laser Dyes

A number of different organic dyes were used to cover the spectral regions of interest. Table IV-2 lists the various dyes, their solvents, concentrations and the

Table IV-2, Laser dyes used in the experiments

Dye	Company	Region (Å)	Solvent	Conc. (M)
Rhodamine-6G	Eastman, New England Nuclear	5950-5750	ethanol (95%)	8×10^{-3}
Coumarin-540A(495)	Exiton	5830-5150	ethanol (95%)	1×10^{-2}
Fluorescein (disodium salt)	Eastman	5460-5300	ethanol (95%)	8×10^{-3}
Coumarin-481F	Exiton	5450-5000 5200-4850	ethanol (95%) { 78% v/v p-dioxane (dry) { 22% v/v ethanol (dry)	1.5×10^{-2} 1×10^{-2}
Coumarin-102	Eastman	5010-4680	p-dioxane (dry)	2×10^{-2}
7-diethylamino-4-methylcoumarin (7-DAM)	Eastman	4900-4700	ethanol (95%)	1×10^{-2}
Coumarin-120	Eastman	4700-4400	ethanol (95%)	1×10^{-2}
p-bis(o-methylstyryl) benzene (Bis-MSB)	Eastman	4500-4250	ethanol (95%)	8×10^{-3}
	Eastman	4300-4100	p-dioxane (dry)	1.2×10^{-3}

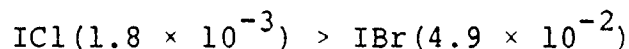
spectral regions where they were used. Usually the dyes were dissolved in 95% ethanol. The lasing maximum of coumarin-481F could be readily shifted by dissolving it in various mixed solvents containing dry p-dioxane and dry ethanol [117].

Reagent grade, resublimed, $^{127}\text{I}_2$ (Shawinigan Chemicals) was distilled under vacuum into the sample cell with no further purification. Halocarbon 25-5S grease (Halocarbon Products Corp.) was used with all the compounds in stopcocks and ground glass joints of the apparatus. The $^{129}\text{I}_2$ was obtained from Oak Ridge National Laboratories as NaI in NaHSO_3 solution. It had a nominal isotopic purity of > 75%. The solution was oxidized by addition of a solution containing 0.1M NaNO_2 in 1M HNO_3 . The liberated $^{129}\text{I}_2$ was extracted with ether, which was then cooled and filtered through glass wool to remove ice crystals. The iodine was separated from the ether by low temperature trap-to-trap distillation, and finally dried by condensing it onto P_2O_5 supported on glass wool. The $^{129}\text{I}_2$ was sublimed into a glass sample cell which was permanently sealed off[†]. $^{129}\text{I}_2$ is a weak β emitter with a half life of 7×10^7 years and particle energy of 0.189 MeV. The sample from Oak Ridge was listed at < 1 mCi radiation. The isotope was prepared in a fume hood using gloves and tongs. No other special

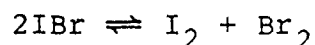
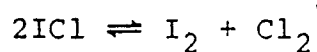
[†]Preparation of $^{129}\text{I}_2$ was done by Ms. N.T. Littlewood

precautions beyond standard laboratory procedures for handling potentially dangerous materials were necessary. Once sealed in the glass sample cell no radiation could be detected as it could not penetrate greater than 1/10 mm of glass.

Iodine monochloride and iodine monobromide can both be synthesized from the direct combination of the constituent elements. These interhalogens have varying degrees of stability with respect to disproportionation. In order of stability with the disproportionation constants for the gaseous compounds and the elements in their standard states at 25 °C [118] in brackets, the compounds are:



where disproportionation corresponds to:



Iodine monochloride (Eastman Kodak, I/Cl ratio 1.10 ± 0.1) was distilled under vacuum through two traps containing P₂O₅ and then into the sample cell. ICl is very reactive, especially with water (10ICl + 5H₂O → I₂O₅ + 10HCl + 4I₂) and must be kept dry. Not only did the original sample itself contain an excess of iodine but dissociation rapidly occurred during any handling of the material. Since I₂ is soluble in solid ICl while Cl₂ is not, the

vapor above ICl is Cl_2 rich and any handling which involved pumping on or distilling the sample preferentially removed Cl_2 [119,122]. Pure samples of ICl could not be obtained and I_2 was always a major contaminant. After the transfer through the traps containing P_2O_5 into the sample cell, the presence of a majority of solid ICl, as opposed to solid I_2 in the cell was confirmed by melting the sample at temperatures slightly above room temperature to a reddish-brown liquid (ICl mp = 27.38°C , I_2 mp = 113.5°C). The sample in the side arm of the cell was maintained at 0°C during the experiments. This yielded a partial pressure of ICl of 3.88 torr [120] while reducing the vapor pressure of any $\text{I}_2(\text{s})$ present to 0.031 torr. An excess of sample was maintained in the cell.

Iodine monobromide also exists as a solid at room temperature (mp = 42°C , sublimes at 50°C) but it is extensively dissociated in the vapor phase where it exists in equilibrium with I_2 and Br_2 . Using an assumed vapor pressure of IBr at 25°C of 7.6 torr the degree of dissociation of gaseous IBr into gaseous I_2 and Br_2 is approximately 8-9% [121]. It is thus difficult to purify. Little information is known about its partial pressures at various temperatures. Iodine monobromide (BDH, 97% IBr excluding I_2) was transferred into a cooled sample container on the gas rack which was then frozen in liquid N_2 and pumped down. The sample was then allowed to come to room temperature

under vacuum. It was cooled to ice temperature and the reddish-brown Br_2 vapor was pumped off. The remaining dark grey crystals were distilled under vacuum directly into the side arm of the cell which was kept at liquid N_2 temperatures. The side arm was then allowed to warm to 0°C and any excess Br_2 was again pumped off. As with ICl the side arm of the sample cell was maintained at 0°C during all experiments.

Both the ICl and the IBr samples were frequently changed to prevent contamination. The sample cells were stored at -20°C when not in use.

To study the effects of the addition of an inert buffer gas to iodine, various amounts of argon and helium were added to the cell. Before any measurements were made, the sample cell was placed on the gas rack and the I_2 was frozen to liquid N_2 temperatures. The cell was then pumped on for approximately 1/2 hour. The I_2 was then allowed to warm to room temperature with the pump shut off. Once again the sample was frozen and the procedure repeated. The cell was then used to measure the spectrum without an inert gas. Following this the cell was rapidly frozen to liquid N_2 temperatures and put on the gas rack. An inert gas was bled into the system up to the desired pressure, the cell was removed from the rack and the spectrum was run again as rapidly as possible to prevent any major change in the laser systems. Accurate inert gas pressures were measured using a capacitance manometer on the gas rack

(DATAMETRICS Barocel Electronic Manometer).

5. Procedures

5.1 Calibration of the PDL

The absolute frequency of the narrow bandwidth pressure scan dye laser was obtained through direct calibration against the single photon spectrum of $^{127}\text{I}_2$ in the reference cell. The precise line frequencies of Gerstenkorn and Luc [29,30] were available from their atlas of iodine lines from 14800 cm^{-1} up to a limit of 19980 cm^{-1} . Sharp, unblended $^{127}\text{I}_2$ lines, whose frequencies were determined from the B-X transition constants of Barrow and Yee [27], were used for calibration in the subsequent region up to 20025 cm^{-1} .

The fringes from a solid quartz etalon provided relative frequency calibration of the intermediate state scans in all spectral regions. The wavelength spacing between etalon fringes was accurately known and the fringes were often used in situations where direct knowledge of the absolute frequency was not necessary but relative measurements were needed. The sharpness and regularity of the fringe patterns produced in any one scan showed that narrow bandwidth laser operation was being maintained. Two solid quartz etalons were used, one a 0.61 cm etalon with $\text{FSR} = 0.556\text{ cm}^{-1}$ (Molelectron) and the other a 1.02 cm etalon with $\text{FSR} = 0.334\text{ cm}^{-1}$ (Burleigh).

The exact FSR of the etalons was determined by calibrating them against $^{127}\text{I}_2$ lines. Because the index of refraction of quartz changes over the visible region, a graph of the index of refraction of quartz versus wavelength was used to establish the FSR of the etalons in spectral regions beyond those directly calibrated. The 1.02 cm etalon was calibrated against $^{127}\text{I}_2$ at 5814 Å. The 0.61 cm etalon was calibrated against $^{127}\text{I}_2$ at 5780 Å and also against Fe/Ne lines from a hollow cathode lamp between 5750 Å and 5820 Å on a 21-ft Ebert spectrograph. The frequency calibration of the PDL could be extended beyond the last useable $^{127}\text{I}_2$ line to 20041 cm^{-1} , using the etalon fringes.

5.2 Calibration of the MDL

The mechanical scan dye laser was calibrated using a Spex model 1400 spectrometer (a 3/4 m Czerny-Turner monochromator equipped with a 1200 l/mm grating blazed at 7500 Å and a ITT model FW130 "Startracker" photomultiplier). The spectrometer slit was simultaneously illuminated with a portion of the laser beam and the emission from a Fe/Ne hollow cathode lamp. The slits were set to the minimum aperture possible that would give a measurable signal. During each scan of the laser, the spectrometer was manually set to the center of various strong well-identified Fe or Ne lines from the lamp. The photomultiplier output was monitored on a Keithley model 610B electrometer. The PMT

output was then switched to one channel of the boxcar integrator. As the laser scanned over the selected frequency position, an output signal of known frequency was recorded simultaneously with the signal channel. A full scan of the laser over a dye profile usually contained at least 6 calibration lines. The spectral line frequencies were obtained by quadratic interpolation of the calibration lines. This scheme for providing calibration markers simultaneously with the sample spectrum was found to give an overall accuracy of $\pm 0.5 \text{ cm}^{-1}$ in the measured spectral line frequencies.

5.3 Maintenance of the System

The use of a spark gap to trigger the nitrogen laser required ongoing maintenance, cleaning and periodic replacement of the copper electrodes in the trigger. As carbon deposits built up in the gap the operating pressure increased. When the spark gap pressure exceeded 40 psig it was necessary to dismantle the system and clean the spark gap lines and repolish the electrodes. Eventually the transfer of copper from one electrode to the other necessitated their replacement. The spark gap would operate approximately 1-2 months between cleanings and about 6 months between replacement of the electrodes. Brass electrodes were found to be unsatisfactory as replacements.

The NRG laser introduced a certain amount of RF noise and trigger instability due to its free-running nature. This trigger instability did not interfere with the experiments; however the RF noise had to be reduced below a certain level before good operation of the boxcar could be achieved. A number of schemes were tried, and it was found that an extra braided copper shield on the cable between the laser head and the power supply greatly reduced the RF noise.

The Mylar sheets that together with a series of aluminum plates formed the storage capacitor in the laser head, had to be periodically replaced when a breakdown produced arcing between the plates. The felt strips surrounding the capacitor plates had to be also replaced as they were periodically burnt when arcing occurred. When the Mylar sheets were replaced, a fine film of transformer oil was spread between them. Great care had to be taken to force all the trapped air from between the sheets.

The front output window on the nitrogen laser had to be removed periodically in order to remove a thin film of copper that accumulated on its surface.

The dye cells in the PDL and MDL were fabricated from three quartz plates glued together at the edges and onto a stainless steel block that made up the back of the cell. It was difficult to seal the edges of the quartz plate if any chipping was present. Dow Corning Silicone Rubber was found to be the only sealant that was not

weakened by the dye solvents. The cleanliness of the dye cell windows and the freedom of the narrow active region inside the dye cell from impurities was found to be crucial for correct operation of the dye lasers.

Chapter V

RESULTS AND DISCUSSION -

IODINE

1. The Dissociation Limit Region in the B $^3\Pi(0_u^+)$ State of $^{127}\text{I}_2$ and $^{129}\text{I}_2$

1.1 Introduction

Two-photon sequential excitation has previously been employed to study the discrete rotational band structure in $^{127}\text{I}_2$ near the dissociation limit of the B $^3\Pi(0_u^+)$ state [12, 13] by means of the technique described in Sec. 2, Chap. III. This study has now been extended to include the corresponding levels in the isotope $^{129}\text{I}_2$. Within the Born-Oppenheimer approximation, the internuclear potentials for different isotopes are the same; therefore, applying the mass-scaled version of long-range potential theory outlined in Sec. 3.3, Chap. II, a combined isotope analysis was possible for iodine. This combined analysis provided a larger body of independent data than was available for each single isotopic form. The B state of iodine was a good candidate for these studies as major perturbations were not observed in the levels approaching dissociation.

The $^{129}\text{I}_2$ levels between $v_B = 70$ and $v_B = 79$ have been studied using two-photon techniques. The probe laser

was fixed on the $v_E = 21$ level of the E state of $^{129}\text{I}_2$ and the pump laser was scanned between 20010 cm^{-1} and 20040 cm^{-1} to map out the dissociation limit region of the B state of $^{129}\text{I}_2$. In some traces lines were also observed from the lower lying $v_B = 69$ level, however these results were not included in the analysis. A few weak lines were positively identified as transitions to the $v_B = 70$ and 73 levels of the mixed isotope $^{127/129}\text{I}_2$ which was present in trace quantities in the sample of $^{129}\text{I}_2$. These results were not included directly in the analysis of the long-range potential, but they were found to obey the same relationships as the results for the other two isotopes.

The spectrum of $^{129}\text{I}_2$ was more difficult to analyse in this region than that of $^{127}\text{I}_2$. The bands in $^{129}\text{I}_2$ were more heavily overlapped with each other and were difficult to resolve into individual rotational lines. Because of this, the analysis could only be extended to $v_B = 79$ in $^{129}\text{I}_2$, as compared to $v_B = 82$ in $^{127}\text{I}_2$. As well, despite the use of computer measurement of the spectra, the line frequencies showed slightly greater scatter in $^{129}\text{I}_2$ when compared to the results on $^{127}\text{I}_2$. A small localized perturbation was observed in the $v_B = 74$ level of $^{129}\text{I}_2$. This level could be split into two groups of lines; those with $J' \leq 13$ and those with $J' > 13$. When fit as a single set of data the deviations varied systematically up to $J' = 13$

with a maximum deviation of 0.032 cm^{-1} . This perturbation was of unknown origin, and it did not seriously affect the results. All of the levels studied occurred at a large enough bond length that their spacings were governed by the long-range potential forces in the molecule. Applying Le Roy's criterion [91], the levels must lie at a large enough bond length such that:

$$R > 2[\langle r_A^2 \rangle^{1/2} + \langle r_B^2 \rangle^{1/2}] \quad \text{V-1}$$

for I $5p_{1/2}$ $\langle r_A^2 \rangle = 6.05473 a_0^2$, $5p_{3/2}$ $\langle r_B^2 \rangle = 6.76919 a_0^2$ [123] resulting in $R > 2[1.69543 \text{ \AA} + 1.89550 \text{ \AA}]$ or $R > 7.182 \text{ \AA}$. Previous RKR calculations [13,27] on the B state of iodine showed that the outer turning points of the vibrational levels with $v_B > 70$ had $R > 7.35 \text{ \AA}$; therefore, their behaviour could be analyzed using the long-range equations developed in Sec. 2, Chap. II.

1.2 Analysis

The rotational terms for the $v_x = 0$ level in the X state up to $J = 28$ were calculated from the standard polynomial expansions [19,33]:

$${}^{129}\text{G}(v) = \sum_{n=1}^3 \rho^n \text{G}_n (v + 1/2)^n \quad \text{V-2}$$

$${}^{129}\text{B}(v) = \sum_{n=0}^4 \rho^{n+2} \text{B}_n (v + 1/2)^n \quad \text{V-3}$$

$${}^{129}\text{D}(v) = \sum_{n=0} \rho^{n+4} \text{D}_n (v + 1/2)^n \quad \text{V-4}$$

The $^{127}I_2$ constants were taken from the analysis of Luc [32] using the value $^{129}\rho = (^{127}\mu/^{129}\mu)^{1/2} = 0.99221$. The isotopic masses used in all calculations are listed in Table V-1. The rotational term values $F_v'(J')$ for each B state vibrational level were obtained by adding the ground state terms to the observed transition frequencies. Because only transitions with low values of J' were observed ($J' \leq 27$) the rotational terms were fit to a linear expression $F_v'(J') = G_v + B_v J'(J' + 1)$ to obtain the constants G_v and B_v for each vibrational level. In the region studied between 20010 cm^{-1} and 20040 cm^{-1} , for the vibrational bands identified, only low J' lines were observed; high J' lines of the vibrational bands would lie to lower wavenumbers than the region being investigated. Quadratic least squares fits to the rotational terms yielded ill-determined D_v values of varying sign. Even though these vibrational bands lay near dissociation where the effects of centrifugal distortion were large, the centrifugal distortion corrections calculated from the free parameters, for such low J' values, were on the order of the experimental error ($\pm 0.025 \text{ cm}^{-1}$). The number of lines analysed and the range of J'_B observed are listed in Table V-2. The vibrational constants G_v are given in Table V-3.

In order to apply the mass-scaling, and since the units of the reduced mass μ were arbitrary here, it was convenient to define $^{127}\mu = 1.0$.

Table V-1. Isotopic Masses^a

Element	Mass Number	Atomic Mass, amu
Chlorine	35	34.96885359
	37	36.96590304
Bromine	79	78.9183320
	81	80.916292
Iodine	127	126.9044755
	129	128.904989

^aA.H. Wapstra, N.B. Grove, Nuclear Data Tables,
A9, 265 (1971)

Table V-2. Summary of rotational line data used in the analysis of the B state dissociation region of iodine isotopic species

Isotope	v_B	No. of lines in analysis	J'_B range of analyzed lines
$^{129}\text{I}_2$	69	12	8-15
	71	41	2-15
	72	90	5-25
	73	59	4-27
	74	62	6-27
	75	34	6-25
	76	73	4-21
	77	102	4-23
	78	41	2-16
$^{127}/^{129}\text{I}_2$	70	12	8-15
	73	37	5-18

D

Table V-3. Vibrational energy levels near the dissociation limit of the B state of iodine isotopic species (relative to $v_X = 0, J_X = 0$ for each species)

Isotope	v_B	$G_V(\text{cm}^{-1})$		
		obs.	Yee, calc. ^a	
$^{129}\text{I}_2$	69	20006.73 ^c	20006.75	20006.625
	70		12.89	12.813
	71	20018.2952 ± 70 ^d	18.29	18.243
	72	23.0021 ± 68	22.99	22.972
	73	27.1103 ± 51		27.055
	74	30.5742 ± 59		30.554
	75	33.4869 ± 56		33.493
	76	35.9192 ± 54		35.952
	77	37.9935 ± 52		37.973
	78	39.6327 ± 98		39.603
	79	40.8847 ± 290		40.890
	80			41.880
	81			42.615
	82			43.138
83			43.490	
$^{127/129}\text{I}_2$	70	20014.0750 ± 23 ^c		20013.976
	73	27.7659 ± 94 ^c		27.705

^aRef. 33

^bAssuming the values for D and C_5 obtained in the present analysis.

^cNot used in the analysis.

^dIn listing the errors, the notation ± 70 means ± .0070.

$$\begin{aligned}
 {}^{127}\mu &= 63.4522378 \approx 1.0 \\
 {}^{127}/{}^{129}\mu &= 63.9484117 \approx 1.0078196 \\
 {}^{129}\mu &= 64.4524067 \approx 1.0157626
 \end{aligned}$$

For any isotopic iodine molecule of reduced mass μ the ratio $\rho = (\mu/i_\mu)^{1/2}$ became $\rho = 1/\mu^{1/2}$. For ${}^{127}\text{I}_2$, ${}^{127}\rho = 1.0$; for ${}^{129}\text{I}_2$, ${}^{129}\rho = 0.99221$ and for the mixed isotope ${}^{127}/{}^{129}\text{I}_2$, ${}^{127}/{}^{129}\rho = 0.99611$.

The B state of iodine undergoes covalent dissociation into ${}^2\text{P}_{1/2}$ plus ${}^2\text{P}_{3/2}$ atoms. These atomic states arise from an unfilled 5p^5 valence configuration (${}^{53}\text{I}$: $[\text{Kr}]4\text{d}^{10}, 5\text{s}^2, 5\text{p}^5$). It has been shown [91,13,27] that the asymptotic term in the long-range potential function for the B state of iodine should have $n = 5$. The $n = 5$ term contributes to the long-range potential when neither of the atoms involved is in an S electronic state. The C_5/R^5 term arises from a first-order quadrupole-quadrupole interaction. The long-range internuclear potential for the B state of the halogen molecules has the form [91,124]:

$$\begin{aligned}
 V(R) &= D - C_5/R^5 - C_6/R^6 - C_8/R^8 \\
 &\quad - C_{10}/R^{10} - \dots
 \end{aligned}
 \tag{V-5}$$

The long-range potential equations in the mass-scaled form can be written in terms of $n = 5$ as:

$$G_V = D_e - [\overline{\Delta G_V}/\rho ({}^{127}\text{K}_5)]^{10/7}
 \tag{V-6}$$

where G_v and the dissociation limit D_e are taken relative to the X state potential minimum, $\overline{\Delta G}_v = 1/2(G_{v+1} - G_{v-1})$ is calculated for each isotope separately, and $^{127}K_5$ is a constant $^{127}K_5 = (10/3)^{127}H_5$;

$$n = n_D + (1/^{127}H_5)(D_e - G_v)^{0.3} \quad \text{V-7}$$

where $^{127}H_5 = \overline{H}_5 / (^{127}\mu^{1/2} (C_5)^{1/5})$ and $^{127}\mu$ is expressed in the correct units of atomic mass units and:

$$(n_D - n) = [E_v / \rho^2 (Q_5')^2]^{3/4} \quad \text{V-8}$$

where $Q_5' = \overline{Q}_5 / (C_5^2)^{1/3}$. The constants \overline{H}_5 and \overline{Q}_5 are numerical constants found in Table 1 of reference 91.

In earlier studies [13,27] the vibrational energies were always measured relative to the $v_X = 0, J_X = 0$ level. To use the mass-reduced forms of the equations it was necessary to express the energies relative to the bottom of the X state potential well. The zero-point energies were calculated for each isotope using the standard isotopic relationship and Luc's constants [32] for $^{127}I_2$:

$$\begin{aligned} ^{127}I_2, G''(0) &= 107.1073 \text{ cm}^{-1} \\ ^{127/129}I_2, G''(0) &= 106.6916 \text{ cm}^{-1} \\ ^{129}I_2, G''(0) &= 106.2742 \text{ cm}^{-1} \end{aligned}$$

The currently measured vibrational and rotational data for $^{129}I_2$ were combined with the previous results for $^{127}I_2$ from reference 13.

The applicability of the mass-reduced form can be readily seen in the Birge-Sponer plot (Figure V-1). The first order energy level differences, in mass scaled form, for both $^{127}\text{I}_2$ and $^{129}\text{I}_2$ have been plotted together as a function of n :

$$\Delta G(n) \equiv \mu^{1/2} \Delta G(v + 1/2) = (1/\rho) \Delta G(v + 1/2) \quad \text{V-9}$$

The two sets of points fell on the same curve. The graph exhibited the positive curvature expected for levels in the B state at large internuclear separation. Le Roy's long range equations did predict a positive curvature for Birge-Sponer plots in the region near the dissociation limit, a region where the outer branch of the potential was accurately described by these equations. Observation of such a curvature was a necessary (though not sufficient) condition for the further application of these expressions. This observation along with the criterion expressed earlier in equation V-1 indicated that these equations could be applied to these levels. As well, the previous application of these formulae to the $^{127}\text{I}_2$ data had produced the expected linear results [13].

The plot of $G(v)$ versus $(\overline{\Delta G}_v/\rho)^{10/7}$ (equation V-6) is shown in Figure V-2. This plot, which shows the same linear relationship for both $^{127}\text{I}_2$ and $^{129}\text{I}_2$, allowed the determination of the dissociation limit D_e from the intercept. The least squares procedure applied to find D_e was suggested

Figure V-1. Birge-Sponer plot of $\Delta G(n)$ against the mass-reduced quantum number n

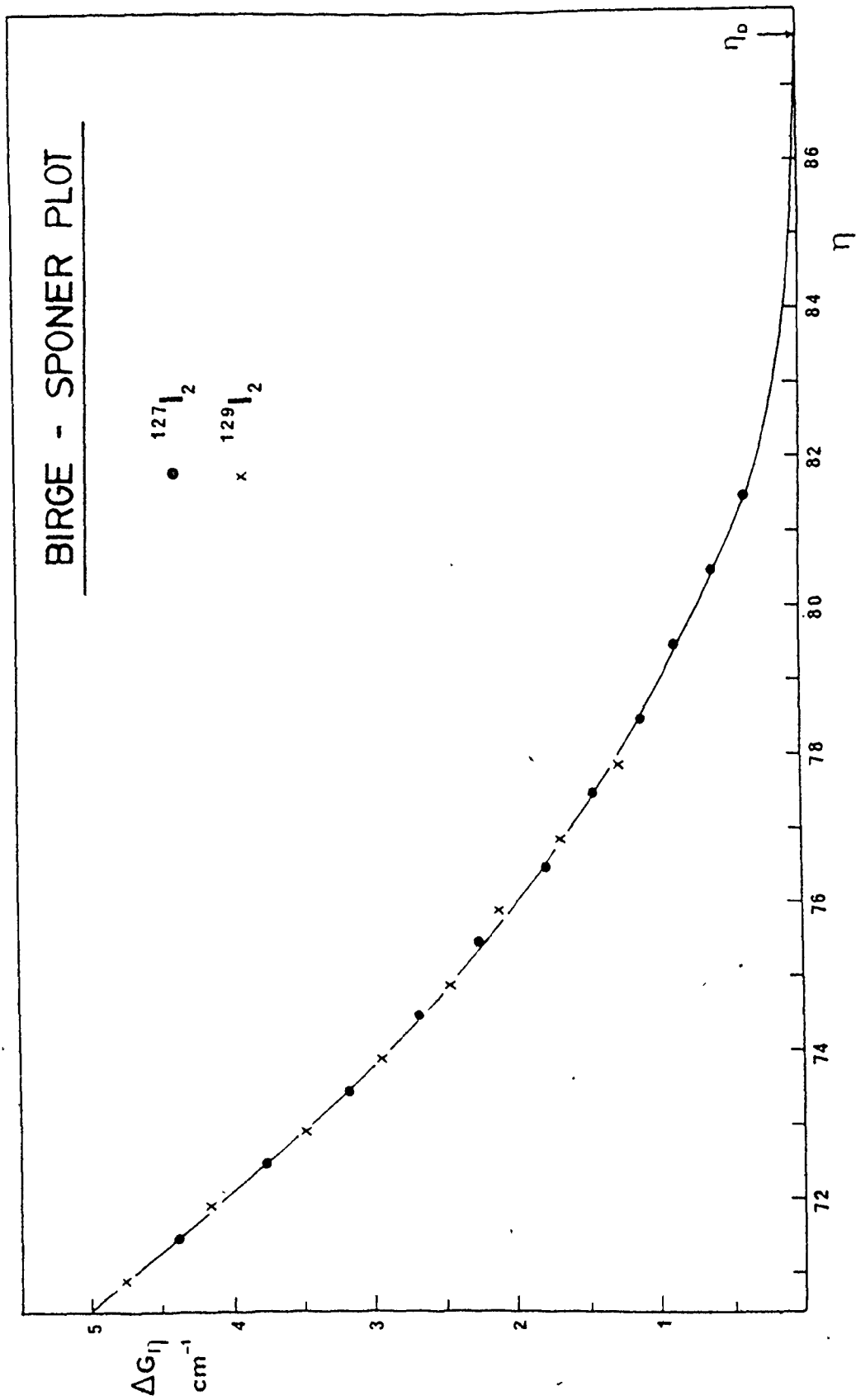
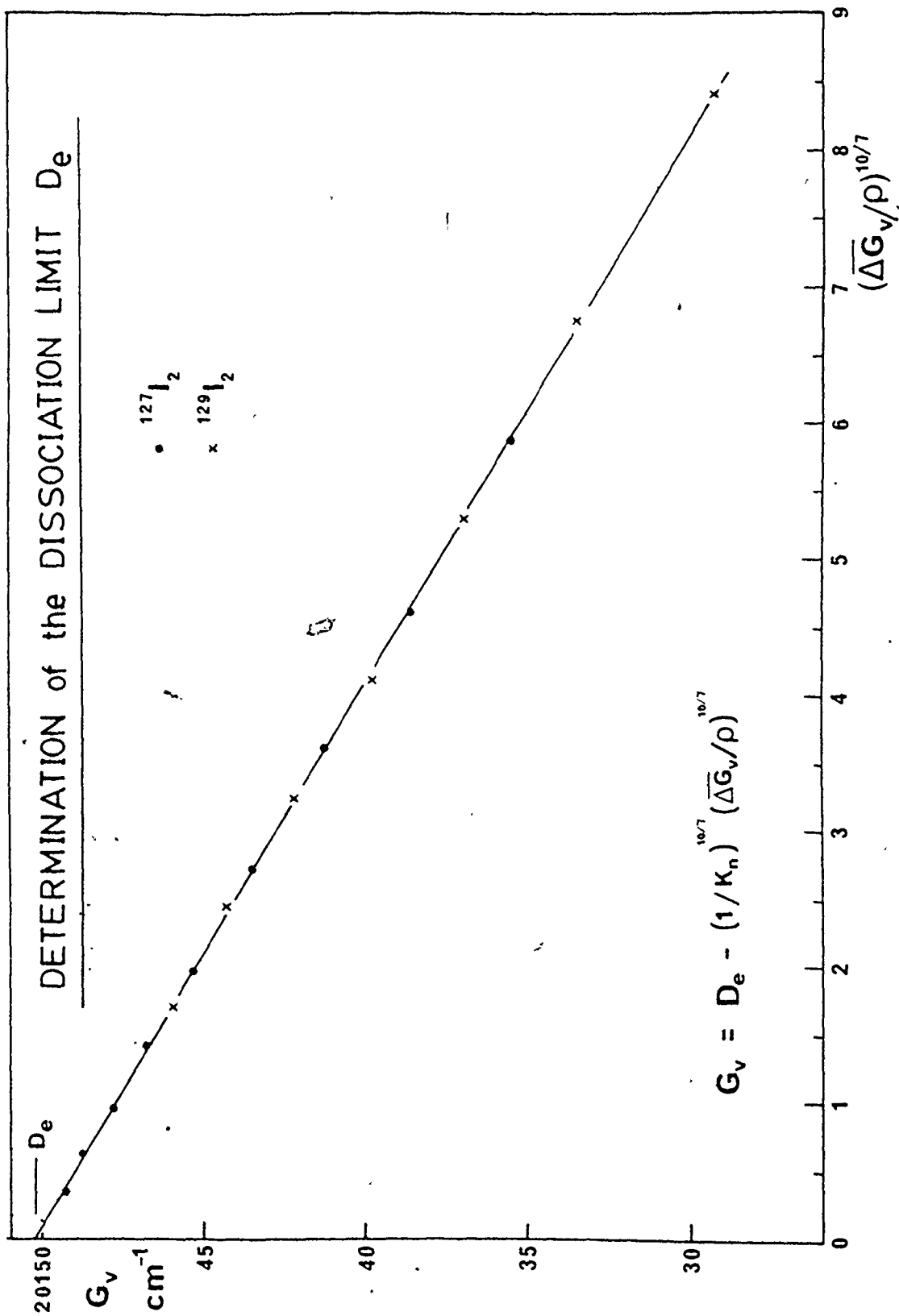


Figure V-2. Determination of the dissociation limit D_e for the combined isotopic species

}

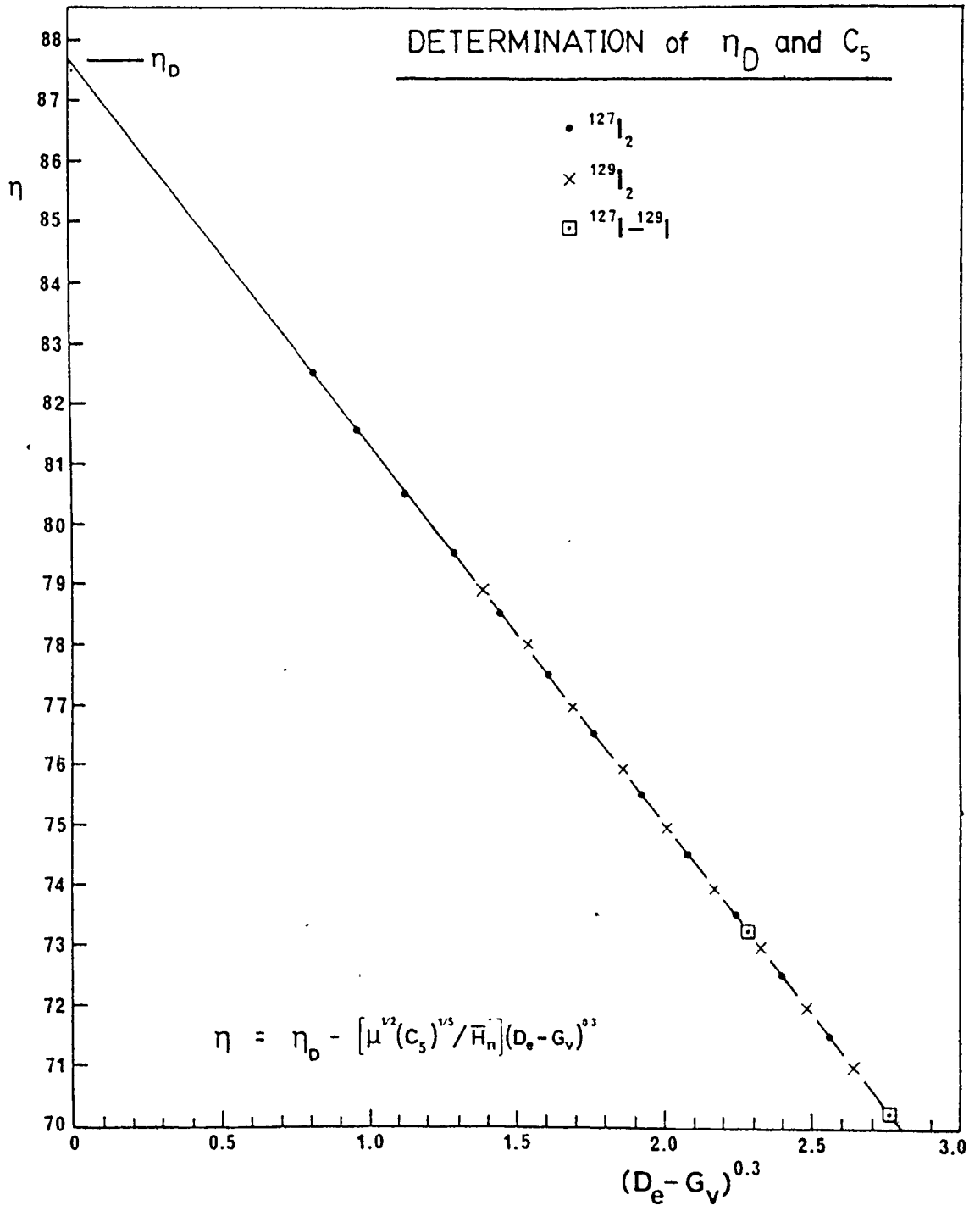


by Le Roy [91]. The value of n was fixed at its asymptotic value and a series of D_e values were calculated by linear regression, successively omitting the deepest observed level from consideration. This gradual approach towards the dissociation limit should ensure that n will be very close to its asymptotic value and should yield a limiting value for D_e . The set of D_e values obtained were plotted against G_v for the lowest retained level and a weighted least squares fit to these results extrapolated to give a limiting value for D_e . This limiting value was $D_e = 20150.171 \pm 0.031 \text{ cm}^{-1}$. After subtracting the zero point energy for $^{127}\text{I}_2$ to obtain $D_0 = 20043.064 \text{ cm}^{-1}$, relative to $v_x = 0, J_x = 0$, this result was compared to the previous result for $^{127}\text{I}_2$ alone [13] of $D_0 = 20043.063 \pm 0.020 \text{ cm}^{-1}$. The agreement was well within experimental error.

The plot of n against $(D_e - G_v)^{0.3}$ (equation V-7) is shown in Figure V-3. Again it produced a single straight line. The points measured for the mixed isotope $^{127/129}\text{I}_2$ were also shown to fall on the line. Values for C_5 and η_D , the long-range potential constant and the mass-reduced "effective" vibrational index at the dissociation limit, were obtained from this data by the same methods of linear regression.

The best values of D_e , C_5 and η_D were used in equation V-7 to produce calculated G_v values for all three isotopes. These values, when compared with experiment,

Figure V-3. Determination of η_D and C_5 . Data points for all three isotopic species are shown.



differed by less than 0.1 cm^{-1} for all the isotopes (Table V-3). The values for $^{127}\text{I}_2$ differed by a maximum of 0.032 cm^{-1} and were not reproduced in the table.

The observed rotational constants for the levels of $^{129}\text{I}_2$ are listed in Table V-4. When the mass-reduced rotational constant $B_v(n) = B_v/\rho^2$ was plotted against n it was found that the points for all three isotopes conformed to a single curve. At high v Le Roy's equations suggested a plot of $(B_v(n))^{3/4}$ versus $(n_D - n)$ (equation V-8) as shown in Figure V-4. Allowing for a certain amount of scatter all the points for all the species fell on the same curve. The scatter of the points was certainly due to experimental error especially for the highest levels where the standard deviation on the B_v values was large. The neglect of centrifugal distortion introduced a systematic error since the points plotted were essentially "effective" B_v values.

The result of the experimental points falling on a curve rather than a straight line was not completely unexpected, as Le Roy has pointed out the approximate nature of the equations involving the rotational constants [91,95]. It was necessary to consider higher power terms in the potential expansion when dealing with rotational constants [98]. This curve was a relatively poor way of obtaining a value for the parameter C_5 ; however, if the values for B_v were known for levels near dissociation, it

Table V-4. Rotational constants near the dissociation limit of the B state of iodine isotopic species

Isotope	v_B	$B_v \times 10^3 \text{ (cm}^{-1}\text{)}$	
		obs.	calc.
$^{129}\text{I}_2$	71	$7.077 \pm .064$	11.589
	72	$6.644 \pm .019$	10.682
	73	$6.080 \pm .014$	9.793
	74	$5.643 \pm .017$	8.925
	75	$5.243 \pm .022$	8.077
	76	$4.900 \pm .024$	7.251
	77	$4.279 \pm .016$	6.448
	78	$3.876 \pm .047$	5.669
	79	$3.532 \pm .107$	4.916
$^{127/129}\text{I}_2$	70	7.410	12.352
	73	5.940	9.615

follows that G_V values were also known and these could be used in a more reliable determination. The limiting slope of the experimental curve at $(n_D - n) = 0$ gave $C_5 = 4.25 \times 10^5 \text{ cm}^{-1} \text{ \AA}^5$ which is higher than the more reliable value of $C_5 = 2.765 \times 10^5 \text{ cm}^{-1} \text{ \AA}^5$ obtained from the G_V data. Using this latter figure to calculate values of B_V from the limiting near-dissociation equation V-8 gave values considerably too large (Table V-4, Figure V-4). These values can be considered upper bounds to B_V , for levels near dissociation.

Table V-5 gives a summary of the final results of this work. In this table values of D_e and n_D have been derived from the values of D_0 and v_D directly calculated in the previous work on $^{127}\text{I}_2$ [13] as a comparison. The larger standard deviations in this work was traced back to the slightly greater scatter in the G_V values for $^{129}\text{I}_2$. This scatter was a direct consequence of the increased number of overlapping lines in this dense spectrum. Derived values of D_0 and v_D are also listed in Table V-5 for each isotopic species.

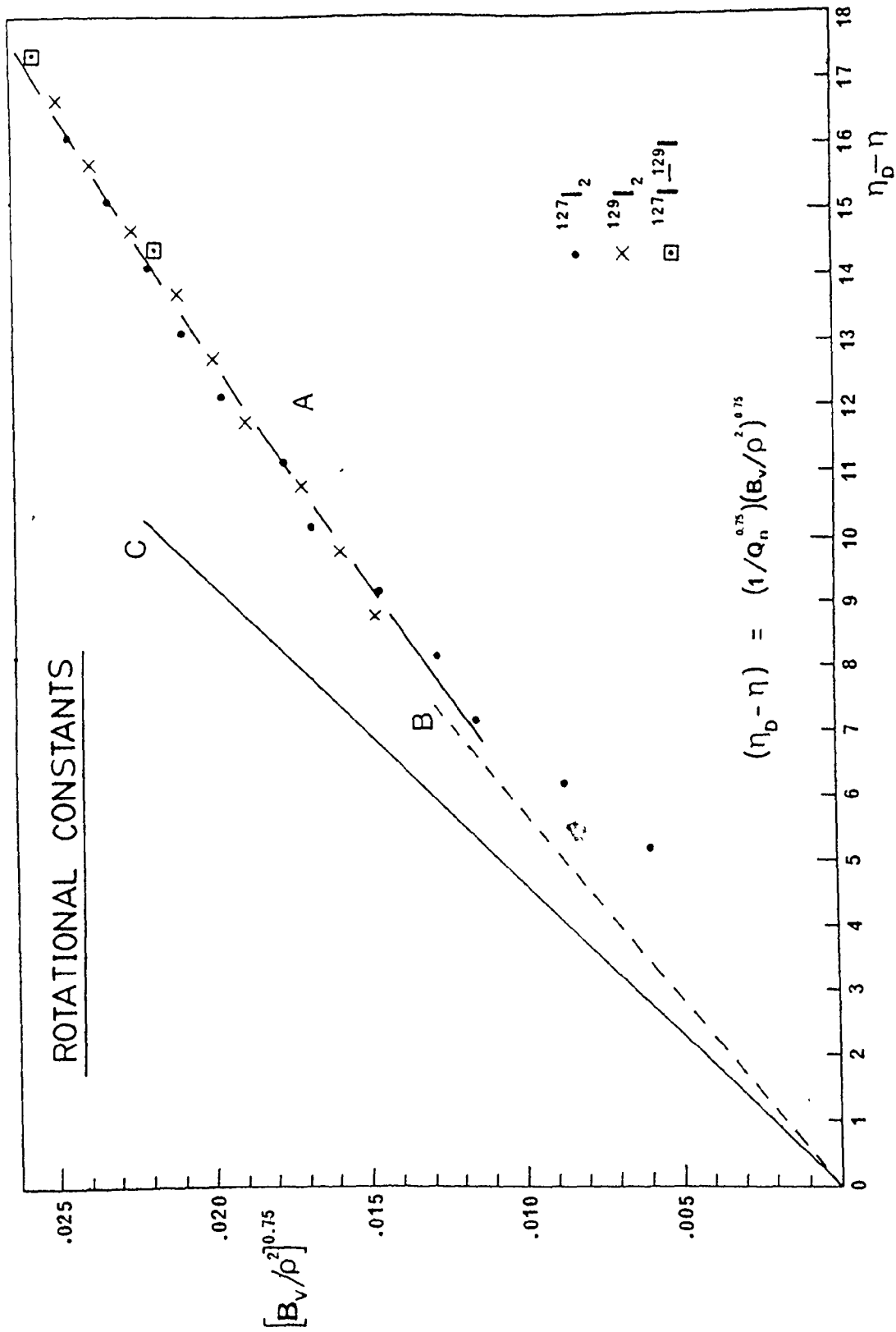
When this new vibrational and rotational data for $^{129}\text{I}_2$ was incorporated into the RKR program previously used to describe the B state of iodine [13], it made a negligible difference. The changes in the vibrational turning points were less than 0.01 \AA for the outer ends of the $v_B = 70-79$ levels of $^{127}\text{I}_2$. These small changes in the potential did

Table V-5. Long range constants for the B state of iodine isotopic species

	Prior results		Present results	
	$^{127}\text{I}_2$	$^{127}\text{I}_2$	$^{127}\text{I}_2$	$^{127/129}\text{I}_2$ $^{129}\text{I}_2$
D_e (cm^{-1})	20150.170		20150.171 \pm .031 ^a	
η_D	87.683		87.676 \pm .149 ^a	
$C_5 \times 10^{-5}$ ($\text{cm}^{-1} \text{ \AA}^5$)	2.776 \pm .132		2.765 \pm .177 ^a	
D_0 (cm^{-1})	20043.063 \pm .020		20043.064	20043.480 20043.897
V_D	87.183 \pm .106		87.176	87.519 87.865

^aCombined results

Figure V-4. Rotational constants for all three isotopic species. Curve A is a least squares quadratic fit, B is the limiting slope at $(n_D - n) = 0$, and C is the calculated line for the best value of C_5

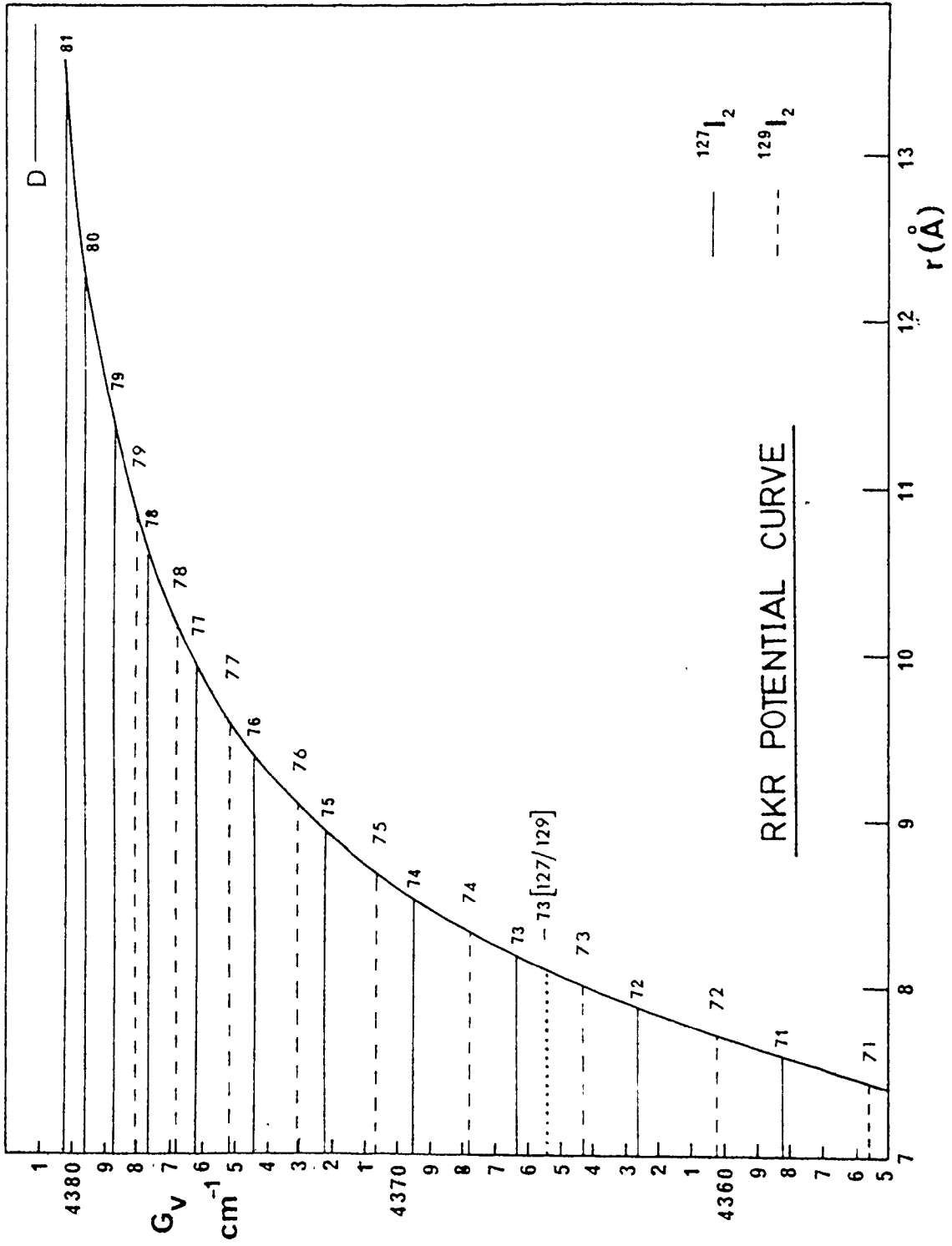


not necessitate the recalculation of the C_6 , C_8 and C_{10} coefficients from the RKR turning points as they would be substantially the same as in reference 13. The RKR potential is illustrated in Figure V-5 for all three isotopic species.

1.3 Discussion

In reexamining the limiting behaviour of levels near dissociation, Le Roy [98] has shown that despite the neglect of higher order terms in the potential, these methods of analysis are the most accurate methods known for obtaining the dissociation limit from experimental vibrational spacings. The use of the mass-reduced forms appeared to be satisfactory in analysing data from different isotopes since the combined vibrational data here gave very consistent results. Because the rotational constants are sensitive to the form of the potential, the increased importance of higher power terms in the long-range potential as dissociation is approached may explain the nonlinear behaviour observed. No obvious perturbations were observed in the spectra except for the one mentioned in $v_B = 74$ of $^{129}\text{I}_2$. The neglect of centrifugal distortion in these calculations has been criticized as a possible defect in this form of analysis [98]. Certainly at high v it is expected that centrifugal distortion would play an increasingly important role; however, no obvious justification for the inclusion of a simple second order term in the fits to the low J data obtained here could be found. Plots of the

Figure V-5. RKR potential curve and higher observed vibrational levels for all three isotopic species. G_v is measured relative to the B state potential minimum



differences from a linear fit did not exhibit an obvious curvature. It will be necessary to obtain either further more accurate data at higher J or calculate values for D_v from other sources, to take these effects into account and correct the B_v data.

The success of this combined isotope analysis of the B state of I_2 provides evidence that such an approach is possible in the halogens. The breakdown of a similar approach in $I^{35}Cl/I^{37}Cl$ found by King and McFadden [15], where the C_5 coefficients were different for the two isotopes, must be due to the molecule and not the method.

2. The 5eV Region of $^{127}I_2$ and $^{129}I_2$

2.1 Introduction

Despite the large amount of experimental data available, the complexity of the energy levels in iodine has produced very few definitive assignments for the higher lying electronic states. It is the states in the 40000 cm^{-1} (or 5eV) region of iodine that are accessible via two-photon excitation using the B state as an intermediate. As was discussed earlier in Sec.1, Chap. II, in the 5eV region of iodine, above the 23 valence electronic states which correlate with ground term (2P) I atoms, the next predicted states are the 18 ion-pair states arising from $I^-(^1S) + I^+(^3P, ^1D)$ combinations (see Figure II-4). The correlations shown for these states may not be correct since ion-pair

states may, on dissociation, short-cut into one or another state pair in which one atom is in the ground state configuration and the other in a Rydberg state [18]. The lowest energy of such a state pair, $I(5p^5, ^2P_{3/2}) + I(5p^4 6s, ^4P_{5/2})$ is 8.33eV compared with the lowest energy ion pair $I^+(5p^4, ^3P_2) + I^-(5p^6, ^1S)$ at 8.95eV. There have been three molecular states positively identified in the region of interest in iodine, one ungerade (u) state and two gerade (g) states. The established states are the D, E and D' states (the F state lies slightly higher in energy and will not concern us).

The best defined u state is the $D \ ^1\Sigma^+(0_u^+)$ state arising from the 1441 configuration of Mulliken. This is the only identified state that can be accessed via a single photon transition from the ground $X \ ^1\Sigma_g^+$ state. The transition $D \ ^1\Sigma^+(0_u^+) - X \ ^1\Sigma_g^+$ has been studied in both absorption and emission [18,38,41,125,126]. Despite these studies, both the vibrational numbering and the constants of the D state have not been firmly established. Most of the data has been gathered from very high vibrational levels in the D state. The molecular constants are known approximately as $T_e \approx 41200 \text{ cm}^{-1}$, $\omega_e \approx 104 \text{ cm}^{-1}$ and $r_e \approx 3.56 \text{ \AA}$. The low vibrational frequency and large equilibrium internuclear separation is typical of an ion-pair state [18].

The g excited states should be accessible spectroscopically by single photon transitions with

intermediate u excited states. The main problem is that few of these intermediate states have been well characterized. Only the B $^3\Pi(0_u^+)$ state is known to a high degree of accuracy [13,27,32]. The A $^3\Pi(1u)$ state has been studied to a lesser degree [127-129]. A recent paper on the A $^3\Pi(1u) - X^1\Sigma_g^+$ transition [129] has extended the original progressions studied; work on the 2770 Å emission of both $^{127}\text{I}_2$ and $^{129}\text{I}_2$ [128], which terminates on the A state, has established a more reliable vibrational numbering and thus more reliable constants for the A state.

In the presence of inert buffer gases the emission spectrum of iodine shows a large number of systems. The best established of these is the E $^3\Pi(0_g^+) \rightarrow$ B $^3\Pi(0_u^+)$ emission in the 4000-4360 Å region. A vibrational analysis of this band system [42] yields $T_e = 41411.8 \text{ cm}^{-1}$, $\omega_e = 101.59 \text{ cm}^{-1}$ and $r_e = 3.7 \text{ Å}$. The emission in the 3400 Å region has been assigned to the D' $^3\Pi(2g) \rightarrow$ A' $^3\Pi(2u)$ transition. The A' state however is not well understood and only an approximate value of $T_e = 40650 \text{ cm}^{-1}$ can be given [43,44] for the D' state. Other studies have tentatively made assignments to other band systems observed in these regions [44,55,127].

Using two-photon methods, Danyluk and King (DK) [9] found 5 excited g states in the 5eV region using vibrational levels in the intermediate B $^3\Pi(0_u^+)$ state as pump levels. This early study used pump levels near the dissociation limit of the B state and employed only the natural isotope

$^{127}\text{I}_2$. Because of this, the absolute vibrational numbering in the 5 states (labeled α , β , γ , δ , and ϵ) could not be determined. Only the origin band of the $\gamma \rightarrow \text{B}$ absorption at $T_0 = 41561 \text{ cm}^{-1}$ was believed to be identified with confidence. Current studies [10] have extended this work to include the two isotopes of iodine $^{129}\text{I}_2$ and $^{127}\text{I}_2$. Also, a wider range of B state pump levels have been employed in the hope of identifying these 5 excited states with greater confidence. All of the previously identified states in the 5eV region of $^{127}\text{I}_2$ were reexamined. In $^{129}\text{I}_2$, although the spectra were overall less intense than in $^{127}\text{I}_2$, all of the states except the weak δ state were observed. The weakness of the $^{129}\text{I}_2$ spectra was believed due to experimental problems with the sealed sample cell. The isotope relationships allowed the determination of absolute vibrational numbering for the states observed in both $^{127}\text{I}_2$ and $^{129}\text{I}_2$.

2.2 Pump Levels and Data Analysis

Levels in the well established intermediate B $^3\Pi(0_u^+)$ state with v_B values ranging from 21 to 81 provided convenient pump levels for the 5eV region of iodine. Only the excited state labeled as E (or ϵ in previous studies [9]) could be accessed from pump levels over the entire range of the B state. The other excited states, in both isotopes, were found to be accessible only from levels in the B state near dissociation.

In the case of the E state, B state levels with v_B values in the range 21-74 and J_B values from 0 to 158 were used as pump levels. The γ excited state was best observed from B state levels with $v_B > 70$. In their earlier work DK [9] also used two lower pump levels with $v_B = 59$ and 63. It was found possible to observe the γ bands on runs with v_B values as low as 58 but most of the spectra analysed were obtained from higher B state pump levels. The rest of the bands, the α , β and δ states, were considerably more difficult to observe experimentally. The spectra of these bands was fragmentary. Pump levels with $v_B \geq 69$ were the only B state levels from which these weaker transitions could be accessed.

Rotational term values for the excited states were obtained by adding the measured probe laser frequencies to the calculated term values of the intermediate B state rotational levels that were pumped. Unfortunately, in order to cover the large range of B state levels employed, a number of different sources of data had to be used to calculate the B state energies. For $^{127}\text{I}_2$ the B state terms were calculated from Luc's Dunham expansion coefficients [32] for $v_B \leq 62$; the experimental constants of Barrow and Yee [27] were then used up to $v_B = 76$; and the experimental constants of Danyluk and King [13] were used up to $v_B = 81$. For $^{129}\text{I}_2$ the B state term values for $v_B \leq 62$ were calculated from Luc's constants for $^{127}\text{I}_2$, using the

standard isotopic relationships with $^{129}\rho = 0.99221$; the calculated values of Yee [33] were then used up to $v_B = 70$; and the experimental values of King et al [14] were used up to $v_B = 79$. This introduced an estimated error of $\pm 0.05 \text{ cm}^{-1}$. This was considerably less than the limiting error in this experiment associated with the bandwidth of the probe laser ($\pm 1.0 \text{ cm}^{-1}$).

Where possible the constants for each excited state vibrational level were obtained from the observed rotational terms by linear regression. The majority of the data obtained in all of the excited states had low J values. Reliable centrifugal distortion coefficients were not obtainable as free parameters in least squares fits. Tellinghuisen et al [38,40] have stated that more meaningful G_v and B_v values could be obtained in this type of analysis by constraining the distortion constants to be consistent with the G_v and B_v values, rather than allowing them to be free parameter or leaving them out entirely. Their iterative method of calculating centrifugal distortion constants from a single rotationless potential curve $V(R)$ and then correcting the observed frequencies is best applied to the ground state of diatomic molecules. The data available in this study did not indicate this type of analysis would greatly improve the results. However for completeness, calculated centrifugal distortion constants D_v based on the formulae from Herzberg [12]:

$$D_e = 4B_e^3/\omega_e^2 \quad \text{V-10}$$

$$\beta_e = D_e \left(\frac{8\omega_e x_e}{\omega_e} - \frac{5\alpha_e}{B_e} - \frac{\alpha_e^2 \omega_e}{24B_e^3} \right) \quad \text{V-11}$$

where possible, were added to the experimental term values before the linear regression. The changes in the results with and without these constants were of the order of the experimental error.

The molecular constants for states with sufficient data from both isotopes (the E, α , β and γ states) were determined using polynomial expansions in the mass reduced quantum number n , as outlined earlier. These expansions act as a confirmation of the vibrational numbering of the states. The generalized expressions are:

$$T(n) = \sum_{n=0} T_n(n^n) \quad \text{V-12}$$

$$B(n) = B_V/\rho^2 = \sum_{n=0} B_n(n^n) \quad \text{V-13}$$

where $^{127}\rho = 1.0$ and $^{129}\rho = 0.99221$. $T(n)$ is the vibrational energy of the v^{th} level relative to the X state potential minimum obtained using the calculated values, 107.1073 cm^{-1} and 106.2742 cm^{-1} for the zero point energies in the ground states of $^{127}\text{I}_2$ and $^{129}\text{I}_2$ respectively [32,14]. Unit changes in the vibrational numbering of the levels of a state, away from the correctly established numbering, produced sharp increases in the reduced χ^2 of the fits to equations V-12 and V-13.



2.3 Results for the E and γ States.

The E state is the most firmly established excited state found in these studies. A total of 867 resolved rotational E+B transitions were analysed for $^{127}\text{I}_2$ and 250 for $^{129}\text{I}_2$. Only $\Delta J = \pm 1$ transitions were observed in the E+B spectra.

The constants for the vibrational levels of the E state for both isotopes are listed in Table V-6. Figures V-6 and V-7 show typical E state spectra for $^{127}\text{I}_2$ and $^{129}\text{I}_2$. The constants for the E state levels in $^{127}\text{I}_2$ with $v_E = 0-22$ were each determined from between 16 and 64 experimental rotational term values. The higher E state levels with $v_E = 23-29$ were less accurately determined using only about 6 term values arising from a few extended runs with Bis-MSB as the probe dye. Transitions to $v_E = 25$ were always too weak for measurement. The constants for the E state levels in $^{129}\text{I}_2$ with $v_E = 3-23$ were each determined from about 12 experimental term values. The levels above and below this region were obtained on only one or two traces. The correct vibrational numbering is given in Table V-6 and the coefficients of equations V-12, V-13, in spectroscopic form, are given in Table V-7 for both isotopes.

In the original work on $^{127}\text{I}_2$ [9], a series of bands labeled ϵ were identified. These bands were pumped from only high vibrational levels in the B state; the correct vibrational numbering had not been originally established.

Table V-6. Term values and rotational constants (cm^{-1}) for the E state of I_2

v	$^{127}\text{I}_2$		$^{129}\text{I}_2$	
	$T_0(v', J' = 0)^a$	$B_v \times 10^2$	$T_0(v', J' = 0)^a$	$B_v \times 10^2$
.0	41354.61(26) ^b	1.9929(56) ^b	41355.97(42) ^b	2.123(47) ^b
1	455.17(37)	1.9919(74)	456.2(1.0)	2.00(14)
2	555.30(24)	1.9863(28)	555.73(27)	1.9617(30)
3	655.60(26)	1.9831(25)	655.86(19)	1.9591(27)
4	755.80(21)	1.9742(18)	754.96(19)	1.9459(17)
5	855.20(25)	1.9681(20)	853.56(27)	1.9407(21)
6	954.36(35)	1.9612(26)	951.77(19)	1.9333(15)
7	42053.11(34)	1.9543(25)	42048.64(50)	1.9333(31)
8	151.32(43)	1.9480(38)	147.68(9)	1.9204(6)
9	249.56(37)	1.9443(39)	244.62(14)	1.9150(72)
10	346.75(21)	1.9394(29)	341.14(33)	1.916(12)
11	443.61(27)	1.9393(35)	438.12(12)	1.8871(43)
12	540.55(27)	1.9352(38)	533.20(29)	1.910(12)
13	636.71(25)	1.9316(39)	628.53(19)	1.9036(60)
14	733.00(22)	1.9216(36)	723.87(32)	1.8929(89)
15	828.30(29)	1.9273(58)	818.10(29)	1.9046(75)
16	924.22(28)	1.9088(65)	911.48(40)	1.921(10)

Table V-6 continued.

v	$^{127}\text{I}_2$		$^{129}\text{I}_2$	
	$T_0(v', J' = 0)^a$	$B_v \times 10^2$	$T_0(v', J' = 0)^a$	$B_v \times 10^2$
17	43018.66(32)	1.885(15)	43006.35(34)	1.901(11)
18	113.06(24)	1.893(13)	99.29(61)	1.905(13)
19	207.45(35)	1.877(18)	193.78(38)	1.849(19)
20	300.47(28)	1.901(14)	286.05(44)	1.889(11)
21	394.25(33)	1.897(19)	379.30(57)	1.867(27)
22	486.22(33)	1.926(50)	470.88(48)	1.884(11)
23	578.87(23)	1.985(48)	563.49(69)	1.74(10)
24	670.62(21)	1.872(45)	[655.5	1.7]c
25			[747.0	1.7]c
26	43853.97(37)	1.896(76)		
27	945.41(22)	1.907(48)		
28	44035.95(20)	1.942(42)		
29	125.84(16)	1.862(36)		

^aRelative to $v'' = 0, J'' = 0$ in the X state

Table V-6 continued.

^bNumbers in parentheses are errors on the last two decimal places in the value.

^cFrom two-point fit

Table V-7. Vibrational and rotational constants (cm^{-1})
for the E excited state

	$^{127}\text{I}_2$	$^{129}\text{I}_2$
T_e	41410.27 ± .15	41410.27 ± .15
ω_e	101.907 ± .041	101.113 ± .041
$\omega_e x_e$	0.2373 ± .0032	0.2336 ± .0032
$\omega_e y_e \times 10^4$	9.05 ± .70	8.84 ± .68
$B_e \times 10^2$	2.0116 ± .0020	1.9959 ± .0019
$\alpha_e \times 10^5$	8.76 ± .44	8.55 ± .43
$\gamma_e \times 10^6$	1.86 ± .23	1.80 ± .22
$r_e = 3.6342 \pm .0018 \text{ \AA}$		

Figure V-6. E state of $^{127}\text{I}_2$
(a). B state pump level 1-60 R(49) at $19641.3102 \text{ cm}^{-1}$
T = 19945.70 cm^{-1}
(b). B state pump level 0-49 P(28) at $19641.3454 \text{ cm}^{-1}$
T = 19671.64 cm^{-1}

Figure V-7. E state of $^{129}\text{I}_2$
(a). B state pump level 0-46 R(46) at $19501.9288 \text{ cm}^{-1}$
T = 19581.32 cm^{-1}
(b). B state pump level 0-47 R(63) at $19501.8183 \text{ cm}^{-1}$
T = 19649.79 cm^{-1}
(c). B state pump level 0-45 P(7) at $19501.7934 \text{ cm}^{-1}$
T = 19503.85 cm^{-1}

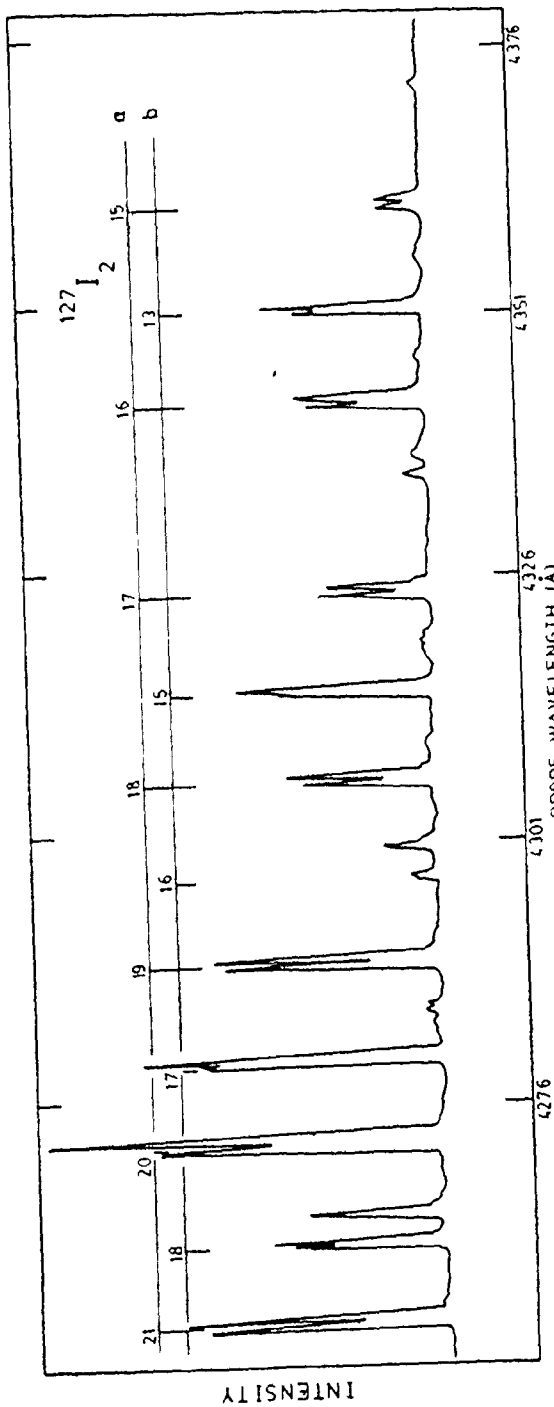


Figure V-6

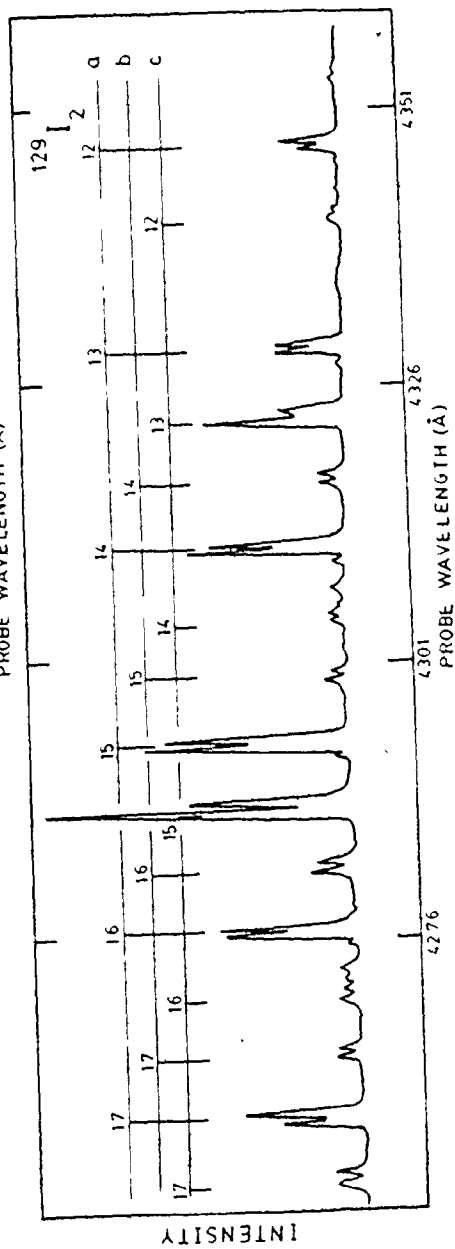


Figure V-7

These present studies showed that the ϵ levels were part of the E state system where ϵ_0 should be renumbered to coincide with $v_E = 12$. The previously measured T_0 values agreed well with those measured in this work; however, the previous rotational constants were about 8% too high. Since the original values were calculated on the basis of only a few rotational terms for each level, this was not unexpected.

Two other research groups, Cunha et al [49] and Williamson [50] repeated the early work of DK on $^{127}\text{I}_2$ using B state pump levels lower in the potential well. Williamson pumped levels with $v_B = 11-17$ and observed E state progressions from $v_E = 0-11$; Cunha et al pumped $v_B = 25-28$ levels and observed $v_E = 0-14$. Their results agreed reasonably well with this work although the values of the rotational constants reported by both sets of workers were 1-2% higher. The calculated vibrational levels of Cunha et al agreed well for low v but began to diverge by $v_E = 14$.

The emission spectrum of iodine in the presence of inert gases showed a discrete spectrum between 4000-4360 Å. This system has been identified as the E→B system and was initially analysed in $^{127}\text{I}_2$ [130] and later extended to include $^{129}\text{I}_2$ [42]. The observed emission bands were primarily from $v_E = 0-7$ to $v_B = 15-30$ levels. Most of the stronger transitions observed by Wieland et al [42] agreed well with these measurements (see Table V-8). Their values for $T_e = 41411.8 \text{ cm}^{-1}$, $\omega_e = 101.59 \text{ cm}^{-1}$ and $\omega_e x_e = 0.2380 \text{ cm}^{-1}$

Table V-8. A comparison of some of the stronger E→B transitions measured by Wieland et al (Table 1, reference 42) with the results obtained here.

Isotope	$v'-v''$	Ref. 42 (cm^{-1})	this work ^a (cm^{-1})	Δ (cm^{-1})
¹²⁷ I ₂	4-13	24544.0	24542.56	1.44
	4-14	24442.0	24439.94	2.06
	4-15	24340.5	24339.12	1.38
	3-15	24240.5	24238.9	1.60
	2-15	24140.5	24138.6	1.90
	1-16	23940.5	23939.5	1.0
	1-17	23843.5	23842.4	1.1
	8-25	23830.5	23830.66	-0.16
	7-24	23814.0	23814.01	-0.01
	0-17	23742.5	23741.8	0.70
	0-18	23647.5	23646.55	0.95
	0-19	23554.0	23553.18	0.82
	1-23	23301.0	23299.65	1.35
	3-26	23257.0	23255.4	1.60

Table V-8 continued

Isotope	$v'-v''$	Ref. 42 (cm^{-1})	this work ^a (cm^{-1})	Δ (cm^{-1})
$^{129}\text{I}_2$	4-14	24448.5	24450.04	-1.54
	4-15	24349.5	24349.8	-0.80
	3-15	24250.5	24250.7	-0.20
	3-16	24152.0	24152.31	-0.30
	0-14	24050.5	24051.05	-0.55
	1-16	23952.0	23952.65	-0.65
	1-17	23856.0	23856.05	-0.05
	1-18	23760.5	23761.3	-0.80
	0-17	23755.5	23755.82	-0.32
	0-18	23660.5	23661.05	-0.55
	0-19	23568.0	23568.14	-0.14
	0-20	23476.5	23477.11	-0.61
	2-25	23249.5	23250.28	-0.78
3-27	23192.5	23193.78	-1.28	

^aB state values from Luc [32]; $^{129}\text{I}_2$ values
calculated using $^{129}\rho = 0.99221$

*

also agreed well. However some of their emission bands, primarily ones assigned to high v_E levels, could not be fit into this E+B scheme unless very large experimental errors were assumed.

Of the remaining excited states, the γ bands were the clearest and strongest progressions observed. These bands were best observed using pump levels near the B state dissociation limit, however they could be observed from pump levels somewhat lower in the B state potential well. The number of rotational terms used to obtain constants for the γ levels of $^{127}\text{I}_2$ ranged from 26 at low v_γ to 7 at $v_\gamma = 12$. For $^{129}\text{I}_2$ the number of terms varied between 7 and 12 for each vibrational level. The molecular constants for the γ vibrational levels are given in Table V-9. Figure V-8 illustrates a typical spectrum of the α , β and γ bands for $^{129}\text{I}_2$.

The γ +B progressions, like the E state, showed only P and R lines and exhibited no evidence of a Q branch; the Q branch may have been too weak to observe. The molecular constants for the γ state are given in Table V-10. The first member of the γ progression was sufficiently strong to be assigned to $v_\gamma = 0$ by inspection. This vibrational numbering was confirmed by least squares fits to equations V-12 and V-13.

The γ series was not observed by either Cunha et al [49] or Williamson [50]. This was probably due to their use

Table V-9. Term values and rotational constants (cm^{-1}) for the γ state of I_2

v	$^{127}\text{I}_2$		$^{129}\text{I}_2$	
	$T_0(v', J' = 0)^a$	$B_v \times 10^2$	$T_0(v', J' = 0)^a$	$B_v \times 10^2$
0	41561.82(28) ^b	1.9685(73) ^b	41562.63(33) ^b	1.95(13) ^b
1	656.12(09)	1.9679(26)	655.95(30)	1.838(76)
2	750.32(12)	1.9624(34)	749.52(36)	1.957(90)
3	843.89(20)	1.9626(52)	843.23(93)	1.98(34)
4	937.86(15)	1.9518(44)	935.51(36)	1.886(89)
5	42030.58(20)	1.9512(53)	42027.64(38)	1.916(93)
6	123.57(53)	1.959(12)	118.76(19)	1.957(52)
7	215.33(20)	1.977(17)	211.11(40)	1.94(12)
8	307.43(19)	1.951(11)	302.10(45)	1.98(13)
9	399.06(20)	1.944(11)	394.48(40)	1.78(13)
10	490.33(19)	1.950(15)	484.13(31)	1.955(87)
11	581.82(30)	1.957(23)	574.31(33)	1.990(93)
12	672.56(34)	1.917(24)		

^aRelative to $v'' = 0, J'' = 0$ in the X state

^bNumbers in parentheses are errors on the last two decimal places in the value.

Table V-10. Vibrational and rotational constants (cm^{-1})
for the γ excited state

	$^{127}\text{I}_2$		$^{129}\text{I}_2$	
T_e	41621.29	$\pm .20$	41621.29	$\pm .20$
ω_e	95.01	$\pm .14$	94.27	$\pm .14$
$\omega_e x_e$	0.222	$\pm .027$	0.218	$\pm .027$
$\omega_e y_e \times 10^4$	28	± 14	27	± 14
$B_e \times 10^2$	1.9702	$\pm .0027$	1.9397	$\pm .0027$
$\alpha_e \times 10^5$	2.72	$\pm .68$	2.66	$\pm .66$
$r_e = 3.6721 \pm .0025 \text{ \AA}$				

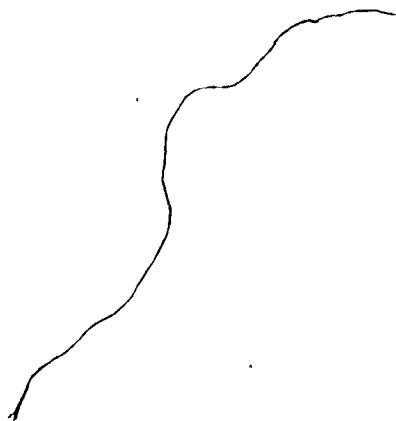


Figure V-8. α , β and γ bands of $^{129}\text{I}_2$.
The B state pump level for the α , β and γ sets
is 0-72 R(1) at $20023.0018 \text{ cm}^{-1}$. The γ' bands
are pumped from the B state level 0-75 R(18)
at $20022.9199 \text{ cm}^{-1}$ ($T = 20035.4821 \text{ cm}^{-1}$)

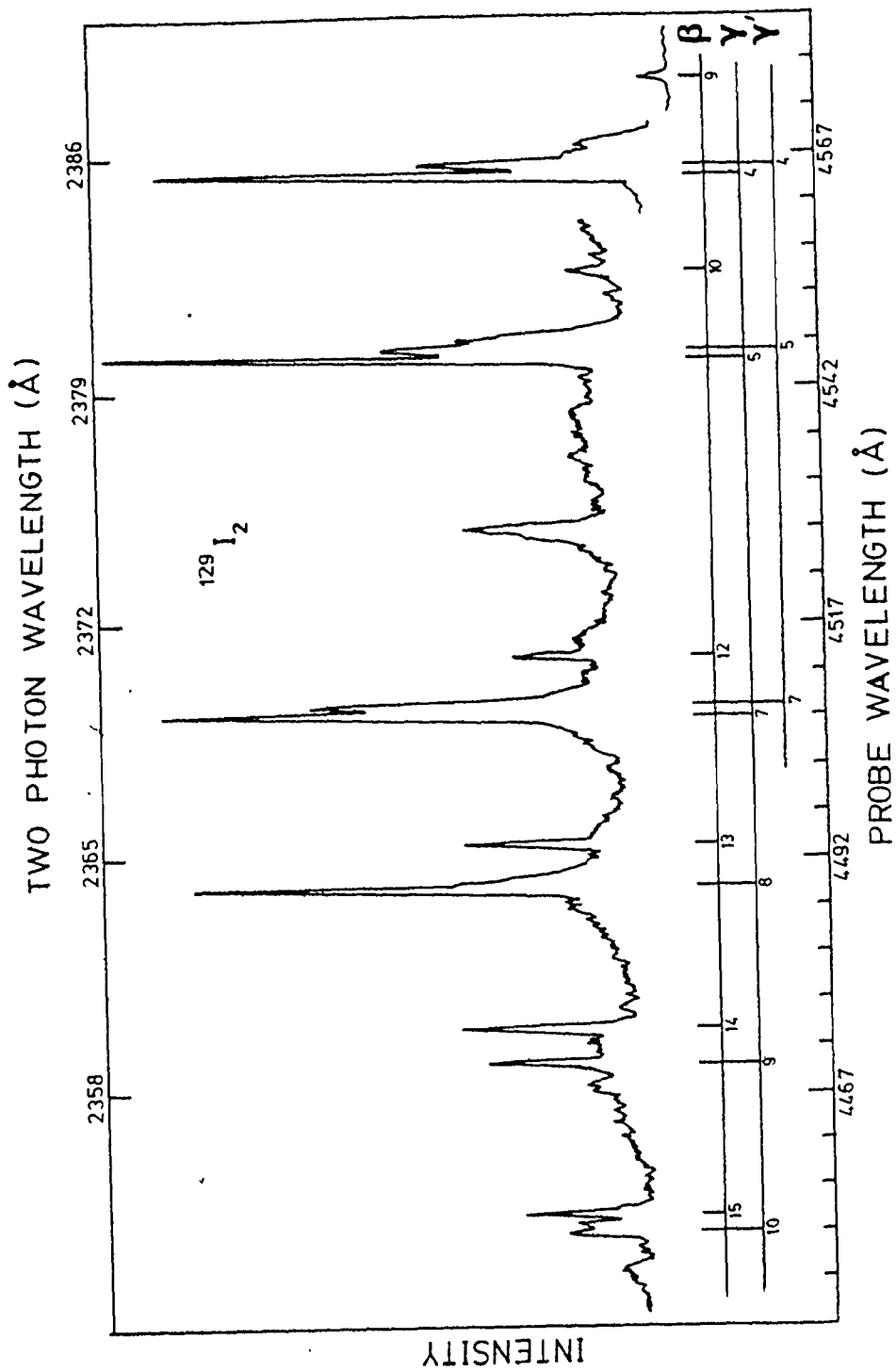
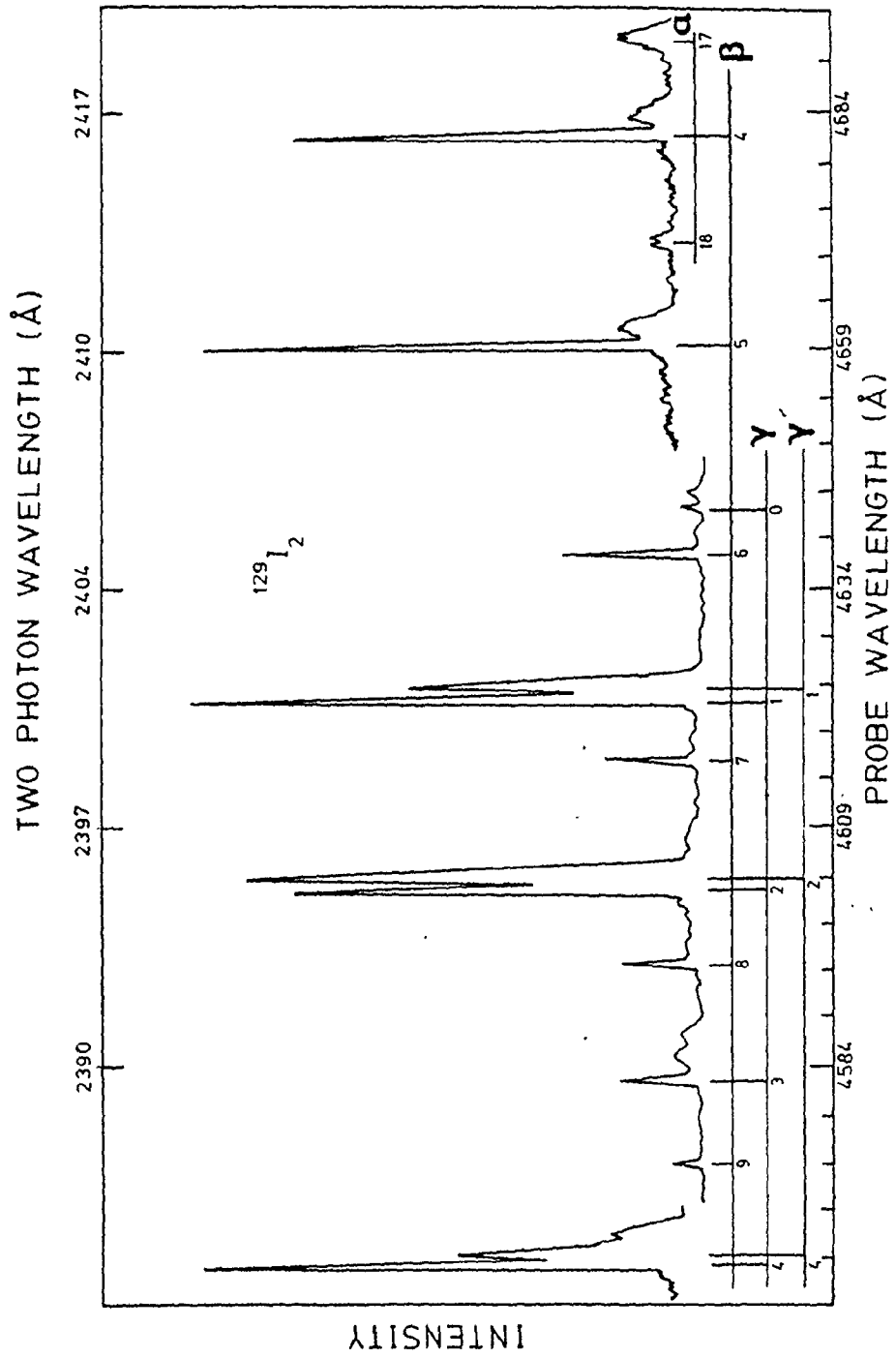


Figure V-8 continued



of pump levels with low v_B values. In the latter work Williamson observed the broadband fluorescence without the use of cut-off filters and the large background noise could obscure bands of lower intensity than the extremely strong E state series.

In their earlier work on these states DK [9] noted irregularities in the T_0 and B_v values for certain levels of the γ state, particularly γ_6 . This work also indicated that the term values showed considerable scatter, particularly levels with $v_\gamma \geq 6$. With the large number of overlapping states in this region it was not unreasonable that some form of rotational perturbation was the likely cause of this scatter.

2.4 Results for the β , α and δ states.

The remaining excited states can only be accessed using vibrational levels within 30 cm^{-1} of the B state dissociation limit. They were difficult to observe experimentally due to their weak nature. The data on both isotopes was fragmentary and the rotational analysis was incomplete. These bands were observed the best in only a few runs based on a limited number of pump lines.

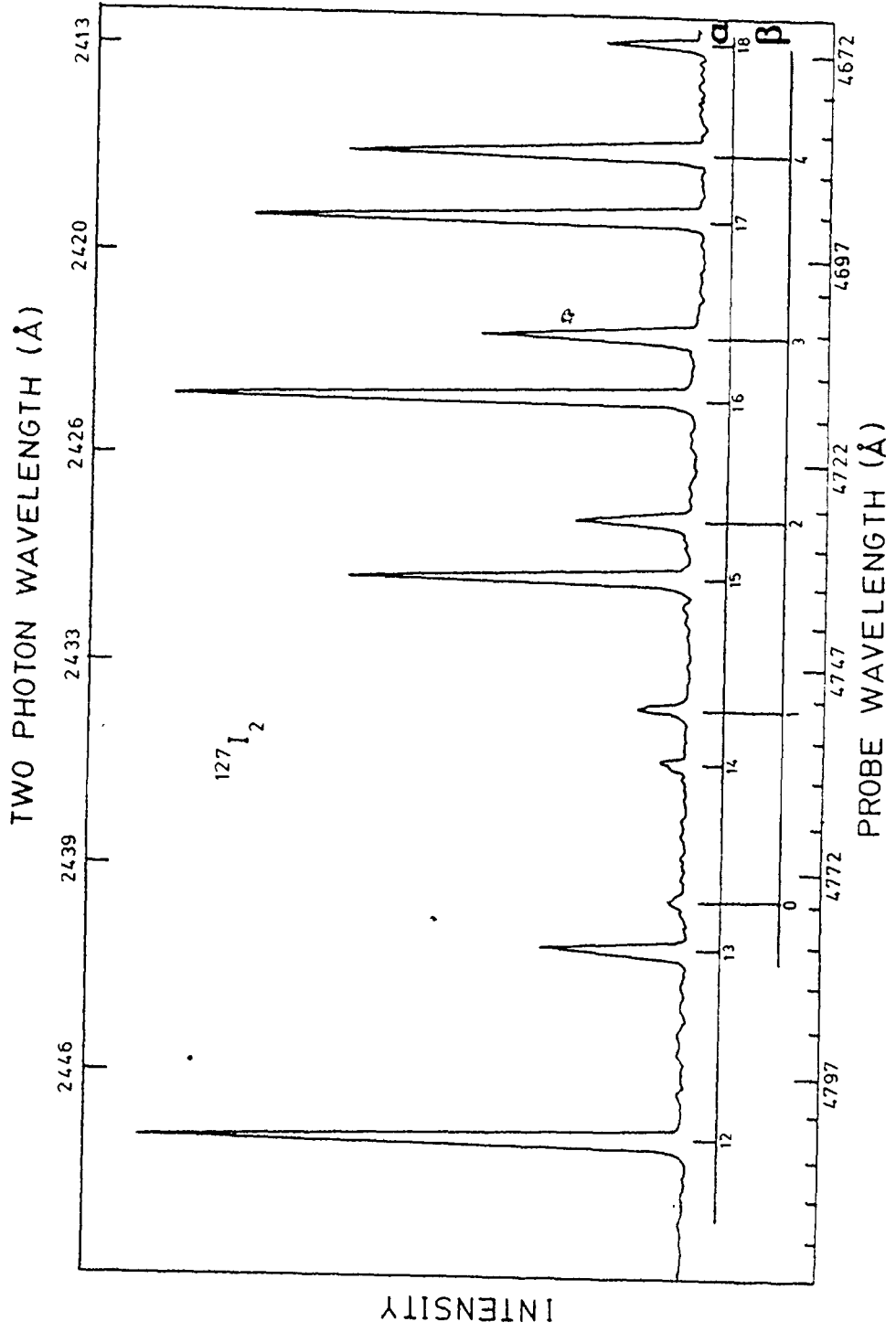
For $^{127}\text{I}_2$ all three series were observed, with similar relative intensities, in spectra based on the following pump levels in the B state; $R_{77}(18)$, $R_{77}(25)$, $R_{78}(11)$, $P_{78}(13)$, $R_{78}(17)$ and $R_{78}(18)$. In general only

the B state levels with $v_B = 77$ and 78 produced good spectra containing α , β and δ progressions. Above or below this point the progressions became increasingly weaker. The α bands were observed using the $R_{69}(24)$ pump level but they were very weak and noisy. Sharp transitions to the α , β and δ bands were observed using $v_B = 81$ as the pump level; however, these bands were again very weak and the relative intensities of the series were different. The weakness of these transitions using this pump level was probably due in part to the low probability of populating B state levels so close to dissociation. Figure V-9 shows α and β bands in $^{127}\text{I}_2$.

For $^{129}\text{I}_2$ the observation of levels, other than the E state and γ state progressions, was found to be very difficult. Using the pump lines $P_{71}(19)$, $R_{72}(0)$, $P_{72}(11)$ and $P_{73}(22)$, spectra could be generated in the $21300\text{-}22500\text{ cm}^{-1}$ probe region. These spectra showed the $\gamma_0\text{-}\gamma_{11}$ bands plus a series of sharp β bands. A different series of weaker bands in the $20500\text{-}21300\text{ cm}^{-1}$ probe region were generated using the pump lines $P_{71}(23)$, $R_{72}(28)$, $R_{73}(18)$ and $P_{73}(22)$. These bands occur in the same region as the α bands for $^{127}\text{I}_2$ and were tentatively identified as α bands in $^{129}\text{I}_2$. No bands could be identified as the δ series for $^{129}\text{I}_2$.

The pump levels in the B state that generated α , β and δ bands were all of low J. These pump levels produced only single unresolved lines in the excited state transitions.

Figure V-9. α and β bands of $^{127}\text{I}_2$. The B state pump level is 0-78 R(11) at $20035.2420 \text{ cm}^{-1}$ (T = 20040.27 cm^{-1})



As a result, the rotational terms for the upper state were obtained over a limited range of J . This produced relatively large uncertainties in the derived constants for these states.

The molecular constants for the vibrational levels of the β state are listed in Table V-11. In $^{127}\text{I}_2$ the constants for the $v_\beta = 0, 9, 11$ bands were all determined from two-point fits to a polynomial in $J(J + 1)$ as they were not observed on all the traces. The β_{10} band was too weak to be observed at all. The probe laser gain profile expired at β_{15} which was partially overlapped by γ_{10} (see Figure V-8). In $^{129}\text{I}_2$ the lowest band that was observable above the background was β_5 . The bands with $v_\beta = 12, 16$ were established using a two point fit to a polynomial in $J(J + 1)$. The β series in $^{129}\text{I}_2$ had an intensity minimum at β_{11} . The rotational constants for the β bands were determined quite poorly from the slope, with so few data points of such low J value. The term values T_0 that were calculated from the intercepts of these lines should be somewhat better determined. As such, application of the isotope effect using equation V-12 should work in establishing the absolute vibrational numbering of the state. The numbering in Table V-11 was established as the correct one and the vibrational and rotational constants determined from these fits are given in Table V-12.

Table V-11. Term values and rotational constants (cm^{-1}) for the β state of I_2

v	$^{127}\text{I}_2$		$^{129}\text{I}_2$	
	$T_0(v', J' = 0)^a$	$B_V \times 10^2$	$T_0(v', J' = 0)^a$	$B_V \times 10^2$
0	40975.7(1.4) ^b	1.6(1.2) ^{b,c}		
1	41078.21(64)	2.40(34) ^b		
2	181.78(65)	2.14(28)		
3	284.99(53)	1.68(21)		
4	385.87(80)	1.91(23)	41385.38(71) ^b	1.86(21) ^b
5	488.68(38)	1.90(11)	485.63(56)	1.98(17)
6	589.93(65)	2.07(18)	585.74(40)	2.08(13)
7	692.27(48)	1.74(14)	686.15(48)	2.08(18)
8	792.11(80)	1.95(22)	786.67(82)	2.22(33)
9	892.87(89)	2.22(32) ^c	886.4(1.1)	2.06(48)
10				
11	42092.44(89)	1.42(32) ^c		
12	191.34(90)	1.83(23)	42182.07(72)	0.8(9) ^c
13	288.71(32)	1.636(80)	278.7(1.2)	2.17(43)
14	386.58(50)	1.83(13)	376.62(20)	2.096(73)
15			473.48(32)	2.00(12)
16			569.68(72)	2.02(93) ^c

Table V-11 continued.

^aRelative to $v'' = 0$, $J'' = 0$ in the X state.

^bNumbers in parentheses are errors on the last two decimal places in the value.

^cTwo point fit, error is experimental.

Table V-12. Vibrational and rotational constants (cm^{-1})
for the β excited state

	$^{127}\text{I}_2$	$^{129}\text{I}_2$
T_e	41029.74 \pm .56	41029.74 \pm .56
ω_e	104.19 \pm .14	103.37 \pm .14
$\omega_e x_e$	0.2212 \pm .0072	0.2178 \pm .0071
$B_e \times 10^2$	1.973 \pm .088	1.943 \pm .087
$\alpha_e \times 10^5$	3.7 \pm 7.7	3.6 \pm 7.5
$r_e = 3.669 \pm .082 \text{ \AA}$		

The identification of the α bands in $^{129}\text{I}_2$ relied on the similarity of the term values obtained to those of $^{127}\text{I}_2$, and on the similarity in the intensity distribution for both species. The α bands for both isotopes showed an intensity minimum at the band labeled $\nu_\alpha = 14$. The constants for the vibrational levels, except for the lowest level, were determined from between 6 and 8 rotational terms with J values between 8 and 19 for $^{127}\text{I}_2$ and 19 and 29 for $^{129}\text{I}_2$. The constants for the vibrational levels of the α state are listed in Table V-13. If the identification of the α bands in $^{129}\text{I}_2$ was correct, the isotopic effect established that the first band observed was $\nu_\alpha = 8(\pm 2)$. Using this numbering the vibrational and rotational constants for the α state were established and are listed in Table V-14. The uncertainty in the vibrational numbering does mean however that the value of T_e could be in error by $\pm 200 \text{ cm}^{-1}$.

The δ bands were the weakest and least understood of the progressions observed. In the weaker spectrum of $^{129}\text{I}_2$ no transitions could be identified as belonging to this series. With no data from the isotope available, the lowest observed level in $^{127}\text{I}_2$ at $T_0 = 41732 \text{ cm}^{-1}$ was arbitrarily assigned to $\nu_\delta = 0$. Eight δ bands were observed with an intensity maximum at δ_3 . Figure V-10 illustrates a region containing γ and δ bands in $^{127}\text{I}_2$. These bands phased in and out with the γ_2 - γ_7 bands. The δ_3 band was almost coincident with γ_5 . Between 4 and 6 pump lines were used,

Table V-13. Term values and rotational constants (cm^{-1}) for the α state of I_2

v	$^{127}\text{I}_2$		$^{129}\text{I}_2$	
	$T_0(v', J' = 0)^a$	$B_v \times 10^2$	$T_0(v', J' = 0)^a$	$B_v \times 10^2$
8	40438.0(1.5) ^b	0.9(1.2) ^{b,c}		
9	539.14(50)	2.32(27) ^b	40533.0(2.0) ^b	1.78(27) ^b
10	642.62(25)	1.93(13)	634.60(77)	1.88(15)
11	744.77(62)	1.96(26)	735.85(82)	1.92(16)
12	846.82(44)	1.99(18)	837.83(52)	1.848(99)
13	948.09(67)	2.22(36)	939.12(70)	1.76(13)
14	41049.46(61)	2.11(32)		
15	149.83(32)	2.20(13)	41141.1(1.8)	1.39(30)
16	249.90(22)	1.904(89)	238.2(1.8)	1.79(32)
17	349.26(76)	1.73(29)	337.65(90)	1.77(15)
18	449.22(56)	1.94(24)	437.4(1.2)	1.64(20)

^aRelative to $v'' = 0, J'' = 0$ in the X state

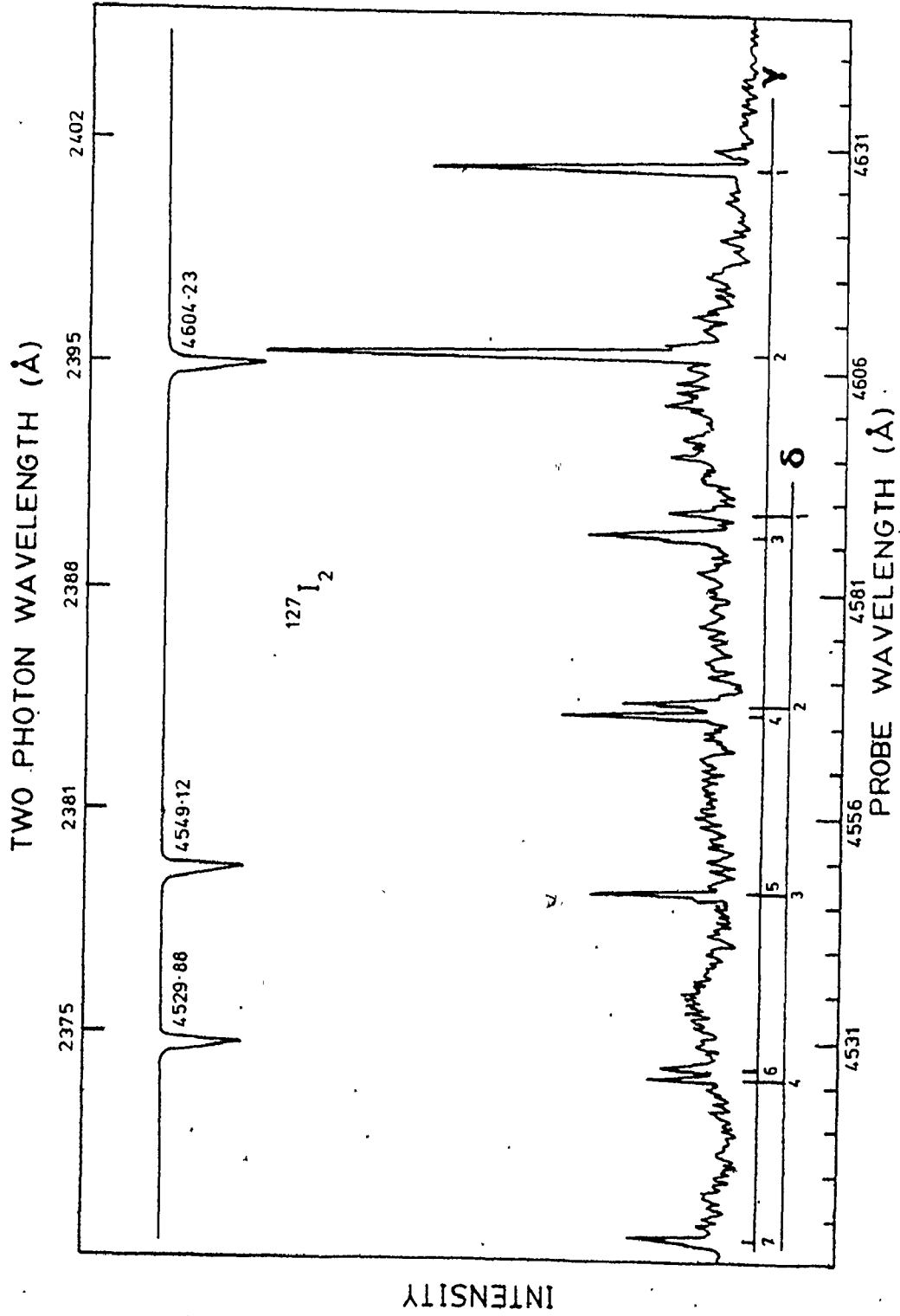
^bNumbers in parentheses are errors in the last two decimal places in the value.

^cTwo point fit, error is experimental.

Table V-14. Vibrational and rotational constants (cm^{-1})
for the α excited state

	$^{127}\text{I}_2$	$^{129}\text{I}_2$
T_e	39648.6 \pm 3.5	39648.6 \pm 3.5
ω_e	107.15 \pm .53	106.31 \pm .53
$\omega_e x_e$	0.218 \pm .019	0.214 \pm .019
$B_e \times 10^2$	2.06 \pm .20	2.03 \pm .20
$\alpha_e \times 10^4$	1.1 \pm 1.4	1.1 \pm 1.4
$r_e = 3.59 \pm .16 \text{ \AA}$		

Figure V-10. γ and δ bands of $^{127}\text{I}_2$. The B state pump level is 0-81 R(1) at $20042.1725 \text{ cm}^{-1}$. The Fe calibration spectrum is also illustrated



INTENSITY

with J values between 0 and 25, to establish the δ bands. Because of the band's weakness and the fact it was heavily overlapped, precise rotational terms for the δ bands were difficult to establish. Table V-15 gives approximate constants for the vibrational levels of the δ state in $^{127}\text{I}_2$. The vibrational interval was reasonably constant at 100 cm^{-1} . Not unexpectedly, the rotational constants B_v were quite widely scattered. Table V-16 gives the best constants that can be determined from this data. The value of B_e listed in Table V-16 is the mean of the observed B_v values.

2.5 Discussion

The E state was sufficiently well known from this work that an RKR potential function could be constructed. The turning points for the lower vibrational levels are tested in Table V-17. Tellinghuisen has developed a Morse function approximation [45] to the E state which agreed well with this potential. In his Morse function R_e was adjusted such that his result agreed with the observed E+B structured continuum of Rousseau and Williams [46]. This adjustment gave a value of $R_e = 3.649 \text{ \AA}$ which compared well with the value of $R_e = 3.6411 \text{ \AA}$ obtained in this work.

Despite the large amount of data on the excited states of iodine it is difficult to identify any one state satisfactorily. Even the E state, which is well known in emission

Table V-15. Approximate term values and rotational constants
(cm^{-1}) for the δ state of $^{127}\text{I}_2$

v	$T_0(v', J' = 0)^a$	$B_v \times 10^2$
0 ^b	41732 \pm 1	1.4 \pm .3
1	41832 \pm 1	1.5 \pm .3
2	41931 \pm 1	1.5 \pm .3
3	42031 \pm 1	1.7 \pm .3
4	42129 \pm 1	1.7 \pm .3
5	42228 \pm 1	2.0 \pm .3
6	42328 \pm 1	1.8 \pm .3
7	42425 \pm 1	1.5 \pm .3

^aRelative to $v'' = 0, J'' = 0$ in the X state

^bArbitrary numbering

Table V-16. Approximate vibrational and rotational constants (cm^{-1}) for the δ excited state of $^{127}\text{I}_2$

	$^{127}\text{I}_2$
T_e	41789
ω_e	100.2
$\omega_e x_e$	0.13
$B_e \times 10^2$	1.63

$r_e = 4.0 \text{ \AA}$

Table V-17. RKR potential turning points for lower vibrational levels of the $^{127}\text{I}_2$ E state

v	G_v (cm^{-1})	R_{\min} (\AA)	R_{\max} (\AA)
0	50.9	3.565	3.710
1	152.4	3.519	3.770
2	253.3	3.488	3.813
3	353.9	3.464	3.849
4	453.9	3.444	3.881
5	553.5	3.427	3.911
6	652.7	3.411	3.938
7	751.4	3.396	3.964
8	849.7	3.383	3.988
9	947.5	3.370	4.011
10	1045.0	3.359	4.034
12	1238.6	3.336	4.075
14	1430.6	3.315	4.114
16	1621.0	3.296	4.151
18	1809.9	3.277	4.185
20	1997.2	3.258	4.218
22	2183.2	3.240	4.248
24	2367.7	3.222	4.278
26	2550.8	3.203	4.305
28	2732.6	3.185	4.331
30	2913.2	3.167	4.356

[42,46] and from this work, has a somewhat ambiguous final identification. In single electron configuration, Mulliken [18] has proposed that the E state is either 2242 $^1\Sigma_g^+(0_g^+)$ or 1432 $^3\Pi_g(0_g^+)$. Both Mulliken and Wieland et al [42] favour the identification of the E state as $^3\Pi_g(0_g^+)$. The E→B emission is thus identified as 1432 $^3\Pi_g(0_g^+) \rightarrow 2431 \ ^3\Pi_u(0_u^+)$. The corresponding absorption, which should be allowed, has not been observed in high temperature spectra [18]. This lack of observation can be used to favour the identification of the E state as $^1\Sigma_g^+(0_g^+)$. Das and Wahl [23] have theoretically calculated that the $^3\Pi_g$ state that must correspond to the E state, in case (a) approximation, is almost exclusively a $^1\Sigma_g^+$ state. This has been used to explain the lack of an absorption spectrum. It is argued that the E→B emission takes place in a region where the B state undergoes configuration mixing with $^1\Sigma_u^+$ and $^3\Sigma_u^-$ states. This mixing produces the observed intensity. However in the present experiments, absorption from E→B has been produced over a wide range of B state vibrational levels and the lack of observation of a high temperature absorption spectrum may just be due to a lack of intensity.

Upon dissociation, the $^3\Pi_g(0_g^+)$ state has been correlated with a $I^-(^1S)$ atom and either a $I^+(^1D)$ atom or a $I^+(^3P_0)$ atom [18]. The former choice conforms to case (c) rules, the latter will occur if there is conservation of spin multiplicity on dissociation.

Identification of the remaining four states was not as straightforward. An important question existed as to why these states were accessible only from B state levels with $v_B > 70$, which have outer turning points at $r > 7 \text{ \AA}$. The transitions from the B state to the α , β , γ and δ states appeared in the spectra at about two orders of magnitude less intensity than the E+B transition. The effects of changes in the iodine vapor pressure and the presence of an inert buffer gas have been examined for these states and the results are given in Sec.4, Chap. V. Like the E state, the β and γ states have large values for the internuclear separation and low values for the vibrational interval. This was described as being typical of the behaviour of ion-pair states [18]. The α state lay approximately 1700 cm^{-1} lower in energy than these other states and may not have corresponded to an ion-pair state. Tai et al [53] and Lehman et al [54] have each identified a 0_g^+ state in the 36000 cm^{-1} region. The fragmentary δ bands could have corresponded to a long extrapolation ($n \sim 50$) from the vibrational levels in the state observed by Tai. Since the δ state was only observed for one isotope of iodine, the absolute vibrational numbering of these levels could not be determined.

The $D' \text{ } ^3\Pi(2_g)$ state, which is the upper state of the 3400 \AA emission bands, could be either the α or β state, more probably the β state. Studies have suggested $T_e = 40,640 \text{ cm}^{-1}$

for D' [43,44]. This was within 400 cm^{-1} of T_e for the β state. Vibrational analysis of the emission bands [43] has given $\omega_e = 103.97 \text{ cm}^{-1}$ and $\omega_e x_e = 0.205 \text{ cm}^{-1}$ which were in good agreement with the values of $\omega_e = 104.19 \text{ cm}^{-1}$ and $\omega_e x_e = 0.2212 \text{ cm}^{-1}$ obtained here for the β state. Guy et al [44] found no evidence of states lying lower than D' and thus attempted to assign the α state to D'. Their assignment, based on the original constants for the α state [9] before the isotope was used to establish the correct numbering, did not appear unreasonable. But according to the new molecular constants for the α state, there were larger differences and the value of T_e lay almost 1000 cm^{-1} below the T_e value determined in the emission study of the D' state.

The emission study of the D' state gave a value of $\Delta T_e = 30341.0 \text{ cm}^{-1}$ for the transition. The value of $T_e = 41030 \text{ cm}^{-1}$ for the β state would yield $T_e = 10689 \text{ cm}^{-1}$ for the lower state. If this lower state dissociated to $2^2P_{3/2} + 2^2P_{3/2}$ atoms as does the X state, a value of $D_e'' = 1858 \text{ cm}^{-1}$ would result. The lower state has been identified as the A' $3\Pi(2u)$ state [18,43]. The above value of D_e'' was significantly larger than Ashby's et al [129] value of 1641 cm^{-1} for the A $3\Pi(1u)$ state, another possible lower state. The value of $T_e = 10689 \text{ cm}^{-1}$ was also lower than Ashby's value of $T_e = 10906 \text{ cm}^{-1}$ for the A state and may confirm the lower state of this emission as A' not A. Despite all this, there was one drawback with the

identification of the D' state with our β state.

Tellinghuisen [43] had observed the $v = 23$ level of A' state at $\sim 2025 \text{ cm}^{-1}$, significantly above the value of $D_e'' = 1858 \text{ cm}^{-1}$ calculated. There was no clear answer to this problem.

The D' $^3\Pi(2g) - B \ ^3\Pi(0_u^+)$ transition would violate the case (c) selection rule of $\Delta\Omega = 0, \pm 1$. Guy et al [44] postulated that the high lying vibrational levels of the B state were perturbed by the $1u$ states that should lie in this region. This perturbation would produce a weak transition and may account for the transitions from the high lying levels of the B state to the α , γ and δ states as well. Unfortunately no evidence of a major perturbation in the high lying vibrational levels of the B state in either isotope has been found [13,14]. A small rotational perturbation around $J = 13$, $v = 74$ in $^{129}\text{I}_2$ may be present. This corresponded in energy to $J = 20$, $v = 73$ in $^{127}\text{I}_2$ which was below the best pump levels for producing excited state transitions in $^{127}\text{I}_2$.

Guy et al [44] have ordered the ion-pair states of iodine in the same order as the states occur in the ion. That is the 6 states arising from $\text{I}^+(^3\text{P}_2)$ should lie lowest in energy, with the 6 states from $\text{I}^+(^3\text{P}_{1,0})$ at higher energy and the 6 states arising from $\text{I}^+(^1\text{D})$ higher still. This ordering appears arbitrary when it is noted that because of

strong spin-orbit coupling in I^+ , its low 3P_0 and 3P_2 states are considerably mixed with 1S and 1D respectively [18].

Das and Wahl's calculations [23] have shown that configurational mixing between the D $^1\Sigma_u^+$, $^3\Pi_u$ and $^3\Sigma_u^-$ states was strongly dependent on the internuclear separation. The dependence of this mixing on r , and the fact that intensities of electronic transitions can vary as r is changed, might explain why only pump levels of high v_B were active in producing probe transitions. There is no information on the configurational composition of the electronic wavefunctions of iodine at $r > 7 \text{ \AA}$. To account for the excited states of iodine correctly, it appeared that contribution from many other excited states, in addition to the covalent and ion-pair states already discussed, especially at large r , must be considered. States that adiabatically correlated with atomic Rydberg states needed to be considered. There were 28 molecular states that dissociated into the lowest energy Rydberg combination $I(^2P_{3/2}) + I(6s)(^4P_{5/2})$ which lay $\approx 5013 \text{ cm}^{-1}$ below the lowest pair of ionic dissociation products. As mentioned previously, these Rydberg states may also enter as the states to which molecular states, that would normally correlate with ion-pair states, can short-cut to (as required by the rigorous noncrossing rule) on dissociation [18].

3. Fluorescence Decay Measurements on $^{127}\text{I}_2$ and $^{129}\text{I}_2$

3.1 Introduction

The fluorescence lifetimes and the kinetics involved in the decay from the B $^3\Pi(0_u^+)$ state of iodine have been extensively investigated [131-139]. After excitation, the decay equation can be written as:

$$\frac{d[\text{I}_2^*]}{dt} = -[\text{I}_2^*]/\tau_{\text{rad}} - S[\text{I}_2][\text{I}_2^*] - Q[\text{M}][\text{I}_2^*] - [\text{I}_2^*]/\tau_{\text{nr}} \quad \text{V-14}$$

The term $-[\text{I}_2^*]/\tau_{\text{rad}}$ represents the spontaneous emission with time constant (radiative lifetime) τ_{rad} . The term $-S[\text{I}_2][\text{I}_2^*]$ is due to the self-quenching process and S is the associated rate constant. The next term is foreign gas quenching with rate constant Q and dependence on the concentration of a foreign gas $[\text{M}]$. The last term accounts for non-radiative de-excitation due to spontaneous predissociation, it has a rate constant $1/\tau_{\text{nr}}$ and is a function of v' and J' .

Equation V-14 may be integrated and rewritten to give

$$[\text{I}_2^*] = (\text{constant}) \exp(-t/\tau_{\text{obs}}) \quad \text{V-15}$$

where

$$1/\tau_{\text{obs}} = 1/\tau_{\text{rad}} + S[\text{I}_2] + Q[\text{M}] + 1/\tau_{\text{nr}} \quad \text{V-16}$$

In the limit of $P_{I_2} \rightarrow 0$ and with no foreign quenching gas present, $1/\tau_0$ is defined as $1/\tau_{\text{rad}} + 1/\tau_{\text{nr}}$. Thus:

$$1/\tau_{\text{obs}} = 1/\tau_0 + S[I_2] \quad \text{V-17}$$

Vibrational and rotational energy transfer cross sections and quenching cross sections for iodine in a large number of vibrational levels of the B state have been measured [131-138]. Magnetic quenching of the fluorescence and its dependence on iodine pressure has given independent measurements of the self-quenching cross sections [139].

However, there is only a limited amount of varied information available on the lifetimes of higher lying electronic states of iodine. Rousseau [47], in an attempt to pin down the electronic assignment of the E state, has measured the resolved E+B fluorescence from a single vibrational level in the E state, and obtained a value of $\tau_E = 27 \pm 2$ nsec (measured $\sim 45557 \text{ cm}^{-1}$, $v_E \approx 45$). This particular value was obtained at two different iodine vapor pressures and the lifetime was thus assumed not to be limited by I_2 self-quenching. The E state lifetime has also been measured by Wilkerson at $\tau_E \approx 50$ nsec (unpublished results discussed in a paper by J. Tellinghuisen [45]). It was not stated how this value was obtained or where in the E+B fluorescence it was measured. The D-X emission of iodine has been considered as a candidate for a tunable

ultraviolet laser [128]. With this in mind Callear et al [140] used a high frequency deflection technique to measure the lifetime of the D-X fluorescence at the intensity maximum of the fluorescence spectrum at 3210 Å. They obtained a lifetime of $\tau_D = 15.5 \pm 0.5$ nsec for a single iodine vapor pressure. Sauer et al [141] have studied fast excited state formation and decay in the pulse radiolysis of argon-iodine systems. For iodine alone, they obtained a radiative lifetime of 6.7 nsec for the long wavelength end of the iodine emission at 3200-3450 Å.

To gain further insight into the excited states accessed via these two-photon methods, and to compare the results with the above studies, preliminary measurements were made of the unresolved fluorescence decay from discrete rovibronic levels in the various excited states. Initially as a check on the basic system, measurements were made on a known long-lived level of the B state. An isolated, well-identified line in the single photon spectrum of iodine was measured at room temperature and again at ice temperature with two different photomultipliers. Following these experiments, the molecules were pumped to an intermediate B state level by the pump laser and then excited to the "E state" levels using a 8 ± 2 nsec probe laser pulse. The observed decay curves resulted from reemission from a rotational level in a given vibrational band of the higher

excited state to the B state manifold. All of the observed decay curves from the higher lying electronic states were found to have $1/e$ lifetimes of less than 20 nsec.

3.2 Fluorescence Lifetimes

The unresolved fluorescence decay curves were detected with a sampling oscilloscope triggered by the N_2 laser at 60 Hz. The scope was connected directly to the photomultiplier output via a short shielded cable. The detected signals, other than the B state signals, were extremely weak and noisy. To obtain better data all the signals were averaged using the minicomputer in conjunction with the sampling scope as a signal averager. The minicomputer's D/A converter was used to drive the X deflection on the scope, moving the sampling point across the scope trace in 180 discrete steps. At each step the A/D converter took 10 readings (at 60 Hz) of the fluorescence signal. The 10 readings were stored as a running average of the value at a given point on the display. In a given run, between 20 and 50 scans of the oscilloscope display were averaged, depending on the signal strength and the noise level. This resulted in between 200 and 500 measurements being averaged for each of the 180 steps across the screen. The final results were stored on a disk.

The noise on the oscilloscope trace appeared to be from two sources, pick-up in the electronics as a whole of

the RF noise from the N_2 laser's spark-gap, and a ringing in the connecting cable that could not be eliminated. A second braided copper shield was pulled over the signal cable in an attempt to cut down the noise, with only limited success. Since most of these signals were observed at the maximum available photomultiplier tube voltage, spike noise from the photomultiplier itself was also a problem. To compensate as much as possible for the noise, a background scan was taken immediately after each run, at identical conditions, with the laser beams blocked off at the cell windows. This background scan was then subtracted off the signal file before further processing.

The B state single photon spectrum was calibrated using Gerstenkorn and Luc's Atlas [29]. A single sharp line in $^{127}I_2$ at $17210.9494 \text{ cm}^{-1}$ was identified as 0-13 P(12) at $17210.9453 \text{ cm}^{-1}$ and 0-13 R(17) at $17210.9590 \text{ cm}^{-1}$. The fluorescence decay from this level (measured through a Corning 2-62 filter) was on the order of 200-400 nsec. The decay curves, recorded at two temperatures, 0°C and 23.2°C , were analysed using a simple, single exponential program. The lifetimes were obtained from a linear least squares fit to the logarithms of the data.

When it was observed that the decay curves of the higher excited states were of the same order as the exciting laser pulse at $8 \pm 2 \text{ nsec}$, a different analysis method was needed. In order to obtain an undistorted measure of the

lifetime it was necessary to deconvolve the effect of the excitation pulse width from the data. A simple logarithmic fit to the data was no longer satisfactory.

The observed fluorescence signal $f(t)$ can be considered as a convolution integral of an (effective) apparatus response function $e(t)$ and the true fluorescence decay $h(t)$.

$$f(t) = e(t) * h(t)$$

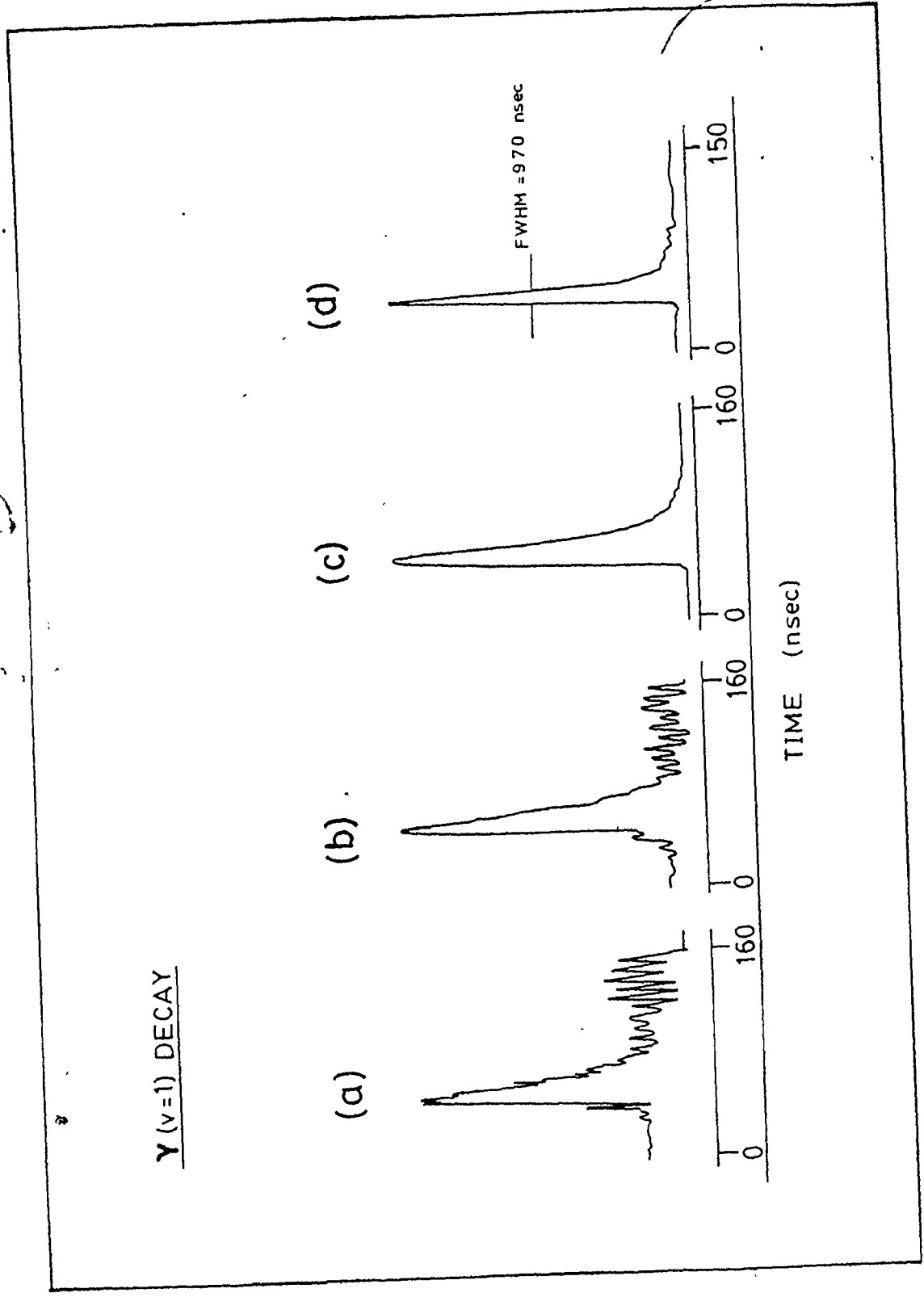
Deconvolution using the Fourier transform appears to be the most direct way of obtaining $h(t)$. If the Fourier transform of each function is designated as $F(\nu)$, $E(\nu)$ and $H(\nu)$, it is well known that in Fourier space, $H(\nu) = F(\nu)/E(\nu)$. The desired impulse response $h(t)$ of the fluorescence system is directly available from the inverse transform, without having to assume any specific form of the decay curve. If this division is attempted, it is found that inclusion of the higher frequency terms in $H(\nu)$, when it is transformed back, made the signal $h(t)$ completely unintelligible. This results from the fact that the first few Fourier coefficients in $H(\nu)$ result from ratios of values that are precisely determined by the experiment. The higher frequency coefficients of $H(\nu)$ are practically the result of zero/zero division. They are mainly determined by the statistical fluctuation in the measured time function and the high frequency noise on the pulse. A single large value in the

high frequency range will completely mask the shape of the deconvolved response function $h(t)$ in the time domain. This problem and a possible solution to it, that of curve fitting in Fourier space, is discussed in reference 116.

The approach used here was to start from an assumed fluorescence decay curve and successively improve it until a satisfactory comparison between it and the observed decay was obtained. The experimental decay data and a measured laser pulse were used as input into a program where they were appropriately scaled (a typical laser pulse is shown in Figure V-11d). It was found that even with background subtraction the ringing signals from the cable could not be completely eliminated from the experimental data. To further smooth the observed signals the data was passed through a variable digital filter to remove most of the noise before further processing. A single exponential decay of known lifetime was then constructed. The assumed decay curve was convolved with the measured laser pulse using Fourier transform techniques. This calculated fluorescence function was then compared to the experimental decay. To do the comparison the two curves were first area normalized to the area of the measured peak. Since the recorded scope traces did not all have the same lead time (lead time is the dead period between the scope-trigger and the actual occurrence of the pulse on the trace), the peak maxima of the two curves

Figure V-11. Fluorescence decay curve of the γ ($v = 1$) band

- (a). Observed signal after background subtraction
- (b). Signal smoothed by digital filter
- (c). Calculated decay ($\tau = 7.0$ nsec)
- (d). Laser pulse



were made coincident before any comparison was done. The sum of the squares of the differences between the two curves was then calculated for points from slightly beyond the peak maxima to the end of the data (the point slightly beyond the maximum was chosen to eliminate any noise spikes on the top of the peak). Because the overlap of the two peaks was important, the program allowed the two peaks to shift relative to each other until, for a given fixed lifetime, a minimum was found in the differences. The lifetime was then incremented by a fixed amount and the process repeated. This was continued until a minimum in the sum squared differences was obtained. The results were then double-checked by displaying on the terminal the final deviations, followed by the observed and calculated decay curves. Figure V-11 shows the decay from the γ_1 band of $^{129}\text{I}_2$, the digitally smoothed data, and the calculated decay curve ($\tau = 7 \pm 2$ nsec).

3.3 Results and Discussion

The unresolved fluorescence from the $17210.9494 \text{ cm}^{-1}$ line in the B state of $^{127}\text{I}_2$ was measured at two iodine vapor pressures; 0°C , $P_{\text{I}_2} = 0.033 \text{ mm Hg}$, and 23.2°C , $P_{\text{I}_2} = 0.284 \text{ mm Hg}^\dagger$. The lifetimes measured were

[†]Iodine vapor measures were calculated from the relationship $\log_{10} P_{\text{atm}} = 13.3740 - (3518.2/T) - 2.018 \log_{10} T$ [142].

$\tau(0^\circ\text{C}) = 469 \pm 17$ nsec and $\tau(23.2^\circ\text{C}) = 220 \pm 10$ nsec.

Using equation V-17, the concentration of I_2 molecules (in molecules/ m^3) can be expressed as $[\text{I}_2] = P_{\text{I}_2}/kT$, where P_{I_2} is the vapor pressure of iodine (Newtons/ m^2), k is Boltzmann's constant (Joules/ $^\circ\text{K}$) and T is the temperature of the vapor phase (in $^\circ\text{K}$). The rate constant S can be expressed in terms of an effective collision cross section σ_S^2 (m^2) as:

$$S = \sigma_S^2 [8\pi RT/\mu] \quad \text{V-18}$$

where R is the gas constant (Joules $^\circ\text{K}^{-1}\text{kmole}^{-1}$) and μ is the reduced mass of the colliding particles (in kg/kmole). The results of these studies were not extensive enough to determine τ_0 and σ_S^2 values directly. Broyer et al [137] have measured the $v' = 13$, $J' = 11$ level of the B state and given the values of $\tau_0 = 1260 \pm 60$ nsec and $\sigma_S^2 = 65.2 \pm 3 \text{ \AA}^2$. The experimental observations in this work were checked by calculating τ_0 values from the τ_{obs} values using Broyer's [137] result for σ_S^2 : at 0°C , $\tau_0 = 580$ nsec; at 23.2°C , $\tau_0 = 1162$ nsec. The fact that the short lifetimes ($\tau < 20$ nsec) obtained for the excited states were not instrument limited was indicated by the following observations: The results in this work agree, with Broyer's results (within large error limits); measurements on different photomultipliers were identical; and the system could measure long lifetimes

(~ 470 nsec) and short laser pulses (~ 9 nsec).

Lifetime measurements were made for both $^{127}\text{I}_2$ and $^{129}\text{I}_2$ on the α , β , γ and E bands. The α_{17} transition was measured in $^{127}\text{I}_2$ and α_{18} in $^{129}\text{I}_2$. The levels β_4 , β_5 and β_6 were measured in $^{127}\text{I}_2$ and β_7 in $^{129}\text{I}_2$. The γ_1 level was studied in both isotopes. The E state levels studied were E_0 , E_2 and E_{19} again in both isotopes. The α , β and γ bands were accessed from pump levels near dissociation in the B state, the E state levels from near $v_B = 26$. Other than defining the rotational level, the fluorescence lifetime of the excited state would not depend on the intermediate state pump level. The lifetime of one δ band, δ_1 was measured for $^{127}\text{I}_2$. The measured lifetimes were based on the assumption that there was only one event occurring and that it could be described by a single exponential decay. The lifetimes of the various states are listed in Table V-18.

A measure of optical absorption is the oscillator strength, defined as [101]:

$$f_{21} = (mc^3/8\pi^2\nu_0^2e^2)(g_2/g_1)(A_{21}) \quad \text{V-19}$$

where A_{21} is the Einstein coefficient for spontaneous emission and g_i is the degeneracy of the i^{th} state. For electronic transitions, the sum of the oscillator strengths of all the transitions arising from any one level to all other levels is unity. If $1/\tau$ is substituted for A_{21} , the

Table V-18. Lifetimes (nanoseconds) at T = 23°C

Band	Lifetime (± 2 nsec)		
	$^{127}\text{I}_2$	$^{127}/^{129}\text{I}_2$	$^{129}\text{I}_2$
E ₂	10,12,11		10
E ₀			10
E ₃	11		
E ₁₉	11		8
γ_1	8		7
γ_2^a	7 ^a		
α_{10}	4		
α_4			5
β_7			8,8
β_6	8		
β_5	8		
β_4	6		
β_8		10	
δ_1	15		

^aOverlap

oscillator strength becomes:

$$f\tau = (mc/8\pi^2e^2)(g_2/g_1)(\lambda_0^2) \\ = 1.4992(g_2/g_1)(\lambda_0^2)$$

V-20

where λ_0 is in centimeters. In the case of these transitions a typical result is the decay of E_2 , $\tau = 11$ nsec and $\lambda_0 = 4304 \text{ \AA}$. The oscillator strength (assuming $g_2 = g_1 = 1$) is then $f = 0.25$. The fluorescence measured probably corresponds to an E→B transition.

The decay curves of the high lying excited states of the two isotopes were all measured at room temperature (23°C) iodine vapor pressures. Only a few trial experiments were made on the E state bands at room temperature (23°C, 0.244 torr) and again at ice temperatures (0°C, 0.029 torr). These measurements showed no change in the observed lifetime, leading to the tentative conclusion that the lifetimes measured were not limited by I_2 self-quenching. As far as the other excited states were concerned there was insufficient intensity at anything below room temperature vapor pressure to measure the signal. The cell was not designed to operate above room temperature. The signals from all but the E and B state levels were on the detection limit of the instrumentation. This method of signal averaging was time consuming. It required 30 seconds to complete 180 data points per sweep of the oscilloscope; thus for weak signals

where 40-50 traces were necessary, the laser system had to remain constant in output power and frequency for 20-25 minutes. The frequency stability of the system was good. However, fluctuations in the output power of the N_2 laser did affect the signal averaging.

Few definite conclusions can be drawn from this data except to say that these excited states all have short lifetimes ($\tau < 20$ nsec). The noise problems and the difficulties encountered in measuring the signals preclude any further refinement of the data. It was difficult even to obtain an accurate description of the laser pulse. If too much light was scattered into the photomultiplier, saturation of the tube would broaden the pulse. A great deal of care had to be taken to shield the tube from measuring any scattered N_2 laser light. It was also observed that the width of the laser line may have depended on the alignment of the dye laser and on the region in the dye profile that the measurement was made. A number of laser pulses were measured in an attempt to obtain measurements near the region of each experimental determination. Saturation of the photomultiplier was tested using neutral density filters. However a variation of the measured pulse width of ± 2 nsec was still observed.

The observed lifetime of $\tau \approx 11$ nsec for the E state ($v_E < 20$) does not seem unreasonable compared to

Rousseau's measurement [47] of 27 nsec for a much higher vibrational level ($v_E \approx 45$). The measurement of $\tau_E \approx 50$ nsec by Wilkerson [13] appears slightly high. The lifetime of the D-X emission of 15.5 nsec measured by Callear et al [140], allowing for the large uncertainty in these measurements, compares favourably with the β state ($\tau \approx 8 \pm 2$ nsec). The α state, another possible assignment of the D state, appears definitely to have a shorter lifetime, $\tau < 5$ nsec, than the other excited states.

It is, in principle, possible that the lifetimes observed may not correspond to the states accessed, but rather to some other state to which the molecule has crossed, either by emitting in the infrared or via a non-radiative transition and then decaying. There is no clearcut way of ruling this out except by saying that an infrared transition of comparable oscillator strength would have a longer lifetime than the ultraviolet transition (the observed lifetime is < 20 nsec). In iodine at room temperature (23°C), using the collisional cross section for the B state, there are approximately 270 nsec, on average, between collisions. This indicates nonradiative processes induced by collision are not likely to occur in 20 nsec.

The observed signals corresponding to transitions to the α and β states are weak and yet the fluorescence decay from these states gives a very short lifetime and

correspondingly a large oscillator strength. It must be remembered however that the intensity observed corresponds to the unresolved emission out of the α or β state to some lower state convolved with the filter transmission characteristics and not directly to a $\alpha \rightarrow \beta$ or $\beta \rightarrow B$ transition. The cut-off filter used in the photomultiplier will just allow ($< 5\% T$) the observation of the fluorescence from the lowest observed α band, α_8 to the bottom of the B state potential well, thus resulting in a low signal intensity for that transition. It is possible the unresolved fluorescence observed is not to the B state at all but rather to the $A' \ ^3\Pi(2u)$ or $A \ ^3\Pi(1u)$ states.

4. The Effects of Collisions and Deactivations on the Excited States of $^{127}\text{I}_2$

4.1 Introduction

Four excited states have been observed in both isotopes of iodine in the 5eV region and the absolute vibrational numbering of these states and their molecular constants have been well established. A fifth state has only been observed in $^{127}\text{I}_2$. The fluorescence lifetimes of these excited states have also been determined. Table V-19 summarizes the details of the excited states observed in $^{127}\text{I}_2$.

Even with this information giving a much clearer picture of the excited states in the 5eV region, it was

Table V-19. Summary of the excited states in the 5eV region of $^{127}\text{I}_2$

Band	T_e (cm^{-1})	ω_e (cm^{-1})	$\omega_e x_e$ (cm^{-1})	r_e (Å)	$B_e \times 10^2$ (cm^{-1})	τ (nsec)
α	39648.6	107.15	0.218	3.59	2.06	4
β	41029.7	104.19	0.2212	3.669	1.973	7-8
E	41410.3	101.91	0.2373	3.6342	2.0116	11
γ	41621.3	95.01	0.222	3.6721	1.9702	7-8
δ	(41789)	(100.2)	(0.13)	(4.0)	(1.63)	(12)

still conceivable that states observed were inter-related. The fact that other than the E state and to some extent the γ state, the states could only be accessed from vibrational levels close to the B state dissociation limit was puzzling. The E state was the only state for which experimental evidence exists using other techniques [42].

If the vibrational levels below the pump level in the B state were to become populated through some form of rapid relaxation, transitions from these levels to the E state could appear as another excited state lying at higher energy. However, the α and β states both lie at lower energies than the lowest level in the E state and thus could not have been arrived at via such a mechanism. On the basis of these ideas at least two separate states must exist in the 5eV region. The γ and E states could be related through B state relaxation and the α and β states could also be related in the same manner.

Although no clear mechanism could be proposed which explained the observation of 5 electronic states as anything less than 2, if there were only two states, the transitions observed should show a distinct dependence on collision. Danyluk and King [9] believed that the effects of collisions were minimal during the 10 nsec. overlap of the two laser pulses at the low (≈ 0.3 torr) cell pressures used. Guy et al [44] felt that even though the time overlap was short, the observed weak intensities of the transitions were such that

the probabilities of collision need not be large.

A series of preliminary experiments were undertaken to examine the collisional properties of these 5 excited states in more detail. These studies involved first measuring the degree of saturation in the transitions and then the effects of self-quenching and foreign-gas quenching. The intermediate state spectra obtained using a number of different excited state levels as two-photon probes were measured. The effect of a time-delay between the pump and probe beams was also studied.

4.2 Saturation of the "E"←B Transitions

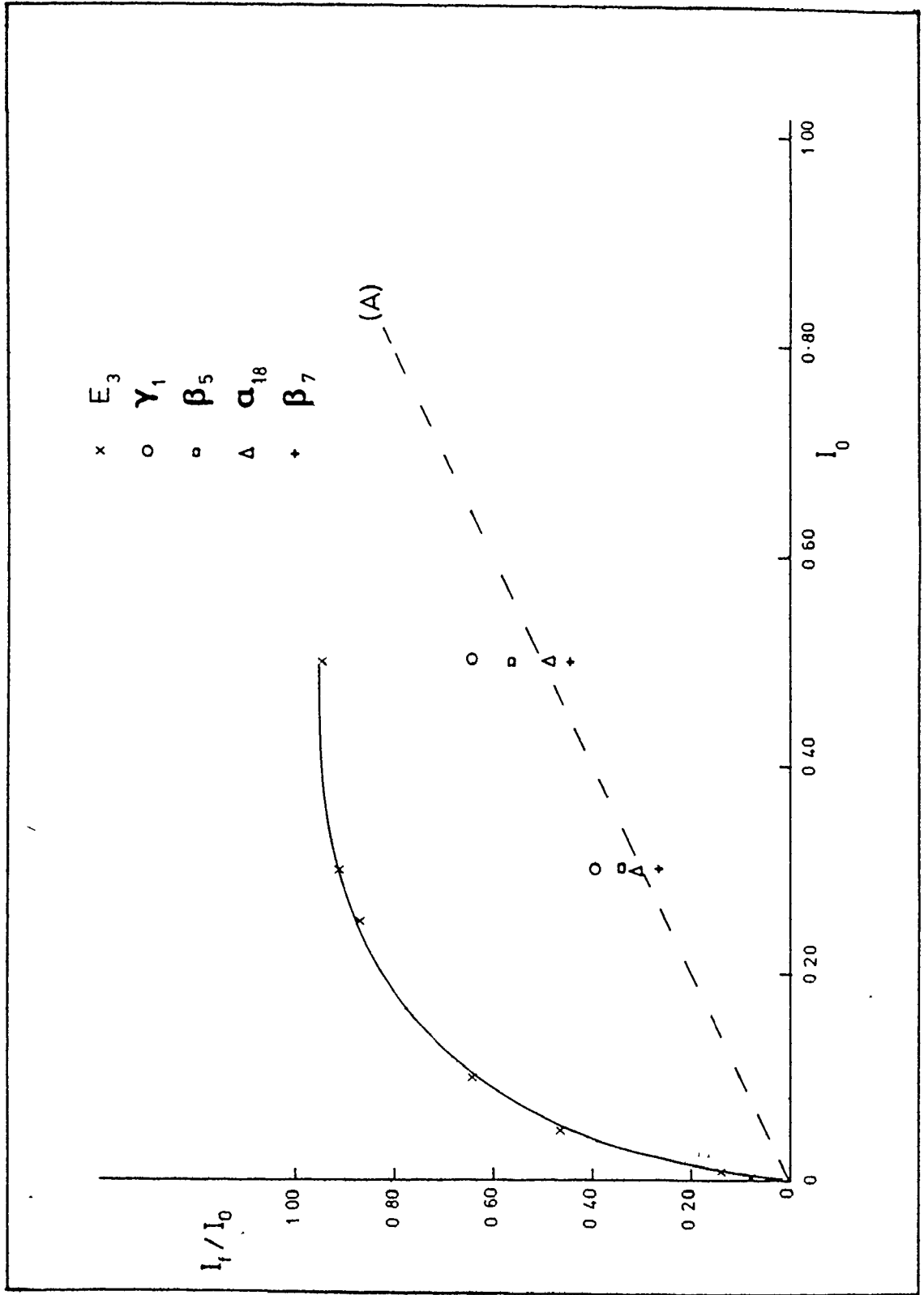
To understand any intensity changes occurring in observed transitions due to outside influences, it was necessary to know if any of the transitions involved were saturated and might exhibit nonlinear behaviour with respect to fluorescence intensity. As the intensity of the incident radiation on an absorbing system increased, the populations of the levels involved, to within a factor of the degeneracies of the states, asymptotically approached each other and the rate of energy absorption approached zero. This phenomenon is known as saturation [101].

The E_2 and E_3 transitions were measured for the E state ($T_0 = 41555.30 \text{ cm}^{-1}$ and 41655.60 cm^{-1} respectively). The $v = 26, R(0)$ transition at 18400 cm^{-1} was used as a pump level. The δ_0 ($T_0 = 41732$), β_5 and β_7 ($T_0 = 41488.68 \text{ cm}^{-1}$ and

41692.27 cm^{-1}), α_{18} ($T_0 = 41449.22 \text{ cm}^{-1}$) and γ_1 ($T_0 = 41656.12 \text{ cm}^{-1}$) bands were also excited using either $P_{78}(19)$ at 20026.65 cm^{-1} or $P_{78}(20)$ at 20025.3 cm^{-1} as the B state pump levels. All of the transitions measured were single, isolated peaks; the peak height, and the product of the peak height and full width at half maximum were found to vary in the same manner. To allow for changes in the laser system a run without neutral density filters (I_0) preceded each run with a filter (I_f) in the probe beam. The ratio I_f/I_0 was calculated for each set. All of the measurements had a 4-5% measurement error associated with them. The possible saturation of the pump transitions was also measured by inserting a 50%T filter in the pump beam. The $v = 26, R(0)$ transition was saturated ($I_f/I_0 = 0.86$), the $P_{78}(19)$ and $P_{78}(20)$ transitions were not ($I_f/I_0 = 0.55$).

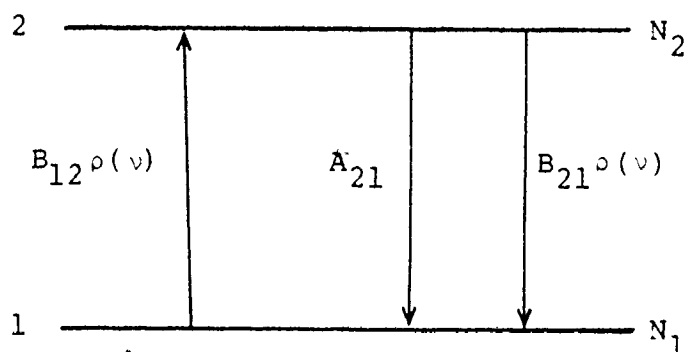
Only a single measurement at 50%T was made on the δ_0 transition ($I_f/I_0 = 0.44$). On the basis of this single result, the $\delta \rightarrow B$ transition was not considered saturated. Figure V-12 shows a graph of the ratio I_f/I_0 versus I_0 for the E_3 , α_{18} , β_5 , β_7 , and γ_1 transitions. The dotted line (A) corresponds to the condition of no saturation. The $E \rightarrow B$ transition exhibited the characteristic curve of a saturated transition: no significant change in the fluorescent intensity was observed until the incident radiation was cut to $< 25\%$ of its original value. The other transitions closely followed the unsaturated line except for the $\gamma \rightarrow \beta$

Figure V-12. Graph illustrating saturation characteristics of the various bands. Broken line A indicates condition of no saturation.



transition which may have been partially saturated. The linear dependence on probe laser intensity observed in the α , β and γ transitions indicated that single photon events were involved and no multiphoton absorption occurred due to the probe laser. The E state curve was also characteristic of a saturated single photon transition.

A simple two-level system can be illustrated as:



where $\rho(\nu)$ is the energy density per unit frequency interval, B_{12} and B_{21} are the Einstein coefficients, N_1 and N_2 are number densities and A_{21} is the spontaneous radiative decay rate. The rate of transitions $1 \rightarrow 2$ can be expressed as: $N_1 B_{12} \rho(\nu)$ and the rate of transitions $2 \rightarrow 1$ as $N_2 [B_{21} \rho(\nu) + A_{21}]$. At equilibrium these two competing rates are equal:

$$N_1 B_{12} \rho(\nu) = N_2 (B_{21} \rho(\nu) + A_{21})$$

$$N_1/N_2 = B_{12} \rho(\nu) / (B_{21} \rho(\nu) + A_{21})$$

In terms of the inverse of this relationship and ignoring all state degeneracies (i.e. $B_{12} = B_{21}$):

$$\frac{N_1}{N_2} = \frac{B_{21}}{B_{12}} + \frac{A_{21}}{B_{12}} \left(\frac{1}{\rho(\nu)} \right)$$

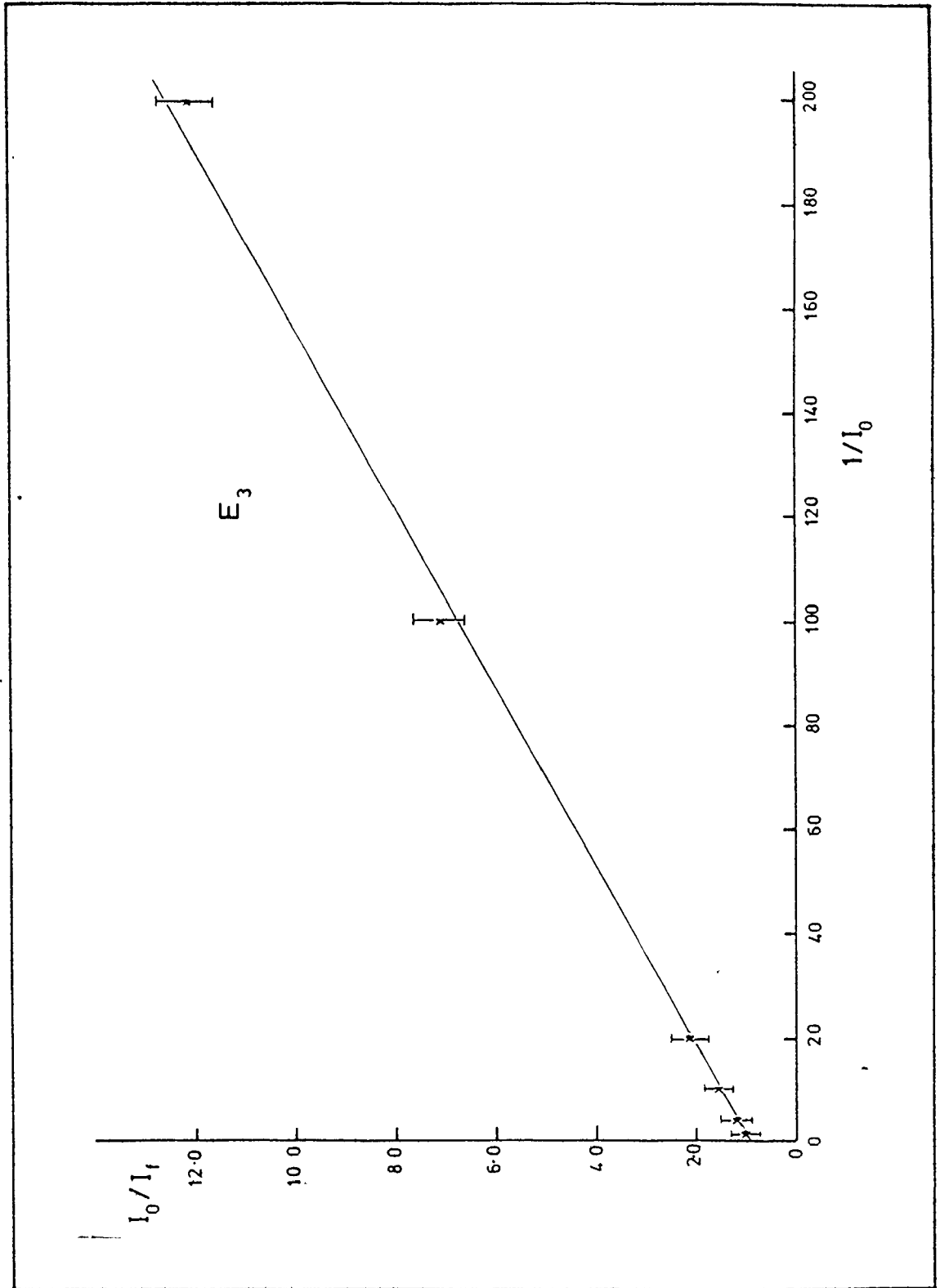
$$= 1 + \text{constant } [1/\rho(\nu)]$$

A plot of I_0/I_f versus $1/I_0$ should produce a straight line. If this argument is extended to a three-level system and no assumptions are made about the intermediate level the results are identical, only the constants change. Any result other than a straight line would be indicative of events involving more than a single photon; Figure V-13 illustrates this for E_3 . Within experimental error it yielded a straight line.

4.3 Self-Quenching and Foreign-Gas Quenching

To determine the effects of collisions, two types of experiments were performed. The change in fluorescence intensity as a function of iodine vapor pressure, i.e. as a function of number density, (self-quenching) and the change observed on the addition of an inert gas to the cell (foreign-gas quenching) were measured. These effects have been extensively studied in the B state of iodine [133-138, 143]. In the two-level B-X system, in the absence of a foreign gas, a simple kinetic relationship [133] can be developed which relates the measured light intensity I to an expression in the radiative life τ , a rate constant for self-quenching S , the concentration of ground state molecules and a rate of excitation. In the presence of a foreign gas a further term involving the foreign gas concentration and a rate constant Q representing foreign-gas quenching can be

Figure V-13. Linear plot of the saturation data for the E_3 band



added. The two rate constants, S and Q, on the basis of the kinetic theory of gases, can be equated to a product of the average particle velocity (calculated using the reduced mass of the colliding particles) and a collision cross-section. The solution of these kinetic expressions depends on the existence of steady-state conditions.

In the experiments considered here, it is a more complex problem. There are three levels involved and the rate equations contain relaxations and collisions between multiple levels. The measured lifetimes of the excited states are very short ($\tau < 20$ nsec) and there exists evidence from measurements on the E state in Sec. 3, Chap. V and reference 47 that the effects of iodine self-quenching on the E state are negligible. There was no change in the fluorescence lifetime over approximately a 10-fold change in I_2 vapor pressure. The other excited states in the 5eV region are expected to be the same since their lifetimes are all similar. Any solution of the kinetics using a steady-state approximation is unlikely to be correct in a pulsed system where the pulse duration is ≈ 10 nsec. However, it may be possible to treat the second transition as simply a detector of the effects in the intermediate state. These two-photon experiments essentially employed a gated detection system with a gate width of 10 nsec. This detection system involved interrogating the molecule during the 10 nsec duration of the probe laser pulse, since it is the fluorescence out of the

excited state in the 5eV region that is actually monitored. Even a two-level system will react differently to pulsed excitation than it would to continuous excitation. On the basis of a simple two-level model, the rate equation can be expressed as:

$$dM/dt = -\sigma c \rho (M - M^*) + M^*/\tau + SMM^*$$

where M and M^* are the concentrations of molecules in the ground and excited states respectively, τ is the radiative lifetime, S is a self-quenching rate constant and the term $\sigma c \rho$ relates the photon field and the absorption cross-section of the transition. If the results from the $v_B = 70$ level are used as typical parameters for B state levels near dissociation from which the α , β , δ and γ states were pumped: $\tau = 3610$ nsec, $\sigma_S^2 = 71 \times 10^{-16} \text{ cm}^2$ [137], and an estimation made of the photon field $\rho = 6.052 \times 10^{10} \text{ photons/cm}^3$ and absorption cross-section $\sigma \approx 2 \times 10^{-15} \text{ cm}^2$, the time evolution of this system can be calculated. A steady-state condition implies that $dM/dt = 0$ for a long time period compared to the time it takes for any changes to occur in the system. In other words, all derivatives go to zero. Such a condition did not occur with these parameters for at least a microsecond after time zero. With pulsed excitation, the system only momentarily attains the condition that $dM/dt = 0$. Solution of the kinetics using a steady-state approximation is not possible. Rather than actually solving the kinetics involved,

it was considered important to observe qualitatively whether or not the excited states all behaved the same way with respect to collisions.

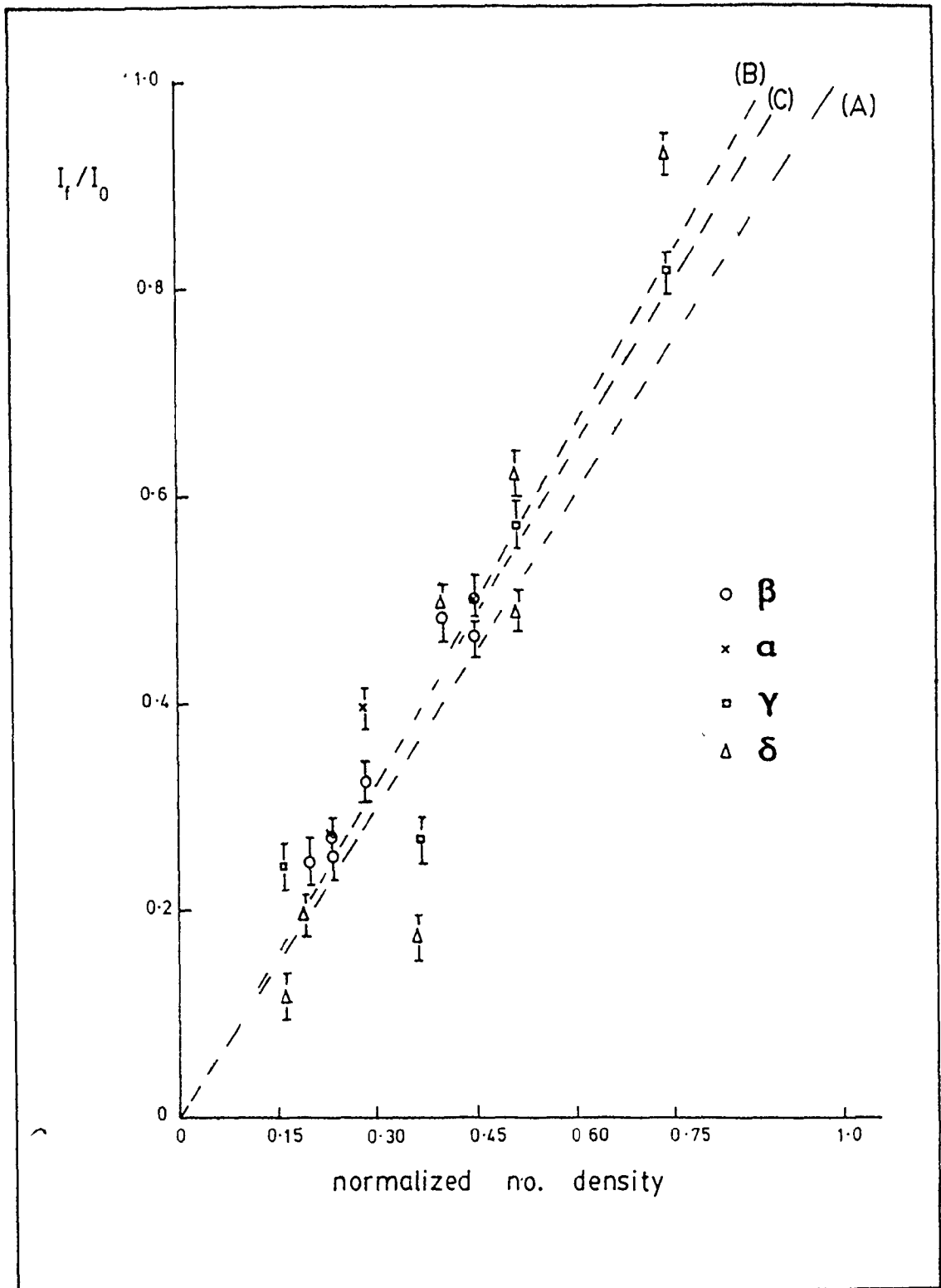
The effect of varying the iodine number density was measured for the α , β , δ and γ states. No attempts were made to measure the E state because of the saturation of this transition. The side arm of the sample cell containing solid $^{127}\text{I}_2$ was cooled to various temperatures below room temperature and the spectra were compared. The iodine vapor pressure at a given side arm temperature was calculated from the equation in reference 142. The actual number density of iodine was calculated using the ideal gas law and the room temperature at which the cell body was sitting. Measurements were restricted to transitions that were not overlapped. In the region studied, the α , γ and δ bands phase in and out with respect to each other and an observed peak is frequently composed of a number of different transitions. If the results were expressed as ratios I_f/I_0 , where I_0 corresponds to the intensity observed at room temperature, and if the number density was normalized to 1.0, all the data could be incorporated on one graph. Table V-20 lists the observed data and Figure V-14 shows a plot of the data. The line (A) corresponds to a slope of 1.0, (B) and (C) are least squares fits to the data with and without the point (1,1). This graph illustrates that, within experimental error, all of the transitions depend on iodine number density in the

Table V-20. Self-quenching of $^{127}\text{I}_2$

Number density (molecules/cm ³)	Normalized number density	I_f/I_0 (± 0.02) of bands		
<u>Run No. 1</u>				
		$\frac{\beta_4}{\beta_5}$	$\frac{\beta_5}{\beta_7}$	$\frac{\alpha_{17}}{\alpha_{18}}$
7.3041×10^{15}	1.0	1.0	1.0	1.0
3.2794×10^{15}	0.45	0.465	0.502	0.500
2.0540×10^{15}	0.28	0.325	0.325	0.385
1.6626×10^{15}	0.23	0.255	0.270	0.273
<u>Run No. 2</u>				
		$\frac{\delta_1}{\delta_2}$	$\frac{\beta_7}{\beta_8}$	
6.6327×10^{15}	1.0	1.0	1.0	
2.6202×10^{15}	0.40	0.484	0.484	
1.3377×10^{15}	0.20	0.185	0.246	
<u>Run No. 3</u>				
		$\frac{\delta_1}{\delta_2}$	$\frac{\delta_0}{\delta_1}$	$\frac{\gamma_1}{\gamma_2}$
6.1405×10^{15}	1.0	1.0	1.0	1.0
4.5457×10^{15}	0.74	0.817	0.932	0.818
3.1319×10^{15}	0.51	0.481	0.623	0.573
2.2162×10^{15}	0.36	0.175	-	0.269
0.9848×10^{15}	0.16	0.119	-	0.244

Figure V-14. Graph of normalized iodine number density vs normalized fluorescence intensity.

- (A). Line of slope = 1
- (B). Least squares fit to data including the point (1,1)
- (C). Least squares fit without the point (1,1)



same manner and do not appear to depend on collisions.

Argon and helium at a number of different pressures were added to the cell to measure the effects of foreign-gas quenching. It was expected that a simple kinetic relationship would not apply under these experimental conditions but the general trends observed for the various states would show any special dependence on collision. The effects of an inert gas on the E state were masked by the saturation of this transition. No changes in E state intensity were observed between spectra with and without argon present. With the addition of 10.0 torr helium, the fluorescence from the α , β , γ and δ states was completely quenched. At 5.0 torr helium the strong γ and δ transitions were just observable above the background. With the addition of 2.5 torr argon the spectra remained measurable, at 5.0 torr argon the fluorescence was once again completely quenched. In the case of the addition of 2.5 torr argon, for a number of different iodine vapor pressures (corresponding to slightly different room temperatures), the ratio I_f/I_0 (where I_0 corresponds to the intensity with no inert gas present) remained the same for the α , β , and δ transitions. The γ bands in this region were overlapped with α bands, and since the γ transition also exhibits a certain amount of saturation, the intensity changes of these bands were not considered reliable. The identical variation of various transitions with foreign-gas pressure indicates that they

are all effected by collisions in an identical manner.

4.4 Time Delay Experiments

As was outlined in Chapter IV, White cell mirrors were used to provide a time delay between the pump and probe laser beams. A delay of 100 nsec was the maximum time practical and it was difficult to completely compensate for the losses in the probe laser beam due to the large number of mirror reflections involved in any delay. This experiment was designed to indicate if any relaxation processes in the B state were contributing to the observations of the excited states in the 5eV region. It could also be used to measure the lifetime of the B state pump level involved in regions that were not possible to study by direct observation of the fluorescence (i.e. near dissociation). This latter experiment was not extremely successful due to the problems involved in maintaining a constant power level in the probe beam. Another problem was that only a limited number of delay times could be measured, delay times that were significantly shorter than the lifetimes of the states involved. Experiments on the E state were the least affected by changes in laser intensity because of the saturation of that transition. The observed intensity changes could be attributed entirely to changes in the B state populations. Measurements were made on the $\nu_B = 26 R(0)$ transition at 18400 cm^{-1} where $\tau_{\text{obs}} = 179 \pm 20 \text{ nsec}$. This was compared to the results of Capelle

and Broida [137] where using their results of $\tau_0 = 780$ nsec and the collision cross section $\sigma_S^2 = 70 \times 10^{-16}$ cm², the expected lifetime at the experimental number density $(nd)_{I_2} = 8.09026 \times 10^{15}$ molecules/cm³ would be $\tau_{calc} = 191$ nsec. Delay experiments on the E state were also run with an inert gas in the cell, where the time delay allowed for collisions to depopulate the E state. The results, within a margin of error, compared well with the expected lifetimes calculated from the work of Capelle and Broida [137].

Time delay experiments on the α , β , δ and γ transitions were very much limited by the experimental difficulty of varying laser intensity. However the relative intensities of the bands remained constant at 8, 33 and 58 nsec delay. No single excited state was found to vary differently from any other when collisions were allowed to effect the B state.

4.5 Discussion

As a final experiment to determine if there were any differences in the manner in which the excited states were reached from the B state, two-photon spectra of the same region of the B state were run using each of the excited α , β , δ and γ states as fixed probe levels. If any form of relaxation process in the B state was occurring and what appeared as two separate excited states was in fact a single state, this would be equivalent to broadening the bandwidth of the probe laser (i.e. allowing a much larger overlap with

the upper excited state). The selectivity of the two-photon method would be lost, and a significantly more complicated spectrum would be expected in the B state. No such effect was observed, and essentially identical spectra were obtained in the B state regardless of the fixed probe position.

The final results of these experiments by themselves are far from complete; however, taken as a whole they do answer the problem of whether these are independent states. Since levels lie below the E state, at least two states must exist; and since all the states except the E state exhibit the same saturation characteristics, the same dependence on I_2 pressure and inert gas pressure, the same time delay behaviour and give identical B state spectra when used as probe transitions, they must exist as independent states.

Quantitative measurements of the effects of collisions have not been made. These will require a further series of experiments, paying special attention to the consequences of a three level system observed with a gated detection system.

Chapter VI

RESULTS AND DISCUSSION -

INTERHALOGENS ICl AND IBr

1. The 5eV Region of Iodine Monochloride, I³⁵Cl and I³⁷Cl

1.1 Introduction

ICl has a strong visible electronic absorption spectrum, the A $^3\Pi_1 + X ^1\Sigma^+$ transition. Both of the electronic states involved dissociate to the same ground state atomic products I($^2P_{3/2}$) + Cl($^2P_{3/2}$). This transition has been extensively studied by Hulthén et al [61,62] and recently reexamined, in both absorption and emission, by Coxon et al [64,65] using conventional single photon techniques. The existence of an electronic state in the E state region, approximately 5eV above the ground state, has been demonstrated by Barnes et al [77], using a limited two-photon method involving an optical parametric oscillator and a nitrogen-pumped dye laser. The linewidths of the two lasers employed in their study were quite broad (2-5 cm^{-1}) and Barnes et al [77] measured only a few vibrational bands. Haranath and Rao [76] have also reported observing about 300 emission bands under low resolution in the 4400 Å to 3800 Å region, from ICl in a condensed electrical discharge. The dissociation limit of the A state has been determined using two-photon methods

by King and McFadden [15]. These latter experiments were performed by scanning the pump laser through a series of discrete vibrational levels near the A state dissociation limit, with the probe laser fixed on a vibrational level in the E state region, as described in Sec. 2, Chap. III. The excited state in the E state region was used by King and McFadden [15] as simply a final state for their experiments, and the exact nature of the state and its molecular constants was not determined.

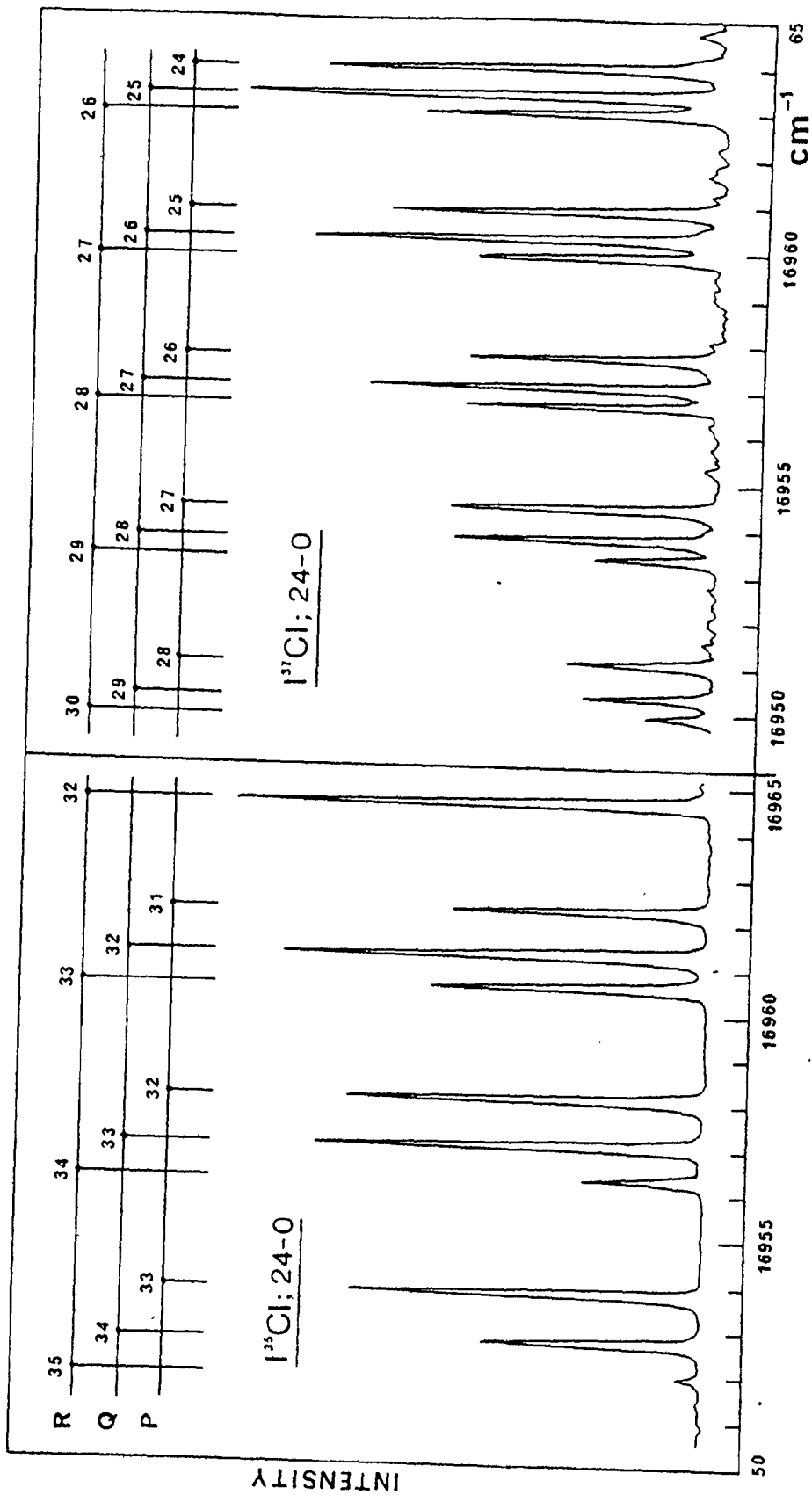
1.2 Selection of Pump Lines

In iodine it was possible to obtain a single photon absorption spectrum of the B state by scanning the pressure scan laser across the B+X absorption and monitoring the B+X broadband fluorescence. The corresponding single photon A+X spectrum of ICl was not observable under the same conditions, because of the decomposition of ICl to I_2 and Cl_2 . This decomposition resulted in the obscuring of the ICl A+X fluorescence by the strong B+X fluorescence of I_2 . Interference by iodine has always been a problem in the spectroscopic study of ICl. Most conventional spectroscopic investigations have had to attempt various methods of minimizing the presence of I_2 . These include stringent purification of commercial ICl to lower the I_2 and H_2O content (H_2O promotes decomposition of ICl to I_2O_5) and careful storage over P_2O_5 .

It was possible to circumvent these impurity problems and obtain clean, clear, high resolution scans of the A+X spectrum by use of the two-photon method. By fixing the probe laser on an appropriate E state level and scanning A-X transitions originating on levels that are low in the A state potential well, spectra of the A state of ICl alone could be obtained over a large range of rotational J values. As outlined in Chap. III each of the isotopic species could be selectively probed and individual A state spectra obtained for each of $I^{35}\text{Cl}$ and $I^{37}\text{Cl}$. The (24,0) band of the A state was used primarily as a source of pump transitions. Examples of the two isotopes' spectra in this region are illustrated in Figure VI-1.

The density of the B+X spectrum of iodine often produced two-photon spectra of the E state containing large numbers of off-resonance lines pumped from transitions underlying the main pump level. This produced complex E state spectra containing multiple sets of lines, for which each pump level had to be individually established. The lighter ICl molecule did not present this multiple pump level problem very frequently. The A+X absorption spectrum was less dense than the B+X absorption of iodine and almost every line pumped resulted in a discrete two-photon spectrum in the E state, with few lines appearing which belonged to anything but the main pump level.

Figure VI-1. Rotational structure in the A+X high-resolution absorption spectrum of ICl. In $I^{35}Cl$, the probe laser is tuned to the (7,24) E+A transition; in $I^{37}Cl$, the probe laser is tuned to the (6,24) E+A transition



The splitting between the observed rotational lines in a vibrational level of the E state depended on the rotational constant of the upper level and the pump level's J value. If the rotational constant of the excited state was large, the splitting correspondingly increased rapidly with J and different J values were readily identified via their characteristic splitting. This made it possible to quickly determine most of the off-resonance lines in the E state spectra and identify the corresponding pump levels from sorted lists of A state frequencies.

The rotational structure of the (24,0) A-X absorption transition consisted of strong P, Q and R branch lines. The (24,0) transition was measured from the band origin to around $J = 36$ and the lines were readily identified with the aid of Hulthén's [61,62] measurements. The term values of each E state rotational level were calculated by adding the measured probe frequency to the term value of the A state pump level as given by Hulthén [62]. A list of pump lines used in this work is given in Table VI-1.

The A-X system of ICl has recently been reexamined by Coxon et al [64,65], and they have made some comments upon Hulthén's work. These include the criticism that, although the measurements made by Hulthén were of high precision, the analysis of their results was based on graphical techniques. Coxon et al [64,65] also believed that the graph of $(T_e - T_f)$ versus $J(J + 1)$ in reference 62

Table VI-1. Pump lines in the A + X transition

Isotope	v	J			
		P	Q	R	
I ³⁵ Cl	24	10	15	17	
		13	23	34	
		15	29		
		28	30(2) ^a		
		31	33		
	23 ^b	19			
		25 ^b	39	31	
				34	
		27 ^b	53	46	54
		28 ^b	56	49	
I ³⁷ Cl	24	12	15	24	
			16	25	
			19	33	
			20	34	
			24	35	
			28		
			30		
			33(2) ^a		
			36(2) ^a		

^aNumbers in parenthesis indicate number of different spectral runs done using the same pump line.

^bv = 23 to v = 28 are off-resonance lines.

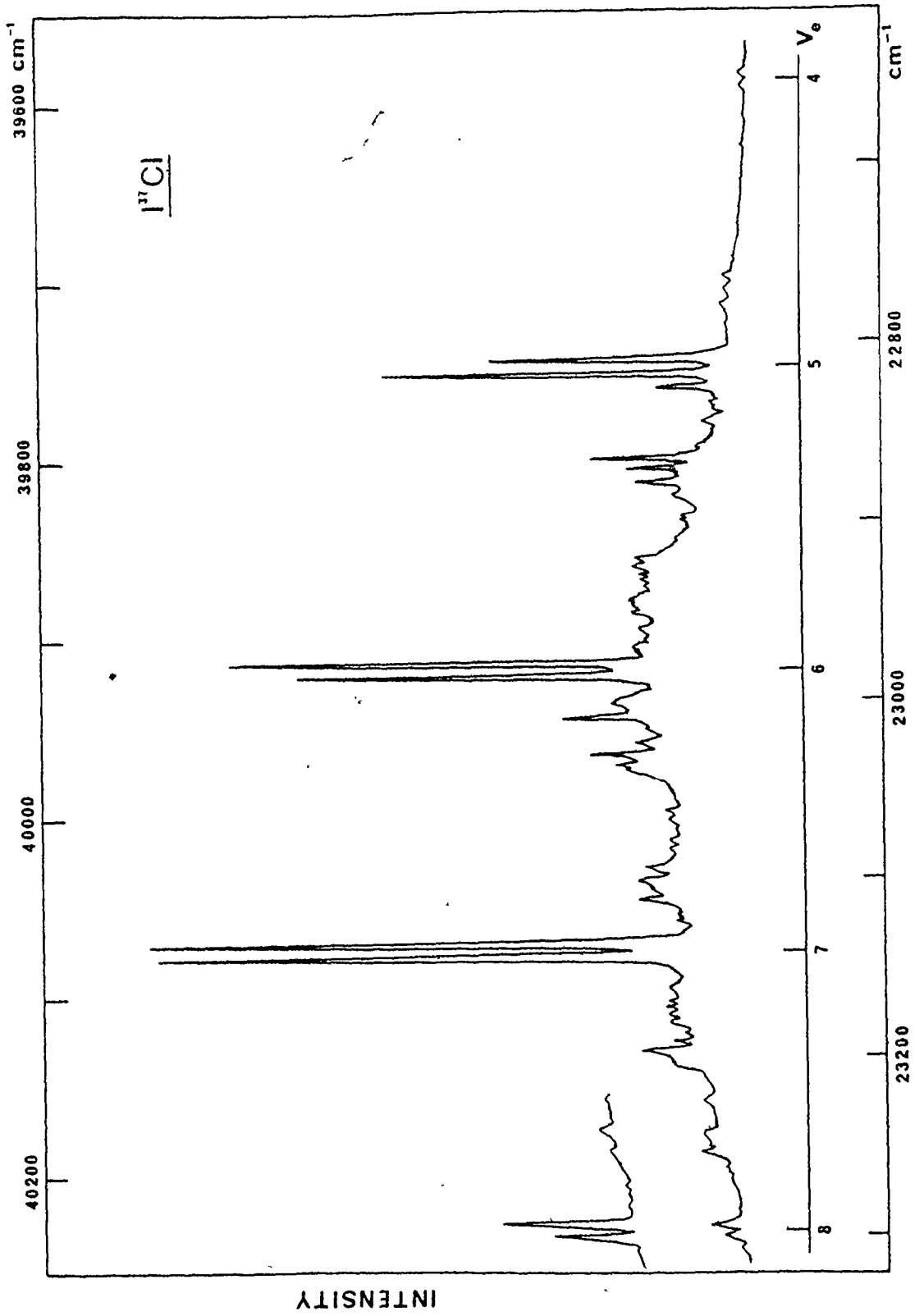
illustrating the Ω -doubling in the A state was not an accurate representation of what actually occurs. The actual measured frequencies of Hulthén et al [62] were recovered from the tables of term energies by Coxon et al [64] in order to analyse them using least squares techniques. However, before doing this, Coxon et al [64] graphically reexamined the form of the Ω -doubling in the A state; this reexamination was aimed primarily at determining a model to be used in their least squares fitting of the experimental data. They found [64] the same linear behaviour in the graphs of $(T_e - T_f)$ versus $J(J + 1)$ as did Hulthén et al [62] for $10 \leq v' \leq 20$. For $v' = 25, 26, 27$ of $I^{35}Cl$ the plots were no longer approximately linear and the magnitude of the Ω -doubling rapidly increased at $J = 71, 66, 54$ respectively. The majority of pump lines employed in this study came from the $(24,0)$ transition at relatively low J values. In both plots of the Ω -doubling, the $v = 24$ level behaved linearly. No use was made of any constants of Hulthén's but the term energies were used directly from the tables in his papers [61,62]. Only a single off-resonance pump line, $R_{27}(54)$ was considered as being associated with a region of anomalous behaviour in the A state. No problems were encountered in incorporating the results from this level with the other data on the molecule.

1.3 Analysis of the E State Spectra

The pump laser was tuned to an A+X absorption frequency corresponding to an identified rotational line for one of the isotopes. The probe laser was then scanned over the dye profile producing E+A transitions. This procedure (for each isotope) gave a spectrum of a series of vibrational bands, each consisting of two rotational lines corresponding to $\Delta J = \pm 1$. Only a single set of vibrational lines could be identified in the region of the coumarin-120 dye profile (4250 Å - 4500 Å). Seven vibrational bands were observed for $I^{35}\text{Cl}$ and five for $I^{37}\text{Cl}$, with vibrational separations of approximately 165 cm^{-1} . No $\Delta J = 0$ or Q branch transitions could be definitely assigned on the spectra, only P, R pairs (Figure VI-2).

The absence of Q branches helped to tentatively identify the type of electronic transition involved. In case (c) coupling, since the A $^3\Pi_1$ state had $\Omega = 1$, a 0+1, E+A transition should have exhibited the same band structure as a case (a) $^1\Pi \leftrightarrow ^1\Sigma$ transition, with the selection rule $\Delta J = 0, \pm 1$. Thus prominent Q branches should have been observed, just as was seen in the 1+0, A $^3\Pi_1 + X ^1\Sigma_0^+$ transition. If the E state had $\Omega = 2$, it would have exhibited the same band structure as a case (a) $^1\Delta \leftrightarrow ^1\Pi$ transition, where, since $\Delta\Lambda \neq 0$, P, Q and R lines would also have been prominent. It was most likely therefore that the E+A transition corresponded to a 1+1

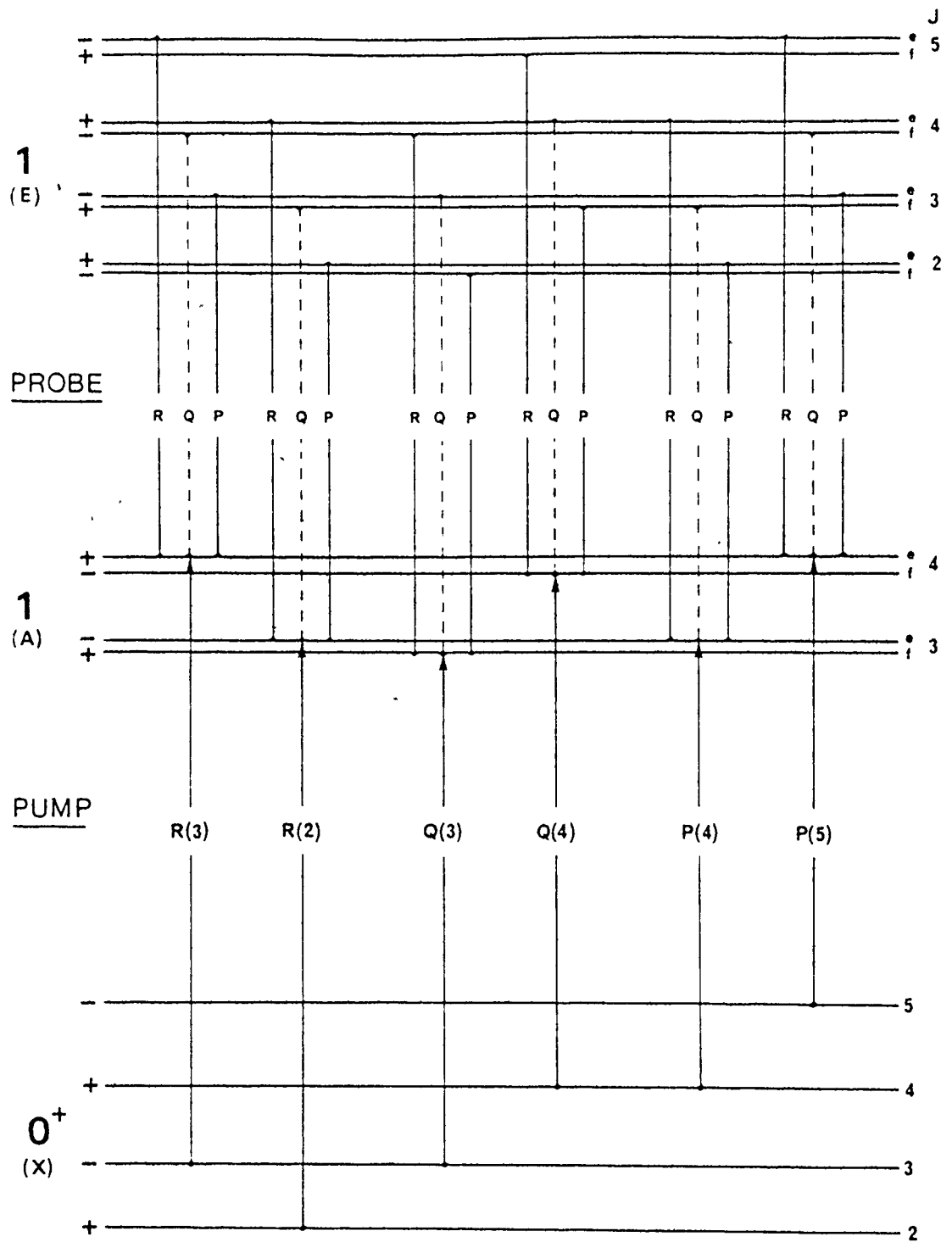
Figure VI-2. E state of $I^{37}\text{Cl}$. The A state pump level is 0-24 Q(33), $T = 17057.661 \text{ cm}^{-1}$. The main progression consists of transitions to rotational levels with $J \approx 32$ and 34 in the E state



transition in case (c) approximation. This transition would have been the analogue of a case (a) $1_{\Pi} \leftrightarrow 1_{\Pi}$ transition where $\Delta\Lambda = 0$ and the Q branch intensity would be rapidly decreased as J increased without going through a maximum (the intensity is approximately proportional to $(1/J)\exp(-F_v(J)hc/kT)$ [19]). The separation in wavenumbers of the P, R pairs observed was approximately given by $2B_v'(2J'' + 1)$. By $J = 6$ the gap was 1.5 cm^{-1} , the bandwidth of the mechanical scan probe laser, and each vibrational transition was just resolvable into a doublet. However, by $J = 6$, the intensity of the Q branch had fallen to approximately 0.15 of its initial value. At higher J values where the gap between P and R lines was sufficient to resolve a Q line, the intensity had dropped too low to observe.

An E state with $\Omega > 0$ should exhibit Ω -type doubling. In the $A \leftarrow X$ transition, for $v_A < 27$, the value $(T_e - T_f)$ increased linearly with $J(J + 1)$. As expected for a $1_{\Pi} \leftrightarrow 1_{\Sigma^+}$ transition in case (a) approximation, the Q transitions terminated on the lower (f) component (using the convention of Brown et al [144] rather than the c, d used by Hulthén et al [62], and P or R transition terminated on the upper (e) component of each rotational level of the A state [62]. The transitions possible are outlined in Figure VI-3. Based on the symmetry selection rules that $\Delta J = 0, \pm 1$ and $+ \leftrightarrow -$, the selection rules in terms of the e, f labels become

Figure VI-3. Typical rotational levels and transitions for a $1 \leftarrow 1 \leftarrow 0^+$ two-photon transition



$$\Delta J = 0, \quad e \leftrightarrow f$$

$$\Delta J = \pm 1, \quad e \leftrightarrow e \text{ and } f \leftrightarrow f$$

Allowing for no Q branch lines in the E state spectra, it can be seen from Figure VI-3, that if a Q line is pumped in the A state, the P and R lines produced in the E state will terminate on the lower f component. If a P or an R line is pumped in the A state, the upper transitions will terminate on the upper e component in the E state.

The term values for each E state rotational level were calculated from the measured probe frequency and Hulthen's A state results. The rotational terms associated with each vibrational level in the E state were then fitted by linear regression to

$$T(v', J') = T_0(v', J' = 0) + B_v J'(J' + 1) \quad \text{VI-1}$$

The largest value of J pumped was J = 56 and even this value was not sufficient to produce meaningful centrifugal distortion terms in fits attempted to higher order polynomials in J(J + 1). It has been suggested that a fixed centrifugal distortion term should be included in these fits as an attempt to account for its effects [50]. This fixed term can be calculated from the Dunham relationship [19].

$$D_e = \frac{4B_e^3}{\omega_e^2} \quad \text{VI-2}$$

If the calculated values ($^{35}\text{D}_e = 2.57 \times 10^{-8} \text{ cm}^{-1}$, $^{37}\text{D}_e = 2.36 \times 10^{-8} \text{ cm}^{-1}$) were incorporated in the fit, the B_v values obtained differed from fits without these terms by less than the error of any one value. In some cases the B values were identical with or without the centrifugal terms. It was thus decided to leave out such an empirically calculated factor.

If the Ω -type doubling is taken into account, two sets of lines exist and effective B_v^f and B_v^e values can be calculated by splitting the fits into two equations with a common T_0 . Transitions pumped by a Q line were used to calculate the B_v^f values and those pumped by P or R lines were used to calculate B_v^e values. The results for the two isotopes are listed in Table VI-2. The $v = 3$ and $v = 9$ levels in I^{35}Cl were fit to an equation involving a single rotational constant, because only a few measurements over a limited range of J values ($J = 26-31$ and $J = 51-56$ respectively) were made.

Although the Ω -doubling coefficient $q = (B_v^f - B_v^e)$ has values that are of the same order of magnitude as the uncertainties in the B values, the I^{35}Cl q is consistently negative, i.e. $B_v^f < B_v^e$. It is not clear whether the scattered results for I^{35}Cl are experimental or related to perturbations affecting the Ω -doubling.

The data from the two isotopes, $I^{35}\text{Cl}$ and $I^{37}\text{Cl}$ can be used to establish the absolute vibrational numbering in the E state. The vibrational term values and the rotational constants were fitted by least squares to a polynomial expansion in the mass reduced quantum number $\eta = \rho(v + 1/2)$ as outlined in Sec. 3.2, Chap. II. A quadratic approximation was applied to the term energies

$$T(v', J' = 0) = T_e + \omega_e(\eta) + \omega_e x_e(\eta^2) \quad \text{VI-3}$$

and a linear approximation to the rotational constants:

$$B(\eta) = B(v)/\rho^2 = B_e - \alpha_e(\eta) \quad \text{VI-4}$$

The reduced masses of the isotopes are

$${}^{35}\mu = 27.41467077 \cong 1.0$$

$${}^{37}\mu = 28.62712943 \cong 1.044226636$$

and the ratios are ${}^{35}\rho = 1.0$ and ${}^{37}\rho = 0.97859415$.

The vibrational term energies in Table VI-2 were corrected to be relative to the bottom of the ground state potential well by the use of the ground state zero-point energies

$${}^{35}G(0) = 191.7713 \text{ cm}^{-1}$$

$${}^{37}G(0) = 187.6733 \text{ cm}^{-1}$$

calculated from the constants given by Hulthén et al [61].

The term energies were then fitted to equation VI-3 using weighted least squares (weighted by $1/\sigma^2$). A distinct minimum in χ^2 was obtained for the vibrational numbering in Table VI-2. The molecular constants are listed in Table VI-3. Independent quadratic fits were also made to the data for each isotope separately and these results (relative to $v_X = 0, J_X = 0$) are also listed in Table VI-3.

The rotational constants B_V^f and B_V^e , where available, were included separately in the fit to equation VI-4. Again the least squares fit was weighted by $1/\sigma^2$; independent fits were also made on each isotope separately. The results are listed in Table VI-4.

An RKR potential was calculated for the E state of ICl and the turning points for the lower vibrational levels are listed in Table VI-5.

1.4 Discussion

Haranath and Rao (HR) [76] have reported an emission spectrum in this region for ICl. Their spectrum was recorded at low resolution and showed red degraded bands heavily overlapped with I_2 emission. They analysed these bands in terms of the upper and lower state vibrational frequencies $\omega_e' = 173 \text{ cm}^{-1}$ and $\omega_e'' = 210 \text{ cm}^{-1}$ of $I^{35}\text{Cl}$. They identified the lower state of this emission as the $A^3\Pi_1$ state. This is very similar to what would be expected for E→A emission from the E state observed in this work,

Table VI-2. Term values and rotational constants (cm^{-1}) for the E state of ICl

Isotope	v'	$T_0(v', J' = 0)^a$	$B_V^f \times 10^2$	$B_V^e \times 10^2$	n^b	$q \times 10^2$ $= B^f - B^e$	
^{35}Cl	3	39493.6 ± 3.6	6.58 ± 0.42		4		
	4	39669.44 ± 0.19	5.641 ± 0.039	5.571 ± 0.014	16	0.07	
	5	39834.36 ± 0.20	5.585 ± 0.034	5.587 ± 0.037	32	-0.002	
	6	39999.47 ± 0.14	5.538 ± 0.015	5.552 ± 0.010	32	-0.014	
	7	40163.12 ± 0.15	5.539 ± 0.019	5.532 ± 0.013	38	0.007	
	8	40326.65 ± 0.29	5.479 ± 0.021	5.495 ± 0.015	32	-0.016	
	9	40485.8 ± 1.4	5.560 ± 0.049		4		
	^{37}Cl	4	39657.05 ± 0.39	5.296 ± 0.073	5.365 ± 0.087	24	-0.069
		5	39818.78 ± 0.40	5.298 ± 0.088	5.349 ± 0.096	30	-0.051
6		39980.90 ± 0.26	5.159 ± 0.050	5.223 ± 0.047	46	-0.064	
7		40141.31 ± 0.40	5.127 ± 0.082	5.206 ± 0.078	44	-0.079	
8	40301.65 ± 0.35	5.082 ± 0.069	5.170 ± 0.066	48	-0.088		

^aRelative to $v_X = 0, J_X = 0$

^bNo. of term values used in each fit

Table VI-3. Molecular constants for the E state of ICl

Constant (cm^{-1})	I ³⁵ Cl		I ³⁷ Cl	
	Combined Isotope			
<u>Combined Isotope Fit</u>				
T_e^a	39107.184 ± 1.771	39107.2 ± 1.8	39107.2	± 1.8
T_e^a		38915.43	38919.53	
ω_e	169.180 ± 0.569	169.18 ± 0.57	165.56	± 0.57
$\omega_e x_e$	0.3721 ± 0.045	0.372 ± 0.045	0.356	± 0.045
<u>Independent Quadratic Fit</u>				
T_e^b		38916.3 ± 1.8	38916.3	± 1.8
ω_e		168.93 ± 0.58	165.8	± 1.2
$\omega_e x_e$		0.3566 ± 0.0044	0.3566	± 0.0089

^aRelative to the bottom of the ground state potential well

^bRelative to $v_X'' = 0, J_X'' = 0$

Table VI-4. Rotational constants for the E state of ICl.

Constant (cm^{-1})	Combined Isotope	I^{35}Cl	I^{37}Cl
<u>Combined Isotope Fit</u>			
$B_e \times 10^2$	$5.6875 \pm .0276$	$5.6875 \pm .0276$	$5.4466 \pm .0276$
$\alpha_e \times 10^4$	$2.27 \pm .40$	$2.27 \pm .40$	$2.13 \pm .40$
<u>Independent Linear Fit</u>			
$B_e \times 10^2$		$5.682 \pm .028$	$5.56 \pm .11$
$\alpha_e \times 10^4$		$2.08 \pm .41$	5.2 ± 1.7

Table VI-5. RKR potential turning points for the E state
of ICl

v	G_v (cm^{-1})	R_{min} (\AA)	R_{max} (\AA)
0	84.41	3.207	3.377
1	252.69	3.150	3.447
2	420.25	3.114	3.497
3	587.10	3.084	3.539
4	753.24	3.060	3.576
5	918.66	3.039	3.611
6	1083.37	3.020	3.643
7	1247.37	3.003	3.673
8	1410.66	2.988	3.702
9	1573.23	2.973	3.730
10	1735.08	2.960	3.757

$$r_e = 3.2888 \pm 0.0079 \text{ \AA}$$

($I^{35}\text{Cl}$; $\omega_e' = 168 \text{ cm}^{-1}$, $\omega_e'' = 211 \text{ cm}^{-1}$). Upon reexamining HR's results under the assumption that the emission corresponded to the E+A emission band, the origin (0,0) band they identified at $4196 \overset{\circ}{\text{\AA}}$ was reassigned to the (0,8) transition. The origin (0,0) was assigned to a reasonably strong band at $3945 \overset{\circ}{\text{\AA}}$ and a number of other strong bands were readily reassigned to various (0, v'') transitions (eg: the (0,7) band at $4166 \overset{\circ}{\text{\AA}}$, (0,6) band at $4137 \overset{\circ}{\text{\AA}}$, (0,5) band at $4108 \overset{\circ}{\text{\AA}}$ and the (0,4) band at $4079 \overset{\circ}{\text{\AA}}$ were all strong transitions lying within $\pm 5 \overset{\circ}{\text{\AA}}$ of the expected values for the E+A emission).

In the work by Barnes et al [77], their vibrational numbering was taken from HR and should also be reassigned. The prominent bands in their excitation spectrum, figure 1 of reference 77 was reassigned by subtracting 10 from their numbering for the E state levels. Their probe wavelength of $4169 \overset{\circ}{\text{\AA}}$ lay very close to the 2-9 ($4172 \overset{\circ}{\text{\AA}}$), 1-8 ($4168 \overset{\circ}{\text{\AA}}$) and the 0-7 ($4167 \overset{\circ}{\text{\AA}}$) transitions in the E+A spectrum. With this reassignment the prominent feature at $6685 \overset{\circ}{\text{\AA}}$ was identified as the 1-9 transition in the X-A spectrum ($6684 \overset{\circ}{\text{\AA}}$), and the peak was reassigned to (2, 9, 1) in their (v_E, v_A, v_X) nomenclature. Another strong band at $6765 \overset{\circ}{\text{\AA}}$ in figure 1 of reference 77 should correspond to the 1-8 transition in the X-A spectrum ($6759 \overset{\circ}{\text{\AA}}$) and the peak was reassigned to (1, 8, 1).

The equilibrium internuclear separation for the E state, $r_e = 3.289 \text{ \AA}$, was much larger than the bond lengths in either the A, ($r_e = 2.685 \text{ \AA}$) or the X, ($r_e = 2.32091 \text{ \AA}$) states. The value of $\omega_e = 168.9 \text{ cm}^{-1}$ in the E state was lower than the values of 211.0 cm^{-1} and 384.3 cm^{-1} in the A and X states respectively [65]. Mulliken [18] has suggested, in terms of iodine, that such a large bond length and low vibrational frequency were indicative of an ion-pair state (i.e. the E bands, $4420\text{-}4000 \text{ \AA}$, in iodine, $R_e = 3.55 \text{ \AA}$ and $\omega_e = 101.6 \text{ cm}^{-1}$ [18]).

To further identify the E state, it was necessary to consider the atomic dissociation products in the appropriate energy region. The dissociation of ICl into 2P ground state neutral atoms produced 4 possible combinations: $I(^2P_{3/2}) + Cl(^2P_{3/2})$, $I(^2P_{3/2}) + Cl(^2P_{1/2})$, $I(^2P_{1/2}) + Cl(^2P_{3/2})$, $I(^2P_{1/2}) + Cl(^2P_{1/2})$. The ground state and the A state both dissociated to the same combination $I(^2P_{3/2}) + Cl(^2P_{3/2})$ which lay at the lowest energy point, $D_e = 17557.511 \text{ cm}^{-1}$ [15]. The highest energy combination was the pair $I(^2P_{1/2}) + Cl(^2P_{1/2})$ which lay at 26042 cm^{-1} or 3.23 eV above the ground X state potential minimum. The observed E state minimum lay at 4.83 eV and therefore the state would have been dissociative in diabatic approximation if it had dissociated into ground state atoms.

The ICl covalent dissociation products of next highest energy lay around 9 eV. These levels involved an iodine atom in a $5s^2 5p^4 6s(4P)$ configuration. The $I(4P_{5/2})$ level lay lowest at 54633.5 cm^{-1} . The lowest energy combination $I(4P_{5/2}) + Cl(2P_{3/2})$ was at 72191 cm^{-1} or 8.95 eV. In case (c) coupling this produced 14 states $(4, 3, 2, 1, 0^+, 3, 2, 1, 0^-, 2, 1, 0^+, 1, 0^-)$, four of which had $\Omega = 1$. Only slightly higher in energy was the combination $I(4P_{5/2}) + Cl(2P_{1/2})$ at 73072 cm^{-1} or 9.06 eV. In case (c) this produced 7 states $(3, 2, 1, 0^+, 2, 1, 0^-)$ two of which had $\Omega = 1$. There was also an ionic combination in the same energy region, the combination $I^+(3P_2) + Cl^-(1S)$ at 72763 cm^{-1} or 9.02 eV. This combination produced 3 states $(2, 1, 0^+)$ one of which had $\Omega = 1$. Thus there were 7 possible $\Omega = 1$ states in a suitable energy region which could correlate with the E state. Mulliken [17] had indicated 3 states with $\Omega = 1$ that dissociated into excited atomic products. Two of these states were correlated with components of a case (a) Π state arising from the $\sigma^2 \pi^4 \pi^3 \sigma^x$ (2431) electron configuration of ICl. Cordes and Sponer [75] found a pair of absorption band systems in ICl in the ultraviolet between 1600 \AA and 2000 \AA . The upper levels of these two systems have been identified as this Π state [17]. The third level with $\Omega = 1$ correlated with a case (b) $3\Sigma^-$ state arising from the $\sigma^2 \pi^3 \pi^3 \sigma^{*2}$ (2332) electron configuration of ICl. This $3\Sigma^-$ state may be a reasonable identification of

the observed E state. The antibonding σ^*2 component in the 2332 electron configuration should result in a larger internuclear separation than the X or A states.

It was expected that the transition $E\ 3\Sigma^- + 1\Sigma^+$ would be extremely weak in single photon absorption and probably not observable since it involved a two-electron jump from the ground state (2440) configuration to the (2332) configuration. The two-photon sequential absorption via the intermediate A state (2431) and then to the E state involved two, one-electron steps. Also any residual case (b) coupling would have further weakened a single photon transition, since the $E\ 3\Sigma^- + X\ 1\Sigma^+$ transition would have been forbidden in case (b) due to the $\Sigma^+ \not\leftrightarrow \Sigma^-$ and $\Delta S = 0$ selection rules.

2. The 5eV Region of Iodine Monobromide, $I^{79}\text{Br}$ and $I^{81}\text{Br}$

2.1 Introduction

The low-lying electronic states of IBr are analogous to those of ICl and have been discussed in the literature in some detail [78-81,84-86]. In IBr there should exist a high-lying excited electronic state resembling the E state of ICl outlined in the previous section. Haranth and Rao [89] have observed about 40 emission bands in IBr in the region 3900-3800 \AA , under low resolution. The existence of an electronic state in the 5eV region has now been established for both isotopic species, $I^{79}\text{Br}$ and $I^{81}\text{Br}$.

The absolute vibrational numbering and the molecular constants of this state have also been determined.

2.2 Selection of Pump Lines

As was outlined in Sec. 1.6, Chap. II, IBr possesses three distinct band systems in the visible and near infrared spectral regions (5400-8000 Å). These correspond to the $B^3\Pi(0^+) - X^1\Sigma^+$, the $\tilde{B}'(0^+) - X^1\Sigma^+$ and the $A^3\Pi(1) - X^1\Sigma^+$ transitions. A convenient intermediate state for use in two-photon spectroscopy of the E state region was the $\tilde{B}'(0^+)$ state. Individual rotational, vibrational levels of this state were accessible using dyes in the visible region around 5500 Å. This meant that $\tilde{B}'(0^+) - X^1\Sigma^+$ transition could be readily calibrated against the single photon iodine spectrum.

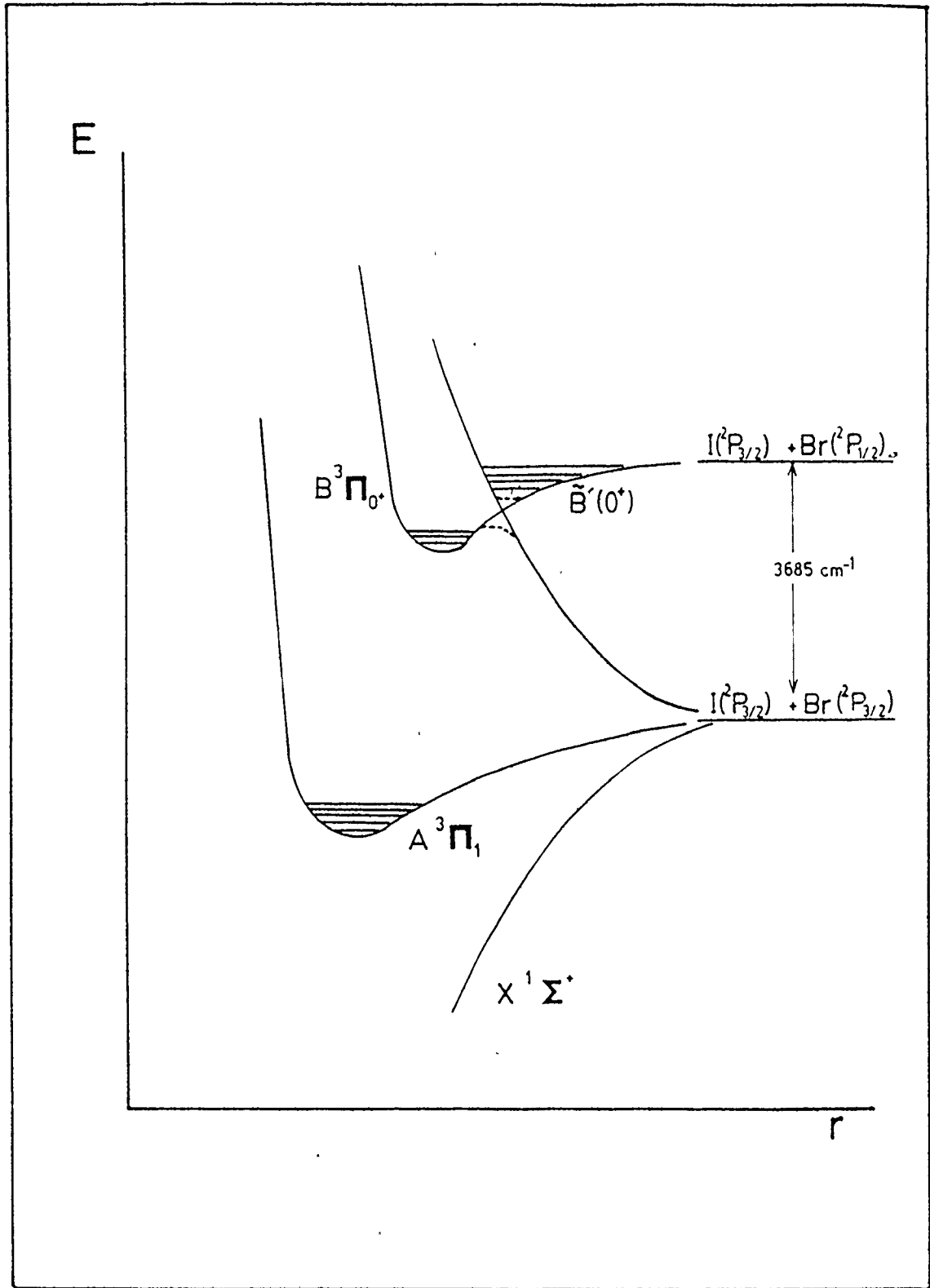
As was the case in ICl, IBr has been found difficult to study by conventional spectroscopic methods due to a 10% dissociation in the gas phase. Because of this dissociation the IBr absorption spectrum is overlapped by the strong absorption spectra of the $^3\Pi(0_u^+) - ^1\Sigma_g^+$ systems of I_2 and Br_2 . The analysis of the visible spectrum of IBr has been further complicated by a strong interaction between the $B^3\Pi(0^+)$ state and a repulsive 0^+ state, resulting in a new $\tilde{B}'(0^+)$ state in adiabatic approximation. The effect of such an avoided crossing has been outlined in Sec. 1.4, Chap. II, and has been extensively discussed in the literature

[57,58,60]. Figure VI-4 illustrates a schematic of this region in IBr.

The ground X ($1\Sigma^+$) state of both $I^{79}\text{Br}$ and $I^{81}\text{Br}$ has been studied by Weinstock et al [85,86] using laser-induced fluorescence. They obtained long progressions of bands in the ground-state vibrational quantum number ($v'' = 0-19$) and thus have established good spectroscopic constants for the ground states of both isotopes.

The vibrational levels ($v' \leq 5$) in the $B^3\Pi(0^+)$ state below the region of the avoided crossing, have been observed [80,88] and their vibrational assignment well established. In the $\tilde{B}'(0^+) - X^1\Sigma^+$ transition only fragmentary bands have been observed in absorption [81,78] and by magnetic rotation spectroscopy [84]. These fragmentary observations consisted mainly of diffuse lines, except for small groups of sharp lines observed for limited sets of J values in particular vibrational levels. Figure 3 of reference 84 illustrates a graph of the term values of the $\tilde{B}'(0^+)$ state, which give rise to sharp spectral lines. This behaviour has been explained by Child et al [58,60] as due to intermediate coupling between the diabatic $B^3\Pi(0^+)$ state and the adiabatic $\tilde{B}'(0^+)$ state. An alternative explanation, in which the vibrational wave function for the $B^3\Pi(0^+)$ state exhibits a node at the apparent crossing point of the bound $B^3\Pi(0^+)$ state with the repulsive 0^+ state, has been put forward by Eberhardt and Sullivan [84].

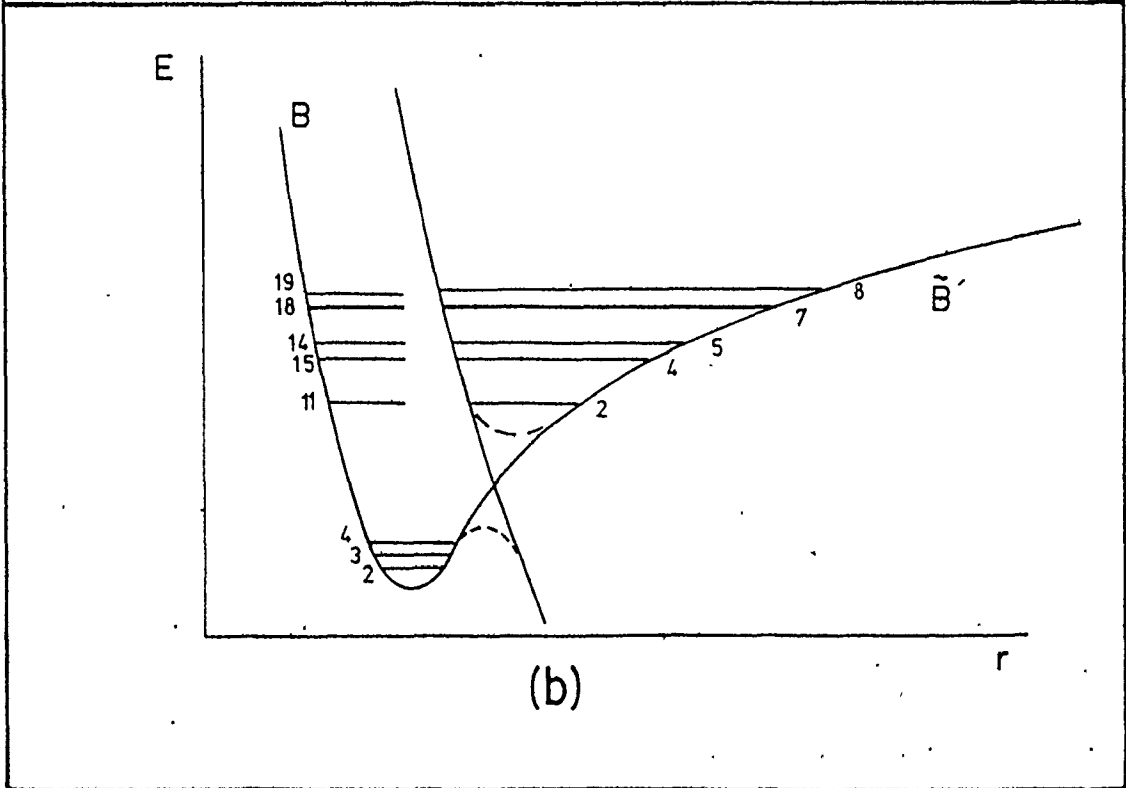
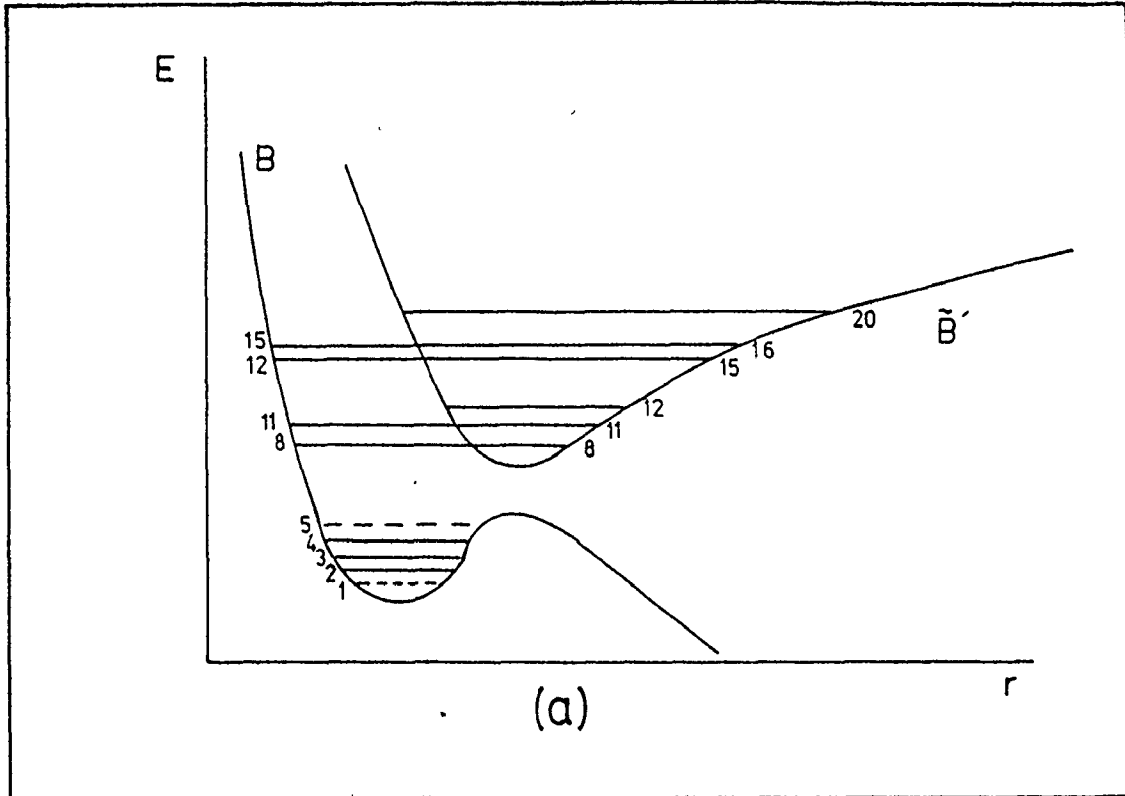
Figure VI-4. Schematic diagram of the valence states of IBr
in the B state region (diagram not to scale)



There is some ambiguity regarding the vibrational numbering adopted in the $\tilde{B}'(0^+)$ state. Eberhardt and Sullivan [84] have used the numbering of Brown [78]. Selin [81] attempted to use the isotope effect to establish the absolute vibrational numbering and from this work believed Brown's numbering should be reduced by 2. His results, however, were sufficiently uncertain that ultimately he maintained Brown's original numbering. Child and Bernstein [58] have suggested this numbering should be reduced by 6, making the lowest observed level $v = 2$ rather than $v = 8$. Child [60], in interpreting the observed spectra in terms of intermediate coupling, has completely renumbered the levels. Using previous experimental results, Child recalculated the term energies relative to the diabatic $B^3\Pi(0^+)$ state and the adiabatic $\tilde{B}'(0^+)$ state, and numbered the levels separately in each state. Figure VI-5 illustrates the two possible numbering schemes.

Two-photon spectroscopy provided another method for studying the intermediate state region of IBr. So far the study of the $\tilde{B}'(0^+)$ state had been limited to a few vibrational levels. These vibrational levels in the $\tilde{B}'(0^+)$ states were only studied in sufficient detail to identify pump lines which could be used in the study of the excited E state. All other previous experimental studies were not sufficiently accurate for this purpose. The two-photon spectra of the $\tilde{B}'(0^+) - X^1\Sigma^+$ transition showed only

Figure VI-5. Two numbering schemes for the \tilde{B}' state in IBr
(a). Selin, Figure 4 of reference 81
(b).. Child, Figure 4 of reference 60



fragmentary bands, which exhibited regions of sharp lines that became broader and weaker as J either increased or decreased away from this region. In the region studied, only three band origins could be established (Figure VI-6). The other bands measured consisted of generally widely spaced lines, with high J values. No systematic study was made of line broadening, nor were the lifetimes of the $\tilde{B}'(0^+) - X^1\Sigma^+$ transition measured. This is a project for further examination.

The term values for each vibrational transition observed in the $\tilde{B}'-X$ transition were calculated by adding the ground X state, $v = 0$ rotational energy to the measured frequencies. The levels were considered accurate to $\pm 0.025 \text{ cm}^{-1}$. The ground state constants were taken from Weinstock et al [86]. The term energies were fit to a second order equation in $J(J + 1)$ as if the $\tilde{B}'(0^+)$ state was an independent adiabatic state. The results obtained are listed in Table VI-6 using the original numbering of Eberhardt and Sullivan [84]. For comparison, Child's calculated results for the $\tilde{B}'(0^+)$ state are listed, along with his numbering scheme, in Table VI-7. In most cases the differences in the term energies in Table VI-7 are probably due to the long extrapolations to the $J' = 0$ intercept. The pump lines used were chosen from these identified vibrational bands. These pump lines are listed in Table VI-8.

Table VI-6. $\tilde{B}'(0^+)$ state of IBr

Isotope	v	T_v (cm^{-1})	$B_v \times 10^2$ (cm^{-1})	$D_v \times 10^7$ (cm^{-1})	Range of J	No. of lines
^{79}Br	27	18131.457(3) ^a	2.27105(201) ^a	1.07(26) ^a	3-29	60
	28	18160.260(15)	2.20748(257)	1.85(13)	17-40	37
	29	18186.927(119)	2.09916(971)	1.19(18)	43-55	20
	30	18210.128(160)	2.06992(1063)	2.36(18)	49-60	30
^{81}Br	8	17212.143(4)	3.22398(432)	6.12 ^b	6-24	55
	26	18094.582(3)	2.33193(187)	1.86(24)	2-29	63
	27	18126.240(12)	2.25519(223)	1.18(10)	22-43	56
	29	18180.684(320)	2.19260(2046)	2.89(33)	51-59	25

^aNumbers in parentheses are errors on the last decimal places of the value.

^bCentrifugal distortion constant poorly determined

Table VI-7. A comparison of this work with the calculations of Child [60] for the $\tilde{B}'(0^+)$ state of IBr

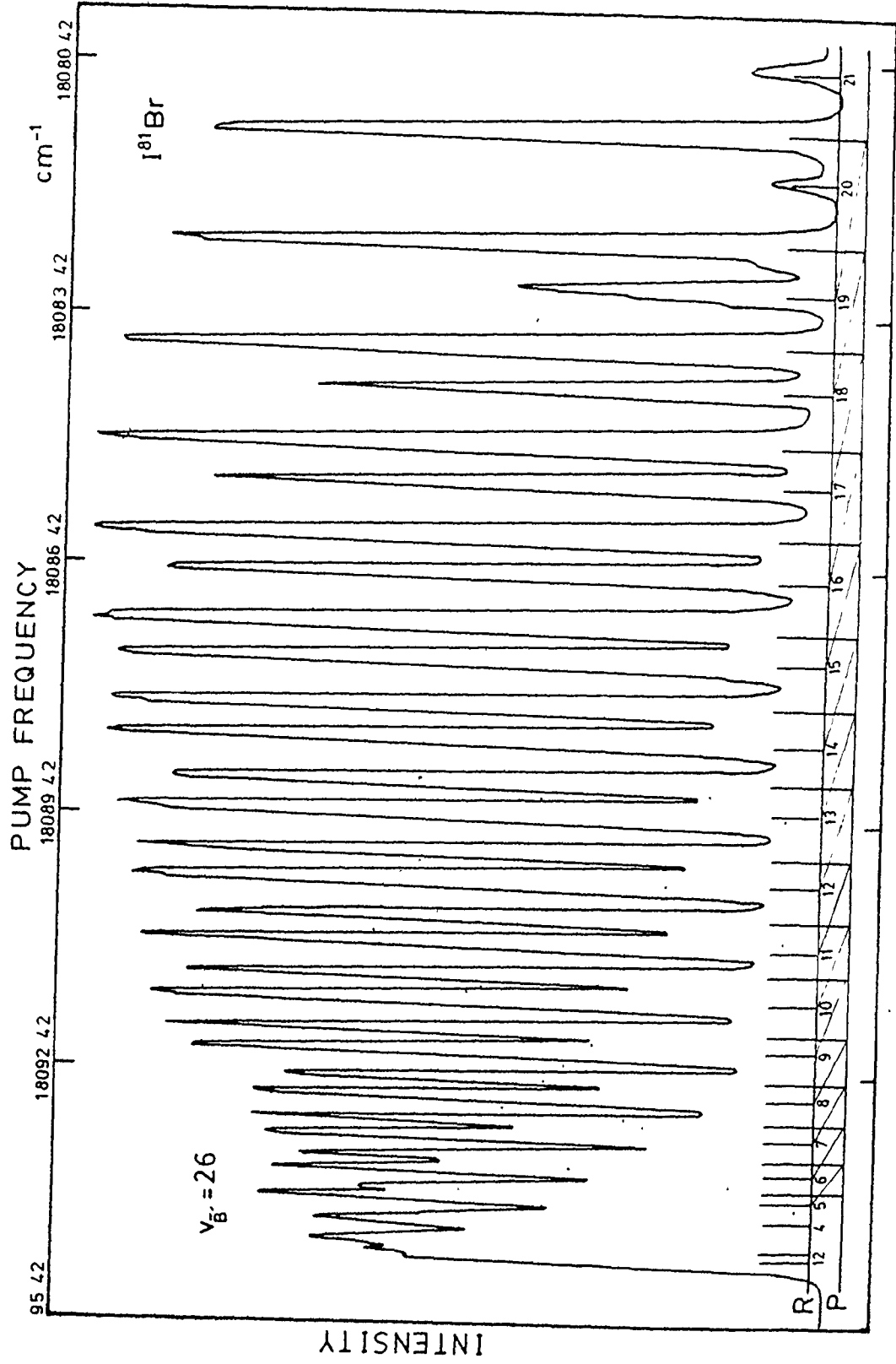
Isotope	v	this work			reference 60		
		T_v (cm^{-1})	B_v (cm^{-1})	v+	T_{v+} (cm^{-1}) ^a	B_{v+} (cm^{-1})	
^{79}Br	27	18131.457	0.02271	17	18132.29	0.02065	
	28	18160.260	0.02207	18	18162.86	0.01995	
	29	18186.927	0.02099	19	18190.44	0.0192	
	30	18210.128	0.02070	20	18215.09	0.0183	
^{81}Br	27	18126.240	0.02255	17	18129.09	0.02035	
	29	18180.684	0.021926	19	18187.5	0.0189	

^aQuoted in reference 60, table 2 relative to the minimum of the X state potential well, corrected here to be relative to $v_X = 0$, $J_X = 0$.

Table VI-8. Pump lines in the $\tilde{B}'(0^+)$ state

Isotope	v	J	
		P	R
$I^{79}Br$	27		3
		8	
	28		22
			29
		29	
			29
			36
		30	
			51
			54
	56		
$I^{81}Br$	8		6
		19	
	27		20
			5
		30	
			39
29		55	

Figure VI-6. Band origin of the $v = 26$ level of the \tilde{B}' state of $I^{81}\text{Br}$



~

2.3 Analysis of the E State Spectra

As was done in the study of ICl, the pump laser was tuned to one of the identified and measured \tilde{B}' -X transitions in one of the isotopic species of IBr. The probe laser was then scanned to induce $E \leftarrow \tilde{B}'$ transitions. This generated a series of vibrational bands for each isotope. Each band consisted of two rotational lines corresponding to $\Delta J = \pm 1$ transitions from the \tilde{B}' pump level. This is illustrated in Figure VI-7 for $I^{79}\text{Br}$, where the pump line was identified as $R_{30}(56)$. This pump level has $v_B = 30$, $J_B = 56$ and an energy $T = 18275.9825 \text{ cm}^{-1}$. The E state lines correspond to rotational levels with $J = 56$ and 58 .

The E state spectra obtained for IBr frequently contained a large number of off-resonance lines. Most of these were not used in the analysis because of the lack of information on the possible intermediate pump levels. Only sets of transitions whose pump level was positively identified through scans of the intermediate state were used. In the region of the coumarin-120 dye profile studied only one set of vibrational levels was positively identified and only a single electronic state in the 5eV region is believed involved. In certain spectra weak lines were tentatively identified as belonging to I_2 . The complicated nature of the spectra, due mostly to the lack of complete knowledge of the intermediate state, made it impossible to rule out the presence of another excited state in the 5eV region. The

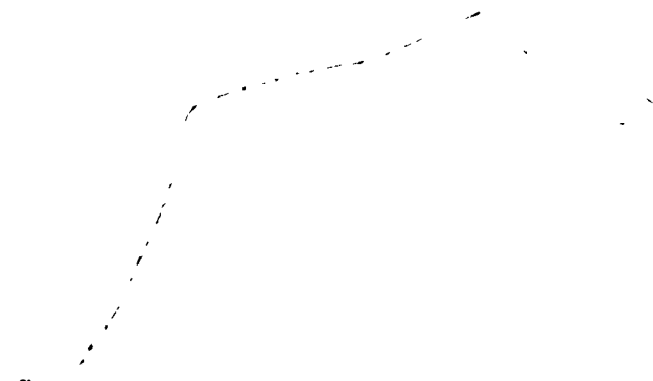
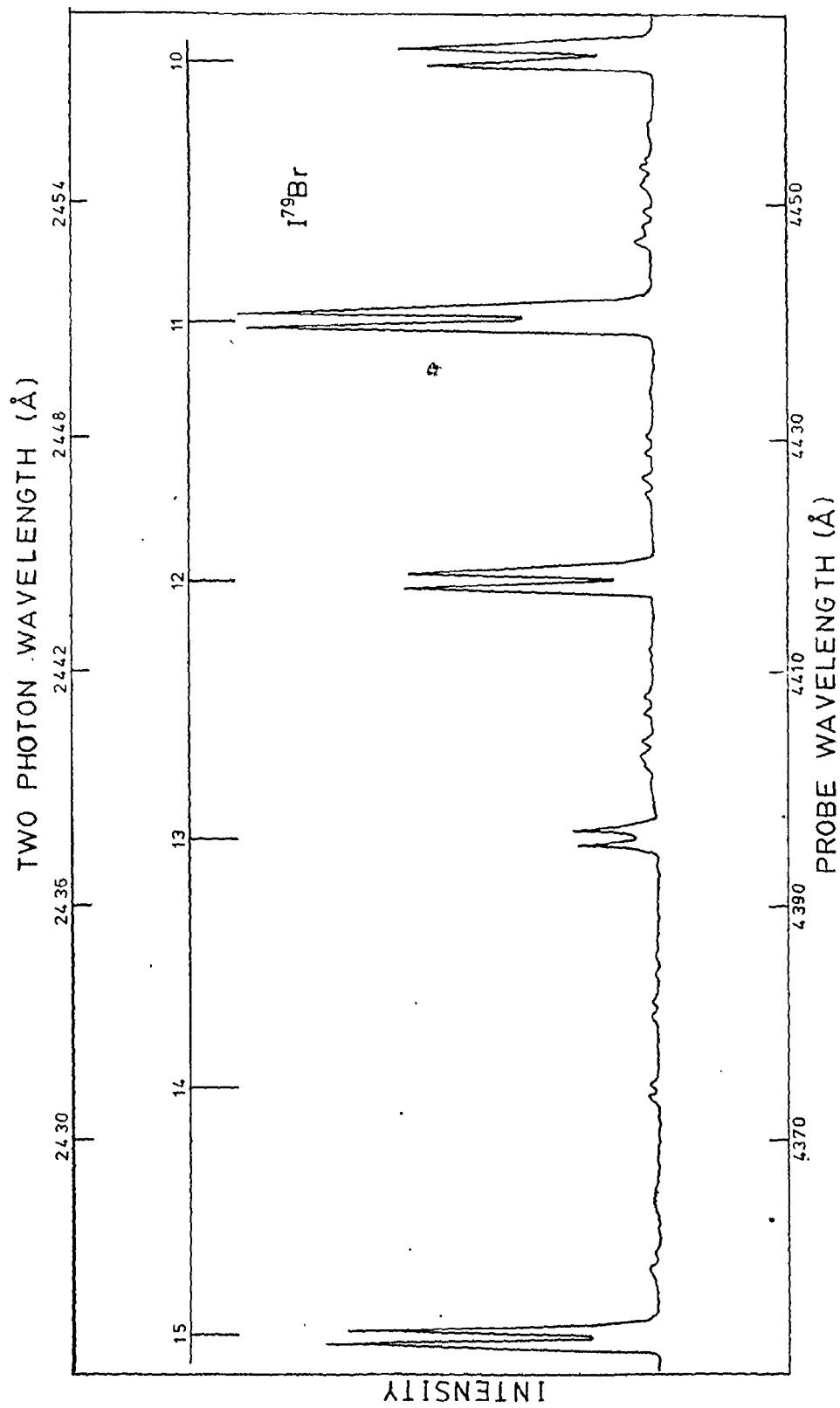


Figure VI-7. E state of $I^{79}\text{Br}$. The B' state pump level is 0-30 R(56), $T = 18275.9863 \text{ cm}^{-1}$. The main progression consists of transitions to rotational levels with $J = 56$ and 58 in the E, state



observed progression contained twelve bands for $I^{79}\text{Br}$ and nineteen bands for $I^{81}\text{Br}$ with a vibrational spacing of $\sim 120 \text{ cm}^{-1}$.

The term values for each E state rotational level were calculated by adding to the measured probe frequency the term value for the \tilde{B}' state pump line calculated previously. The E state term values were fitted by linear regression to a first order equation in $J(J + 1)$. The highest J level observed corresponded to $J = 58$ and second order fits were attempted to obtain centrifugal distortion constants. No definite values could be obtained for D_v ; the values calculated were of varying sign and had significant errors. The first order results are listed in Table VI-9. For $I^{81}\text{Br}$ the $v = 2$ level was observed for only two values of J and the result in Table VI-9 is based on a two point fit. This level was not included in subsequent calculations. On the whole, the results for $I^{81}\text{Br}$ were not as well determined as those for $I^{79}\text{Br}$.

The vibrational term values, T_0 of the E state were fitted to a power series in $n = \rho(v + 1/2)$. The correct vibrational numbering was determined using the combined isotope analysis outlined in Sec. 3.2, Chap. II. The reduced mass of $I^{79}\text{Br}$ was defined as ${}^{79}\mu = 1.0$ and thus the ratio $\rho = ({}^{79}\mu / {}^{81}\mu)^{1/2}$ became $\rho = 1 / ({}^{81}\mu)^{1/2}$. The vibrational term value expression in quadratic approximation is:

Table VI-9. Term values and rotational constants (cm^{-1}) for the E state of IBr

Isotope	v	T_0^a	$B_v \times 10^2$	Range of J	no. of lines
^{79}Br	9	40469.51(27) ^b	2.9483(124) ^b	4-58	10
	10	40584.82(20)	2.9419(113)	4-58	16
	11	40699.50(20)	2.9248(104)	4-58	18
	12	40813.80(22)	2.9083(106)	4-58	15
	13	40928.91(22)	2.8551(110)	7-58	15
	14	41039.96(24)	2.9646(117)	4-58	10
	15	41154.71(20)	2.8899(104)	4-58	18
	16	41267.60(20)	2.8842(113)	4-58	16
	17	41378.91(32)	2.9063(140)	27-58	12
	18	41491.08(42)	2.8542(155)	7-58	8
19	41602.45(23)	2.8707(117)	4-58	12	
20	41712.87(53)	2.8509(232)	29-56	4	

Table VI-9 continued

Isotope	v	T_0^a	$B_v \times 10^2$	Range of J	no. of lines
$I^{81}Pr$	0	39415.50 (56)	3.6759 (1647)	7-21	4
	1	39534.66 (56)	3.0217 (1647)	7-21	4
	2 ^c	39651.91	3.0123	7-21	2
	3	39769.77 (56)	2.9109 (1647)	7-21	4
	4	39886.53 (56)	3.1355 (1647)	7-21	4
	5	40003.47 (56)	2.9944 (1647)	7-21	4
	6	40119.57 (56)	2.8178 (1647)	7-21	4
	8	40350.26 (30)	2.7601 (154)	7-57	7
	9	40464.32 (27)	2.8028 (144)	6-57	6
	10	40578.48 (47)	2.7772 (140)	6-57	10
	11	40692.59 (26)	2.7681 (150)	7-57	9
	12	40803.99 (34)	2.8465 (170)	6-57	7
	13	40917.13 (43)	2.8404 (190)	6-57	5
	14	41029.67 (35)	2.8791 (201)	6-57	6
	15	41142.26 (34)	2.8218 (170)	6-57	7
	16	41253.91 (34)	2.8268 (170)	6-57	7
	17	41365.14 (50)	2.8144 (194)	6-57	3
	18	41476.05 (43)	2.8163 (190)	6-57	5
	19	41586.85 (34)	2.7652 (170)	6-57	7

Table VI-9 continued

^aRelative to $v_X = 0$, $J_X = 0$

^bNumbers in parentheses are errors on the last decimal places of the value.

^cValues for $v = 2$ were based on a two point fit and are not included in the analysis.

$$T_0 = T_e + \omega_e'(\eta) + \omega_e x_e (\eta^2) \quad \text{VI-5}$$

where ${}^{81}_0 = 0.9923587$ and ${}^{79}_0 = 1.0$. The vibrational term values T_0 were corrected to be relative to the ground X state potential minimum rather than $v_X = 0, J_X = 0$ by adding on the ground state zero-point energy to the values in Table VI-9. The ground state zero-point energies were calculated from Weinstock's constants [86]:

$${}^{79}_G(0) = 134.1470 \text{ cm}^{-1}$$

$${}^{81}_G(0) = 133.1030 \text{ cm}^{-1}$$

In this manner all the data could be fitted to a single polynomial exactly satisfying the isotope relationships. A very distinct minimum in χ^2 was obtained for the vibrational numbering given in Table VI-9 when the term energies (weighted by $1/\sigma^2$) were fit to equation VI-5. The coefficients were also obtained using independent quadratic fits to the two sets of isotopic data using the numbering determined previously. The coefficients are listed in Table VI-10.

The rotational constants were treated in the same manner. The mass-reduced rotational constant can be expressed in a linear approximation as:

$$B(\eta) = B_v/\rho^2 = B_e - \alpha_e(\eta) \quad \text{VI-6}$$

Table VI-10. Molecular constants for the E state of IBr

Constant (cm^{-1})	Combined Isotope	I^{79}Br	I^{81}Br
<u>Combined Isotope Fit</u>			
T_e^a	39490.779 ± 0.364	$39490.78 \pm .36$	$39490.78 \pm .36$
T_e^b		39356.63	39357.68
ω_e	$119.296 \pm .690$	$119.30 \pm .69$	$118.38 \pm .69$
$\omega_e x_e$	$0.21276 \pm .00305$	$0.2128 \pm .0031$	$0.2095 \pm .0031$
<u>Independent Quadratic Fit</u>			
T_e^b		39352.45 ± 2.99	$39357.18 \pm .36$
ω_e		$119.68 \pm .41$	$118.62 \pm .08$
$\omega_e x_e$		$0.2210 \pm .0137$	$0.2220 \pm .0039$

^aRelative to the minimum of the ground state potential well

^bRelative to $v_X''=0, J_X''=0$

The rotational constants for the two isotopes were determined from this combined polynomial exactly obeying the isotope relationships and from independent linear fits to the data. These constants are listed in Table VI-11.

Using these results, the centrifugal distortion constant D_e was calculated for each isotope from ω_e and B_e values using the relationship $D_e = 4B_e^2/\omega_e^3$ [19]. The values calculated were on the order of 10^{-9} cm^{-1} . Since these small values did not contribute significantly even at the maximum observed J value, the term values for the E state were not recalculated incorporating these centrifugal distortion corrections.

An RKR potential was constructed for the lower vibrational levels in the E state from the combined results. The vibrational turning points are listed in Table VI-12.

2.4 Discussion

Haranath and Rao (HR) [89] have observed about 40 emission bands in the region 3900-3800 Å, produced from IBr vapor in a condensed discharge. The results were obtained under low resolution and the bands were diffuse and red-degraded. There was also considerable overlap from iodine and bromine emission lines. HR analysed the bands in terms of $\omega_e' = 104.0 \text{ cm}^{-1}$ and $\omega_e'' = 140.0 \text{ cm}^{-1}$ and identified the lower state of this system as the $A^3\Pi_1$ state. Their bands were reassigned to the E+A emission expected from our E state;

Table VI-11. Rotational constants of the E state of IBr

Constant (cm^{-1})	Combined Isotope	I^{79}Br	I^{81}Br
<u>Combined Isotope Fit</u>			
$B_e \times 10^2$	$3.0738 \pm .0090$	$3.0738 \pm .0090$	$3.0270 \pm .0090$
$\alpha_e \times 10^4$	$1.287 \pm .065$	$1.287 \pm .065$	$1.258 \pm .065$
<u>Independent Linear Fit</u>			
$B_e \times 10^2$		$3.0084 \pm .0162$	$3.0856 \pm .0113$
$\alpha_e \times 10^4$		7.25 ± 1.10	$2.009 \pm .092$

Table VI-12. RKR turning points for the lower vibrational levels of the E state of IBr

v	G_v (cm ⁻¹)	R_{\min} (Å)	R_{\max} (Å)
0	59.59	3.284	3.437
1	178.46	3.235	3.499
2	296.91	3.202	3.544
3	414.93	3.177	3.583
4	532.52	3.156	3.617
5	649.69	3.138	3.648
6	766.43	3.122	3.677
7	882.75	3.108	3.705
8	998.64	3.094	3.731
9	1114.11	3.082	3.756
10	1229.15	3.071	3.781
11	1343.76	3.061	3.805
12	1457.95	3.051	3.828
13	1571.72	3.042	3.850
14	1685.05	3.033	3.873
15	1797.97	3.025	3.894
16	1910.46	3.018	3.916
17	2022.52	3.010	3.937
18	2134.15	3.004	3.957
19	2245.36	2.997	3.978
20	2356.15	2.991	3.998

$$r_e = 3.35721 \text{ \AA}$$

but instead of being transitions to low levels in the A state well, their transitions appeared to match up with transitions to $v'' \geq 8$. Strong bands which they had assigned as progressions in the upper state were reassigned to $(2, v'')$, $(1, v'')$ and $(0, v'')$ progressions in the lower state vibrational levels. This change in assignment yielded $\omega_e' = 120 \text{ cm}^{-1}$ from their results. The strong band at 3856 \AA assigned to $(0,0)$ was reassigned to a $(0,10)$ transition that occurred at 3853 \AA . The next strongest transition at 3841 \AA assigned to $(1,0)$ was reassigned to $(0,9)$, which occurred at 3838 \AA .

No Q branch lines corresponding to $\Delta J = 0$ transitions were observed in the $E^+ \tilde{B}'$ spectra. The \tilde{B}' state has $\Omega = 0^+$, and under the case (c) selection rule, $\Delta \Omega = 0, \pm 1$, there were two possibilities for the $E^+ \tilde{B}'$ transition, $0^+ \leftarrow 0^+$ and $1 \leftarrow 0^+$. A case (c) $1 \leftarrow 0^+$ transition would have a structure similar to that of a case (a) ${}^1\Pi \leftrightarrow {}^1\Sigma$ transition. A ${}^1\Pi - {}^1\Sigma$ transition would be the same under case (a) and (b) with $\Delta J = 0$ and $\Delta J = \pm 1$ transitions allowed. Strong P, Q, R lines should be observed. A case (c) $0^+ \leftarrow 0^+$ transition would have a structure similar to a case (a) ${}^1\Sigma - {}^1\Sigma$ transition. Again there would be no difference between case (a) and (b) and only $\Delta J = \pm 1$ transitions would be allowed. A single P and a single R branch line should be observed. It was most probable therefore, that the $E^+ \tilde{B}'$ transition was a $0^+ \leftarrow 0^+$ transition under case (c).

The dissociation of IBr into neutral $^2P_{1/2, 3/2}$ atoms results in four pairs of atomic combinations. The ground $X^1\Sigma^+$, the $A^3\Pi_1$ state and the $B^3\Pi(0^+)$ state all dissociate into the lowest energy combination $I(^2P_{3/2}) + Br(^2P_{3/2})$ with $D = 14660 \text{ cm}^{-1}$ [78]. The $\tilde{B}'(0^+)$ state dissociates into the next highest atomic combination $I(^2P_{3/2}) + Br(^2P_{1/2})$ at approximately 18345 cm^{-1} [78]. The highest energy combination $I(^2P_{1/2}) + Br(^2P_{1/2})$ occurs at 25948 cm^{-1} or 3.22eV relative to the ground state potential minimum. As was the case in ICl, the E state of IBr at 4.88eV would be dissociative in diabatic approximation if it separated into ground state atoms.

The IBr covalent dissociation products of next highest energy occur in the $8.5\text{-}9\text{eV}$ region. Unlike ICl they are not as close together in energy. The lowest lying atomic pair is $I(^4P_{5/2}) + Br(^2P_{3/2})$ at 8.59eV . This pair would result in 14 states in case (c) approximation of which two have $\Omega = 0^+$. At higher energy, the combination $I(^4P_{5/2}) + Br(^2P_{1/2})$ at 9.05eV would result in 7 states with one having $\Omega = 0^+$. Between these two covalent pairs would lie the ionic combination $I^+(^3P_2) + Br^-(^1S)$ at 8.92eV . This combination would produce 3 states, one of which has $\Omega = 0^+$. This resulted in 4 possible $\Omega = 0^+$ states in the correct energy region.

The interpretation of the E state in IBr closely followed that of ICl. Mulliken [17] had considered the excited states of ICl using simple MO theory. These considerations were applied to IBr. Mulliken had identified three states with $\Omega = 0^+$ which dissociated to either excited atomic products or ionic ones. One of these levels was correlated with the components of a case (a) Π state which, like ICl, was identified as the upper state of the two band systems observed by Cordes and Spomer in the 1600-2000 Å region [75]. The other two states with $\Omega = 0^+$ correlated with a case (a) $3\Sigma^-$ state and a case (a) $1\Sigma^+$ state, both of which arose from the $\sigma^2 \pi^3 \pi^* 3\sigma^* 2$ (2332) electron configuration.

In an early fluorescence study of IBr, Loomis and Allen [145] excited low pressure IBr vapor with 1849 Å light, producing a series of lines that cut off at 2500 Å. At this point the line structure ceased and a number of diffuse, headless bands extending to 3700 Å were found. No corresponding sequence was observed in ICl. Mulliken has pointed out [17] that this resembles the UV fluorescence spectrum of I_2 following excitation to the D state. He postulated this fluorescence in IBr follows excitation to energy levels belonging to the $\sigma^2 \pi^4 \pi^* 3\sigma^x$ configuration.

In ICl it was postulated that the E state corresponded to the $3\Sigma^-$ state arising from the (2332) electron configuration. Unlike the E $3\Sigma^- - X 1\Sigma^+$ transition in ICl,

which would not be allowed in case (a) approximation, an $E \ ^1\Sigma^+ - X \ ^1\Sigma^+$ transition in IBr would be allowed. However, it would still correspond to a two-electron jump from the ground $X \ ^1\Sigma^+$ (2440) state to the $E \ ^1\Sigma^+$ (2332) state. The E state of IBr with an equilibrium bond length $r_e = 3.357 \text{ \AA}$ and $\omega_e = 119.3 \text{ cm}^{-1}$, in comparison to the X state with $r_e = 2.469 \text{ \AA}$ and $\omega_e = 268.67 \text{ cm}^{-1}$, does exhibit ion-pair character [18]. The ionic combination $I^+(^3P_2) + Br^-(^1S)$ that lies in this energy region would only give rise to triplet states. Both of the states under consideration, the $^1\Sigma^+$ and the $^3\Sigma^-$, arise from the (2332) configuration with its antibonding σ^*2 component, which should increase the equilibrium bond length. The evidence is as yet insufficient to assign the E state of IBr to one single electronic configuration.

Chapter VII

CONCLUSION

The early studies of $^{127}\text{I}_2$ have now been improved by the use of more pump levels, advanced measurement techniques, and the use of the isotopic molecule $^{129}\text{I}_2$. The B state dissociation limit region has been studied in $^{129}\text{I}_2$ up to $v_B = 79$ and the results for the two isotopes successfully combined in a single mass-reduced set of equations. Of the five excited states in the 5eV region of iodine, four of these have been studied in both isotopes; combined isotope analysis has established the absolute vibrational numbering, and thus reliable molecular constants. The fifth excited state, the δ state, was found to be too weak to study in $^{129}\text{I}_2$. Initial work has been started on the measurement of the fluorescence lifetimes of these high-lying excited states, and the effects of saturation, iodine vapor pressure and the presence of inert buffer gases were examined.

In $^{35}\text{Cl}/^{37}\text{Cl}$ and $^{79}\text{Br}/^{81}\text{Br}$ these studies have verified the excellence of these two-photon methods for unravelling complicated, overlapping spectra containing more than one species. A single excited state in the 5eV region of these molecules has been measured and a combined isotope analysis has been applied to establish the absolute vibrational numbering and the molecular constants. Unlike

I_2 and ICl , the intermediate \tilde{B}' state in IBr used in these experiments did not have a body of detailed measurements existing in the literature. No systematic study of this region was undertaken here; however, more accurate measurements than currently available in the literature were made on a few of the vibrational levels of this state.

The work on the spectroscopy of iodine, and certainly that on the interhalogens ICl and IBr , has not answered every question. The study of the vibrational levels of the high lying excited states should be done under higher resolution to resolve more of the rotational structure on these bands. This would help in establishing whether or not Q branch lines exist at low J. Both ICl and IBr need to be investigated in more detail in the 5eV region using a greater range of probe laser dyes. Only a single excited state has so far been measured in either of these molecules in this region. In IBr , the avoided crossing region of the B and \tilde{B}' states should be further studied using the isotope selectivity and detailed resolution of these two-photon methods in the intermediate state region. Resolution of the fluorescence from the high lying excited states in iodine and the interhalogens would provide further information on the processes involved. This would establish the lower states involved in the fluorescence and in the case of IBr provide another means of studying the complicated \tilde{B}' state region.

The lifetime measurements in general need refinement. The lifetimes of the high lying excited states in ICl and IBr should be measured. Along with those in I_2 , these measurements should be done at a number of different vapour pressures. The lifetimes of the vibrational levels in the B state of I_2 near dissociation should be examined along with the lifetimes of the "X bands" that occur near dissociation of the A state in ICl [15]. The lifetimes of the vibrational levels of the B and \tilde{B}' states, involved in the avoided crossing in IBr should be studied in detail. The study of the effects of self-quenching and foreign-gas quenching should be expanded to include all three molecules. A more detailed set of experiments should be undertaken with careful attention being paid to the three level kinetics involved.

Much of the spectroscopy that needs to be done necessitates changes in the laser spectrometer system. An optical multichannel analyser should be incorporated to resolve the fluorescence. The mechanical scan probe laser should be replaced with a dye laser with a narrower bandwidth, to allow better resolution of the vibrational levels in the E state region. The bandwidth ideally should be variable since the initial discovery of a state is greatly facilitated by a broad bandwidth probe which overlaps a large number of transitions. It is also necessary to overlap as many upper state levels as possible when using two-photon detection of

the intermediate state structure.

Calibration is an ongoing problem in laser systems. The optogalvanic effect [146-149] has been suggested as a means of directly calibrating dye lasers. Attempts were made during the course of this work to stimulate this effect in commercial hollow cathode lamps with very limited success (the pulsed dye laser used in this study would only stimulate a single strong Ne transition). It may be necessary to develop special discharge lamps to observe the effect. The I_2 atlas of Gerstenkorn and Luc [29] should be stored in the computer and computer searching used to match up calibration spectra. In regions outside the B-X system of I_2 , a calibration method is lacking for the narrow bandwidth pressure scan laser. It may be possible to use absorption lines in atomic species such as cesium along with reference etalons to accomplish this.

The measurement of lifetimes requires two immediate improvements: the incorporation of a high speed preamplifier to increase the signal strength; and the use of a transient recorder to capture each laser pulse. The latter instrument would greatly decrease the time spent averaging the signal. The ringing noise problems encountered during these experiments may be due to ground loop problems in the signal lines and could possibly be eliminated.

The measurement of the intermediate state lifetime by directly observing the fluorescence from this state will

not be possible in ICl and IBr due to the interference from other fluorescing species. The use of a White cell to introduce an optical delay in the probe laser path to delay it relative to the pump laser is one method, using two-photon detection, to measure this lifetime. Due to the large number of mirror reflections required, this was not totally successful when applied. The same idea could alternatively be used by employing two nitrogen lasers, one of which would be delayed relative to the other, to pump the dye lasers. The synchronization of this may be a problem and a single nitrogen laser could be used by delaying the beam pumping one of the dye lasers from the other by only a single set of reflections off a widely spaced set of mirrors. This delayed nitrogen pulse could be used to actually pump the dye laser or act as a trigger for a fast shutter in front of a flashlamp pumped dye laser. The use of a single nitrogen laser may introduce too many losses which may have to be compensated for by going to a more powerful excimer laser as a pump source. This method of optical delay could also be used to study the vibrational levels in the B state of iodine near dissociation, where direct observation of the fluorescence is not possible.

Work on self-quenching and foreign-gas quenching would be greatly facilitated by the construction of a sample cell that contains a capacitance manometer built into it. In this way, accurate pressure measurements could be made at all

times during the experiments. Outside of the work involved in the spectroscopy, the partial pressures of the various molecules present in the samples of ICl and particularly IBr must be studied. This would be a necessary step towards understanding any collisional data on these molecules.

The minicomputer is currently under-used in this system. It may be possible to expand its control of the equipment to the actual operation of the dye lasers themselves. This would necessitate the change from a free-running nitrogen laser to a more reliable, reproducible, triggered system. It would also involve accurate measurement of the output powers of all the various lasers. The computer could be used to normalize the spectra to the output of the nitrogen laser and remove any pulse-to-pulse variation.

There is no question that two-photon sequential absorption spectroscopy in conjunction with computerized data acquisition is a very sophisticated method of investigating the excited states of diatomic molecules. The use of all available isotopes without resorting to often difficult enrichment processes is another point in favour of these methods. The future development of the equipment lies in improved dye laser resolution, increased knowledge of the lasers' output characteristics and increased use of computer control.

Chapter VIII

REFERENCES

1. J. I. Steinfeld, P. L. Houston, Lasers and Coherence Spectroscopy, J. I. Steinfeld (ed), Chapter 1 (Plenum Press, New York, 1978)
2. M. D. Danyluk, Ph.D. Thesis, McMaster University, Hamilton, Ontario, 1978
3. R. A. Gottscho, R. W. Field, R. Bacis, S. J. Silvers, J. Chem. Phys. 73, 599 (1980)
4. R. A. Gottscho, J. B. Koffend, R. W. Field, J. Mol. Spectr. 82, 310 (1980)
5. R. A. Gottscho, P. S. Weiss, R. W. Field, J. Mol. Spectr. 82, 283 (1980)
6. P. F. Bernath, R. W. Field, J. Mol. Spectr. 82, 339 (1980)
7. P. J. Domaille, T. C. Steimle, D. O. Harris, J. Chem. Phys. 68, 4977 (1978)
8. M. D. Danyluk, G. W. King, Chem. Phys. Lett. 44, 440 (1976)
9. M. D. Danyluk, G. W. King, Chem. Phys. 22, 59 (1977)
10. G. W. King, I. M. Littlewood, J. R. Robins, Chem. Phys. 56, 145 (1981)
11. R. A. Bernheim, L. P. Gold, P. B. Kelly, C. Kittrell, D. K. Veirs, Phys. Rev. Lett. 43, 123 (1979)
12. M. D. Danyluk, G. W. King, Chem. Phys. Lett. 43, 1 (1976)
13. M. D. Danyluk, G. W. King, Chem. Phys. 25, 343 (1977)
14. G. W. King, I. M. Littlewood, J. R. Robins, N. T. Wijeratne, Chem. Phys. 50, 291 (1980)

15. G. W. King, R. G. McFadden, Chem. Phys. Lett. 58, 119 (1978)
16. G. W. King, I. M. Littlewood, R. G. McFadden, J. R. Robins, Chem. Phys. 41, 379 (1979)
17. R. S. Mulliken, Phys. Rev. 46, 549 (1934)
18. R. S. Mulliken, J. Chem. Phys. 55, 288 (1971)
19. G. Herzberg, Molecular Spectra and Molecular Structure, Volume 1 Spectra of Diatomic Molecules, (Van Nostrand Rienhold, 1950)
20. R. S. Mulliken, Phys. Rev. 36, 1440 (1930)
21. J. A. Coxon, Molecular Spectroscopy - Specialist Periodical Reports, R. F. Barrow, D. A. Long, D. J. Millen (eds), Volume 1, Chapter 4, (Chemical Society of London, 1973)
22. A. J. Downs, C. J. Adams, Comprehensive Inorganic Chemistry, J. C. Bailar Jr., H. J. Emeleus, Sir Ronald Nyholm, A. F. Trotman-Dickinson (eds), Volume 2, Chapter 26, (Pergamon Press, 1973)
23. C. Teichteil, J. P. Malrieu, Chem. Phys. Lett. 49, 152 (1977)
24. G. Dass, A. C. Wahl, J. Chem. Phys. 69, 53 (1978)
25. R. Mecke, Ann. Phys. 71, 104 (1923)
26. R. J. Le Roy, J. Chem. Phys. 52, 2683 (1970)
27. R. F. Barrow, K. K. Yee, J. Chem. Soc. Faraday II 69, 684 (1973)
28. J. Wei, J. Tellinghuisen, J. Mol. Spectr. 50, 317 (1974)
29. S. Gerstenkorn, P. Luc, Atlas du Spectra D'Absorption de la Molecule de L'Iode (14800-20000 cm-1), (Editions du C. N. R. S., Paris, France, 1978)
30. S. Gerstenkorn, P. Luc, Rev. Phys. Appl. 14, 791 (1979)
31. S. Gerstenkorn, P. Luc, A. Perrin, J. Mol. Spectr. 64, 56 (1977)
32. P. Luc, J. Mol. Spectr. 80, 41 (1980)

33. K. K. Yee, J. Chem. Soc. Faraday II 72, 2113 (1976)
34. S. Gerstenkorn, P. Luc, J. Mol. Spectr. 77, 310 (1979)
35. R. Bacis, S. Churassy, R. W. Field, J. B. Koffend, J. Verges, J. Chem. Phys. 72, 34 (1980)
36. J. B. Koffend, R. Bacis, R. W. Field, J. Mol. Spectr. 77, 202 (1979)
37. J. B. Koffend, F. J. Wodarczyk, R. Bacis, R. W. Field, J. Chem. Phys. 72, 478 (1980)
38. J. Tellinghuisen, M. R. McKeever, A. Sur, J. Mol. Spectr. 82, 225 (1980)
39. J. Tellinghuisen, Chem. Phys. Lett. 18, 544 (1973)
40. J. Tellinghuisen, D. L. Albritton, J. Mol. Spectr. 57, 160 (1975)
41. R. D. Verma, J. Chem. Phys. 32, 738 (1960)
42. K. Wieland, J. Tellinghuisen, A. Nobs, J. Mol. Spectr. 41, 69 (1972)
43. J. Tellinghuisen, Chem. Phys. Lett. 49, 485 (1977)
44. A. Guy, K. S. Viswanathan, A. Sur, J. Tellinghuisen, Chem. Phys. Lett. 73, 582 (1980)
45. J. Tellinghuisen, Phys. Rev. Lett. 34, 1137 (1975)
46. D. L. Rousseau, P. F. Williams, Phys. Rev. Lett. 33, 1368 (1974)
47. D. L. Rousseau, J. Mol. Spectr. 58, 481 (1975)
48. E. W. Condon, Phys. Rev. 32, 858 (1928)
49. S. L. Cunha, J. A. Lispoa, R. E. Francke, H. P. Grienbisen, B. P. Chakraborty, Opt. Commun. 28, 321 (1979)
50. A. D. Williamson, Chem. Phys. Lett. 60, 451 (1979)
51. M. Kawasaki, K. Tsukiyama, M. Kuwana, K. Obi, I. Tanaka, Chem. Phys. Lett. 67, 365 (1979)
52. K. Chen, L. E. Steinhock, E. S. Young, Chem. Phys. Lett. 59, 222 (1978)

53. C. Tai, F. W. Dalby, G. L. Giles, Phys. Rev. A20, 233 (1979)
54. K. K. Lehmann, J. Smolarek, L. Goodman, J. Chem. Phys. 69, 1569 (1978)
55. H. Hemmati, G. J. Collins, Chem. Phys. Lett. 75, 488 (1980)
56. K. Kasatani, Y. Tanaka, K. Shibuya, M. Kawasaki, K. Obi, H. Sato, I. Tanaka, J. Chem. Phys. 74, 895 (1981)
57. A. D. Bandrauk, M. S. Child, Mol. Phys. 19, 95 (1970)
58. M. S. Child, R. B. Bernstein, J. Chem. Phys. 59, 5916 (1973)
59. M. S. Child, Molecular Spectroscopy - Specialist Periodical Reports, R. F. Barrow, D. A. Long, D. J. Millen (eds), Volume 2, Chapter 7 (The Chemical Society, London, 1974)
60. M. S. Child, Mol. Phys. 32, 1495 (1976)
61. E. Hulthén, N. Johansson, U. Pilsater, Ark. Fys. 14, 31 (1958)
62. E. Hulthén, N. Johansson, L. Koffman, Ark. Fys. 18, 479 (1960)
63. M. A. A. Clyne, J. A. Coxon, Proc. Roy. Soc. A298, 424 (1962)
64. J. A. Coxon, R. M. Gordon, M. A. Wickramaaratchi, J. Mol. Spectr. 79, 363 (1980)
65. J. A. Coxon, M. A. Wickramaaratchi, J. Mol. Spectr. 79, 380 (1980)
66. G. W. Holliman, J. I. Steinfeld, Chem. Phys. Lett. 12, 431 (1971)
67. M. D. Havey, J. J. Wright, J. Chem. Phys. 68, 4754 (1978)
68. S. J. Harris, W. C. Natzle, C. B. Moore, J. Chem. Phys. 70, 4215 (1979)
69. W. G. Brown, G. E. Gibson, Phys. Rev. 40, 529 (1932)

70. M. A. A. Clyne, I. S. McDermid, J. Chem. Soc. Faraday II, (a) 72, 2242 (1976); (b) 72, 2252 (1976)
71. C. D. Olson, K. K. Innes, J. Chem. Phys. 64, 2405 (1976)
72. M. A. A. Clyne, I. S. McDermid, J. Chem. Soc. Faraday II, 73, 1094 (1977)
73. R. D. Gordon, K. K. Innes, J. Chem. Phys. 71, 2824 (1979)
74. R. D. Gordon, J. Mol. Spectr. 78, 350 (1979)
75. H. Cordes, H. Sponer, Z. Phys. 63, 334 (1930)
76. P. B. V. Haranath, P. T. Rad, Ind. J. Phys. 31, 156 (1957)
77. R. H. Barnes, C. E. Moiller, J. F. Kircher, C. M. Verber, App. Phys. Lett. 24, 610 (1974)
78. W. G. Brown, Phys. Rev. 42, 355 (1932)
79. L. E. Selin, Ark. Fys. 21, 479 (1961)
80. L. E. Selin, B. Soderborg, Ark. Fys. 21, 515 (1961)
81. L. E. Selin, Ark. Fys. 21, 529 (1961)
82. M. A. A. Clyne, J. A. Coxon, J. Mol. Spectr. 23, 258 (1967)
83. W. H. Eberhardt, W. Cheng, H. Renner, J. Mol. Spectr. 3, 664 (1959)
84. W. H. Eberhardt, W. Sullivan, J. Mol. Spectr. 70, 270 (1978)
85. E. M. Weinstock, J. Mol. Spectr. 61, 395 (1976)
86. E. M. Weinstock, A. Preston, J. Mol. Spectr. 70, 188 (1978)
87. J. J. Wright, M. D. Havey, J. Chem. Phys. 68, 864 (1978)
88. M. A. A. Clyne, M. C. Heaven, J. Chem. Soc. Faraday II, 76, 49 (1980)
89. P. B. V. Haranath, P. T. Rao, Ind. J. Phys. 31, 368 (1956)

90. H. Krockel, E. Tiemann, D. Zoglowck, *J. Mol. Spectr.* 85, 225 (1981)
91. R. J. Le Roy, Molecular Spectroscopy - Specialist Periodical Report, R. F. Barrow, D. A. Long, D. J. Millen (eds), Volume 1, Chapter 3 (The Chemical Society, London, 1973)
92. R. J. Le Roy, R. B. Bernstein, *J. Chem. Phys.* 52, 3869 (1970)
93. R. J. Le Roy, R. B. Bernstein, *J. Mol. Spectr.* 37, 109 (1971)
94. R. J. Le Roy, R. B. Bernstein, *Chem. Phys. Lett.* 5, 42 (1970)
95. R. J. Le Roy, *Can. J. Phys.* 50, 953 (1972)
96. E. Merzbacher, Quantum Mechanics (John Wiley & Sons, 1961)
97. R. J. Le Roy, *Can. J. Phys.* 52, 246 (1974)
98. R. J. Le Roy, private communication
99. R. J. Le Roy, Semiclassical Methods in Molecular Scattering and Spectroscopy, M. S. Child (ed) pp 109-126 (NATO Advanced Studies Institute Series, D. Reidel Publishing Co., 1979)
100. C. J. Schutte, The Theory of Molecular Spectroscopy, Volume 1: The Quantum Mechanics and Group Theory of Vibrating and Rotating Molecules (North Holland Publishing Co., 1976)
101. J. I. Steinfeld, Molecules and Radiation: An Introduction to Modern Molecular Spectroscopy (Harper & Row, 1974)
102. K. R. Way, W. C. Stwalley, *J. Chem. Phys.* 59, 5298 (1972)
103. W. C. Stwalley, Paper AA5, Proceedings of the 27th Symposium on Molecular Structure and Spectroscopy, Columbus, Ohio, 1972 (unpublished)
104. P. L. Kelley, H. Kildal, H. R. Schlossberg, *Chem. Phys. Lett.* 27, 62 (1974)
105. F. P. Shafer, Dye Lasers, Topics in Applied Physics, Volume 1, 2nd edition (Springer-Verlag, 1977)

106. W. A. Fitzsimmons, L. W. Anderson, C. E. Riedhauser, J. M. Vrtilik, IEEE, J. Quantum Elect. QE-12, 624 (1976)
107. T. W. Hansch, Appl. Optics 11, 895 (1972)
108. R. Wallenstein, T. W. Hansch, Appl. Optics 13, 1625 (1974)
109. J. E. Lawler, W. A. Fitzsimmons, L. W. Anderson, Appl. Optics 15, 1093 (1976)
110. J. G. Hirschberg, R. R. Kadesch, J. Opt. Soc. of Amer. 48, 177 (1958)
111. J. E. Mack, D. P. McNutt, F. L. Roesler, R. Chabbal, Appl. Optics 2, 873 (1963)
112. D. H. Rand, J. N. Shearer, J. Opt. Soc. of Amer. 46, 463 (1956)
113. G. H. McCall, Rev. Sci. Instrum. 43, 865 (1972)
114. J. W. White, J. Opt. Soc. of Amer. 32, 285 (1942)
115. R. N. Jones, Computer Programs for Absorption Spectrophotometry (program PC-120), Bulletin No. 11, National Research Council of Canada (1968)
116. U. P. Wild, A. R. Holzwarth, H. P. Good, Rev. Sci. Instrum. 48, 1621 (1977)
117. J. A. Halstead, R. R. Reeves, Opt. Commun. 27, 273 (1978)
118. F. A. Cotton, G. Wilkinson, Advanced Inorganic Chemistry 3rd edition (Interscience, New York, 1972)
119. R. E. Buckles, J. M. Bader, Inorg. Synth. 9, 130 (1971)
120. R. H. Lamoreaux, W. F. Giauque, J. Phys. Chem. 73, 755 (1969)
121. J. McMorris, D. M. Yost, J. Amer. Chem. Soc. 53, 2625 (1931)
122. G. V. Calder, W. F. Giauque, J. Phys. Chem. 69, 2443 (1965)
123. C. C. Lu, T. A. Carlson, F. B. Malik, T. C. Tucker, C. W. Nestor, Atomic Data 3, 1, (1971)

124. R. J. Le Roy, J. Mol. Spectr. 39, 175 (1971)
125. H. Cordes, Z. Phys. 97, 603 (1935)
126. J. Tellinghuisen, Chem. Phys. Lett. 29, 359 (1974)
127. R. A. Ashby, Can. J. Phys. 57, 698 (1979)
128. K. S. Viswanathan, A. Sur, J. Tellinghuisen, submitted to J. Mol. Spectr.
129. R. A. Ashby, C. W. Johnson, J. Mol. Spectr. 84, 41 (1980)
130. J. Waser, K. Weiland, Nature 160, 643 (1947)
131. R. L. Brown, W. Klemperer, J. Chem. Phys. 41, 3072 (1964)
132. J. I. Steinfeld, W. Klemperer, J. Chem. Phys. 42, 3475 (1965)
133. R. B. Kurzel, J. I. Steinfeld, J. Chem. Phys. 53, 3293 (1970)
134. R. B. Kurzel, J. I. Steinfeld, D. A. Hatzenbahler, G. E. Leroi, J. Chem. Phys. 55, 4822 (1971)
135. G. A. Capelle, H. P. Broida, J. Chem. Phys. 58, 4212 (1973)
136. J. A. Paisner, R. Wallenstein, J. Chem. Phys. 61, 4317 (1974)
137. M. Broyer, J. Vigue, J. C. Lehmann, J. Chem. Phys. 63, 5428 (1975)
138. K. Sakurai, G. Tiaiele, H. P. Broida, Chem. Phys. Lett. 41, 39 (1976)
139. E. O. Degenkolb, J. I. Steinfeld, E. Wasserman, W. Klemperer, J. Chem. Phys. 51, 615 (1969)
140. A. B. Callear, P. Erman, J. Kuripa, Chem. Phys. Lett. 44, 599 (1976)
141. M. C. Sauer, W. A. Mulac, R. Cooper, F. Grieser, J. Chem. Phys. 64, 4587 (1976)
142. Selected Values of the Thermodynamic properties of the

Elements, R. Hultgren, P. D. Desai, D. T. Hawkins,
M. Gleiser, K. K. Kelley, D. D. Wagman (eds)
(American Society for Metals, 1973)

143. R. B. Kurzel, E. O. Degenkolb, J. I. Steinfeld, J. Chem. Phys. 56, 1784 (1972)
144. J. M. Brown et al, J. Mol. Spectr. 55, 500 (1975)
145. F. W. Loomis, A. J. Allen, Phys. Rev. 33, 639 (1929)
146. D. S. King, P. K. Schenck, K. C. Smyth, J. C. Travis, Appl. Optics 16, 2617 (1977)
147. R. B. Green, R. A. Keller, S. S. Luther, P. K. Schenck, J. C. Travis, Appl. Phys. Lett. 29, 727 (1976)
148. D. S. King, P. K. Schenck, Laser Focus, March 1978
149. T. F. Johnston Jr., Laser Focus, March 1978